

DESIGN, CHARACTERIZATION, AND OPTIMIZATION
OF AN INEXPENSIVE RAMAN SPECTROSCOPIC SYSTEM
FOR SAMPLE IDENTIFICATION

By

PAIGE ELIZABETH EAGAN

A DISSERTATION PRESENTED TO THE GRADUATE SCHOOL
OF THE UNIVERSITY OF FLORIDA IN PARTIAL FULFILLMENT
OF THE REQUIREMENTS FOR THE DEGREE OF
DOCTOR OF PHILOSOPHY

UNIVERSITY OF FLORIDA

2003

Dedicated to. . .

my solid foundation, Mom and Dad

my creative inspiration, Kristen

the love of my life, Eric

ACKNOWLEDGMENTS

Many individuals have contributed to the fruition of this dissertation. They are not only scientific colleagues, but good friends and supporters. First, I wish to acknowledge my graduate advisor, Dr. J.D. Winefordner, for his continued guidance and encouragement. Jim sustained a large research group while giving each student the opportunity for intellectual freedom and creativity. Additionally, he strongly encouraged personal growth through teaching and service. It is the latter for which I am most appreciative, because it afforded me the space to explore nonresearch areas of analytical chemistry.

I am grateful to have had the opportunity to work with Dr. N. Omenetto. Nico's unadulterated enthusiasm for knowledge was truly inspirational and motivational. Such enthusiasm is a quality that I will strive to purvey to my students in the future.

Contributions from Dr. B.W. Smith and Dr. I.B. Gornushkin should not be overlooked. Ben was a great resource for equipment and advice. Igor provided helpful research conversations, computer programs, and patience. My work would not be what is without their assistance.

I would like to extend my appreciation to all members of the Winefordner and Harrison groups with whom I have interacted. Each of them added to the overall experience, lessons, and memories of graduate school. The initiation of my project is accredited to Dr. Dimitri Pappas. I am thankful for his encouragement, support, knowledge, and friendship. Dr. Nathan Pixley was also instrumental in my success in the

lab and his friendship is likewise treasured. A special acknowledgement is bestowed to Tiffany Correll. She has made the lab not only bearable, but enjoyable. I am thankful that I have had the opportunity to work beside her for the past 3 years and have developed a great friendship. Kevin Turney has provided much entertainment, advice, and great conversation for which I am grateful. Many computer and formatting solutions have been provided by Dr. Jamshid Temirov.

Appreciation is extended to all support staff in the Chemistry department, including machine, electronic, and IT shops. Special thanks are owed to Jeanne Karably for her efficient management of the analytical office and endearing upbeat personality.

It would be remiss of me not to mention influential figures who have been significant driving forces in my life: Rev. Mary Koppel (friend), Ms. Theresa Zucchero (friend), Ms. Sarah McCarthy (friend), Ms. Ester Freeman (high school chemistry teacher), Mr. Kenneth Phillips (middle school algebra teacher), Dr. Valeria Kleiman (Physical Chemistry graduate professor), Dr. John Bordley (Physical Chemistry undergraduate professor), Dr. John Shibata (Physical Chemistry undergraduate professor), Dr. Ed Kirven (Organic Chemistry undergraduate professor), Dr. James Lowe (Organic Chemistry undergraduate professor), and Dr. Cornelius Klots (Visiting Chemistry professor retired from Oak Ridge Labs).

Last, but not least, I would like to acknowledge my family. I attribute my success in life to my parents, Colonel (Ret.) Patrick D. Eagan and Mrs. Nancy Eagan. My achievements to-date would have not been possible without the solid foundation and unconditional support they have provided. Additionally, I was surrounded by a wealth of support from my grandparents while growing up – each provided a special means of

encouragement. I am glad that Granny will be able to experience this achievement with me; I know Pop-pop and Grandmother are celebrating from above. My sister, Kristen, has been a large and positive force for me and I appreciate her perspective on life. Much appreciation is extended to Dr. Eric Oxley. He has provided an incredible amount of advice, support, and encouragement. I am most appreciative for his unwavering friendship and love.

TABLE OF CONTENTS

| | <u>Page</u> |
|--|-------------|
| ACKNOWLEDGMENTS | iii |
| ABSTRACT | ix |
| CHAPTERS | |
| 1 INTRODUCTION | 1 |
| General Background | 1 |
| Scope of Dissertation Research | 4 |
| 2 FUNDAMENTALS OF RAMAN SPECTROSCOPY | 7 |
| Introduction | 7 |
| Classical Wave Model | 10 |
| Quantum Mechanical Model | 13 |
| Selection Rules | 17 |
| Competing Spectroscopic Techniques | 18 |
| 3 DESIGN OF LOW-END RAMAN SPECTROSCOPIC SYSTEM | 22 |
| Introduction | 22 |
| Source | 24 |
| Background | 24 |
| Source Selection | 29 |
| Source Specifications | 32 |
| Experimental Characterization | 33 |
| Fiber Optic Probe | 38 |
| Background | 38 |
| Fiber Optic Probe Selection | 42 |
| Fiber Optic Probe Specifications | 43 |
| Experimental Characterization | 46 |
| Laser-to-Fiber Coupling | 48 |
| Spectrometer | 48 |
| Background | 48 |
| Spectrometer Selection | 50 |
| Spectrometer Specifications | 54 |
| Experimental Characterization | 57 |

| | |
|--|------------|
| Operating conditions | 57 |
| Spectrometer optical resolution..... | 58 |
| Spectrometer response..... | 62 |
| Computer and Data Collection Software..... | 64 |
| Background..... | 64 |
| Computer and Data Collection Software Specifications | 64 |
| Experimental Characterization | 65 |
| Concluding Remarks | 67 |
| 4 PERFORMANCE OF LOW-END RAMAN SPECTROSCOPIC SYSTEM..... | 69 |
| Introduction..... | 69 |
| Signal and Performance Considerations..... | 69 |
| Peak Intensity Theoretical Calculation..... | 69 |
| Number density | 70 |
| Scatterer cross section | 71 |
| Solid angle | 71 |
| Path length..... | 72 |
| Photon flux | 72 |
| Transmittance..... | 72 |
| Efficiencies..... | 75 |
| Calculation results | 79 |
| Spectra and S/N Values | 79 |
| Limit of Detection (LOD) | 81 |
| Noise Considerations..... | 86 |
| Fixed Pattern Noise (FPN) | 86 |
| Limiting Noise Source..... | 96 |
| Signal and background shot noise..... | 99 |
| Signal and background flicker noise..... | 100 |
| Detector noise..... | 100 |
| Limiting noise source determination..... | 101 |
| Concluding Remarks | 104 |
| 5 DATA ANALYSIS FOR LOW-END RAMAN SPECTROSCOPIC SYSTEM..... | 109 |
| Introduction..... | 109 |
| Background Information..... | 109 |
| Samples and General Experimental Parameters | 110 |
| Sample Grouping Analysis | 113 |
| Hierarchical Cluster Analysis (HCA)..... | 117 |
| Fundamentals | 117 |
| Application to plastics grouping | 119 |
| Principal Component Analysis (PCA)..... | 119 |
| Fundamentals | 119 |
| Application to plastics grouping | 123 |
| Linear Discriminant Analysis (LDA)..... | 123 |
| Fundamentals | 123 |

| | |
|---|---------|
| Application to plastics grouping | 127 |
| Grouping Analysis Conclusions | 130 |
| Sample Identification Analysis..... | 130 |
| Correlation Methods..... | 130 |
| Fundamentals | 131 |
| Application of correlation methods to plastics identification | 132 |
| Identification Analysis Conclusions..... | 155 |
| Concluding Remarks | 157 |
| 6 SURFACE-ENHANCED RAMAN SCATTERING SPECTROSCOPY WITH LOW-END RAMAN SPECTROSCOPIC INSTRUMENT | 158 |
| Introduction..... | 158 |
| General Background | 158 |
| Simple SERS Substrate Preparation and Use with Low-End System | 161 |
| Concluding Remarks | 170 |
| 7 CONCLUDING REMARKS AND FUTURE WORK | 173 |
| Conclusions..... | 173 |
| Future Research Directions..... | 174 |
| LIST OF REFERENCES..... | 181 |
| BIOGRAPHICAL SKETCH | 187 |

Abstract of Dissertation Presented to the Graduate School
of the University of Florida in Partial Fulfillment of the
Requirements for the Degree of Doctor of Philosophy

DESIGN, CHARACTERIZATION, AND OPTIMIZATION
OF AN INEXPENSIVE RAMAN SPECTROSCOPIC SYSTEM
FOR SAMPLE IDENTIFICATION

By

Paige Elizabeth Eagan

August 2003

Chair: James D. Winefordner

Major Department: Chemistry

Raman spectroscopy probes molecular vibrations resulting from the inelastic scattering of incident light. The resulting spectra are information-rich and often provide chemical and structural knowledge concerning the analyte. Only a small number of photons (1 in 10^8) undergo the inelastic collision that leads to Raman scattering. Although the Raman effect is a weak phenomenon, the peaks are relatively narrow and can produce a fingerprint for various samples, which is ideal for identification purposes. Within the past decade, the use of Raman spectroscopy as an analytical tool has surged due to a number of instrumental developments, hardware improvements, and application needs.

The research endeavors described in this dissertation focus on the development of a low-end Raman spectroscopic system. The system was designed, characterized, and optimized with respect to instrument function and data analysis. Design criteria stipulated low cost, portability, broad application base, fiber optic sampling,

commercially available components, simple data analysis, and ease of use. Primary emphasis was placed on the inexpensive aspect.

The first phase of research concentrated on instrument components. A dispersive, fiber optic Raman spectroscopic system within the aforementioned constraints has been developed. While several Raman instruments are commercially available, they meet a different set of needs. These high-end systems generally provide excellent resolution, low detection limits, and relatively short measurement times. Yet, an increase in design complexity, a decrease in ease of use, and a rise in system costs are additionally associated with these systems. The low-end Raman instrument developed in this research is foreseen as an inexpensive alternative for routine identification purposes. Attention was also placed on a number of signal and noise considerations.

After the instrumental phase of the research waned, emphasis was placed on the use of correlation analysis for sample identification. Post-consumer plastics were selected as the samples for this phase of research because they possess relative spectral simplicity while maintaining in-class variations. Additionally, they are readily available and have been successfully evaluated with other independent Raman and correlation studies. A number of spectral factors (e.g., continuum background and fixed pattern noise) were considered and their effects on correlation efficiency were evaluated. In general, a correlation approach presented promising results for sample identification.

To improve on the instrument's detection limits, surface-enhanced Raman scattering (SERS) spectroscopy was attempted with the system. A simple and inexpensive method of preparation was used for the production of SERS substrates, which involved the deposition of silver on copper circuit boards *via* internal electrolysis.

The deposition of gold in a similar manner was evaluated as a potential SERS substrate. The results for this portion are mixed; the gold modified surface has not demonstrated consistent signal enhancement, while the silver has yielded positive results.

CHAPTER 1 INTRODUCTION

Raman spectroscopy probes the vibrations of molecules as they relate to the inelastic scattering of incident light. The resulting spectra are information-rich and often provide the researcher with chemical and structural knowledge concerning the analyte. Only a small number, approximately 1 in 10^8 photons, undergo the inelastic collision that leads to the Raman scattering effect. Although the Raman effect is a weak phenomenon, the associated peaks are relatively narrow and can produce a fingerprint for various samples, which is ideal for identification purposes. Over the past 2 decades, the use of Raman spectroscopy as an analytical tool has dramatically increased and found a wide-range of applications.

General Background

For centuries, the scattering of light and its relation to the world around us has been a point of curiosity. It was Leonardo de Vinci who concluded that the color of the sky was related to light scattering by suspended particles in the air; later, Maxwell hypothesized that these particles possessed a molecular origin.¹ The Raman effect was first theoretically described in 1923 by A. Smekal. The phenomenon was experimentally observed 5 years later by C.V. Raman,^{2,3} who was awarded the Nobel Prize in 1930. Raman spectroscopy became one of the two most common spectroscopic techniques used to interrogate molecular vibrations. It was deemed the tool of choice until the 1940s when infrared (IR) spectrometers became available commercially.¹ The Raman spectroscopic technique remained virtually dormant for the next 3 to 4 decades.

Advances in the Raman spectroscopy field have mirrored instrumental developments and improvements. These technical innovations have made the routine use of Raman spectroscopic analysis a more tangible reality in a broad area of disciplines.

The first major technological advancement that helped propel the use of Raman spectroscopy was the development of the laser in the late 1960s. This had an early pervasive effect on the Raman field. Using a powerful monochromatic excitation source that has the ability to focus numerous photons into a small volume, researchers were able to better interrogate and manipulate the Raman scattering effect. Most of the pre-1986 Raman literature was dominated by physical and structural investigations,¹⁻⁴ with little mention of chemical analysis applications. A number of fundamental and technical barriers continued to impede the realization of such chemical analyses. Obstacles included weak scattering intensities, fluorescence interferences, and inefficient light collection and detection. These limitations were addressed in the past 15 years by several spectroscopic instrumentation innovations. Notable technological advancements include the development and optimization of charge coupled device (CCD) detectors, holographic notch filters, more efficient spectrometer designs, near-infrared (NIR) diode lasers, and collection optics.^{5,6} These developments helped researchers to overcome the major instrumental impediments; and resulted in higher signal-to-noise ratios (S/N), greater rejection of Rayleigh scattered light, higher quantum efficiencies (Q), greater sensitivity, decreased integration times, avoidance of fluorescence interferences, and increased ease of use. The period of time from c.1986 to present has been coined the age of the Raman renaissance.

A number of enhancement techniques has also been exploited, adding to the versatility and analyte sensitivity of Raman analyses. The principal enhancement practices are surface-enhanced Raman scattering (SERS), resonance Raman scattering, and surface-enhanced resonance Raman scattering (SERRS) spectroscopies. Additional types of Raman spectroscopy are classified as nonlinear techniques and include stimulated Raman scattering, coherent Stokes Raman scattering, and coherent anti-Stokes Raman scattering (CARS). The latter has found the most use to date of these nonlinear types.

Raman spectroscopy has become a mainstay among spectrochemical analysis techniques and has been applied to a number of research fields. The diverse disciplines and studies include materials,⁷⁻⁹ pharmaceuticals,¹⁰⁻¹² medical diagnostics,¹³⁻¹⁸ reaction monitoring,¹⁹⁻²¹ environmental monitoring,²²⁻²⁴ mineralogy,²⁵⁻²⁷ art restoration,²⁸⁻³⁰ and forensics.³¹⁻³³ Current research incorporates both fundamental studies and application-based directives. Academic research embraces the broadest range and can often be categorized as fundamental studies, instrumental development, or applications. Industry has recently become more interested in the use of Raman spectroscopy for on-line monitoring and quality control. Pharmaceutical companies are investing time, money, and manpower in this technique with expectations that the Food and Drug Administration (FDA) will approve the method in the near future. Other government agencies are considering the use and approval of Raman spectroscopy as well. The Department of Defense (DOD) and the Department of Energy (DOE) have demonstrated the utility of Raman spectroscopy for on-site chemical identification and characterization of unknown compounds and are reviewing the technique for approval as a standard analysis method.³⁴

Such government-level activity indicates the increased interest and importance of Raman spectroscopy. The main roadblock to widespread government implementation is the difficulty in establishing frequency and intensity standards (e.g., the resulting spectra need to be instrument independent). Differences in spectrometer designs and gratings (if used) render spectra that cannot be easily nor accurately compared. The National Institute of Standards (NIST) and the American Society for Testing and Materials (ASTM) have been active in establishing Raman standards for both frequency and intensity.³⁵

Scope of Dissertation Research

The research endeavors described in this dissertation focus on the development of a low-end Raman spectroscopic system. The system was designed, characterized, and optimized with respect to instrument function and data analysis. This instrument could be applied to routine qualitative analyses and identification applications.

The system was designed within the constraints of specific criteria. The developed instrument was to comprise inexpensive and commercially available components, while possessing the potential for portability. Ease of use and fiber-optic sampling were also considerations. The instrument was intended for qualitative and identification purposes and simple data analysis techniques were sought. Lastly, a broad application base was desired. Such a system has been successfully developed and is detailed in this dissertation. Figure 1-1 provides a flow diagram of the various system criteria and their relative priorities in design considerations. The terms “low-end” and “inexpensive” are used interchangeably when referring to the developed Raman system. Cost and quality of components are often closely related. Thus with cost deemed the most important factor, sacrifices were made on quality of parts leading to a “low-end” system classification.

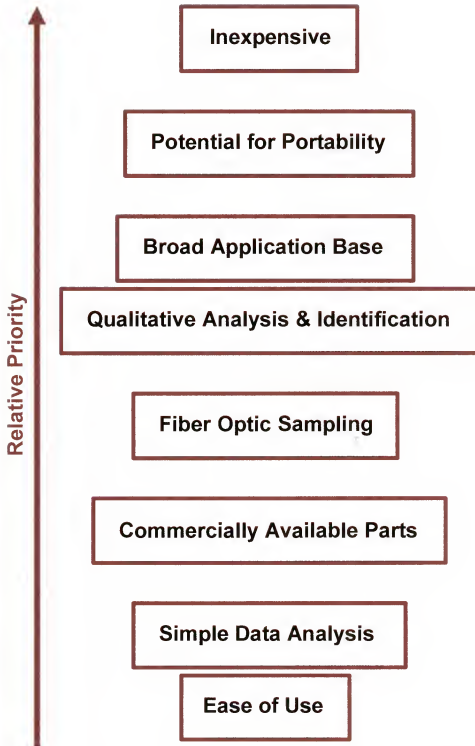


Figure 1-1. Various Criteria in the low-end Raman spectroscopic system design. They are listed in order of relative priority.

Fundamental considerations are addressed in Chapter 2, briefly accounting for classical and quantum mechanical descriptions. The merits and limitations of Raman spectroscopy are discussed and compared to competing spectroscopic techniques.

Design of the Raman spectroscopic system is presented in Chapter 3. Each of the major instrument components are described in terms of background information, selection considerations, manufacturer specifications, and experimental characterization.

In Chapter 4, the performance of the developed Raman system is evaluated. Considerations are made with respect to signal intensities, noise and noise source identification, experimental parameter effects on S/N, and continuum background.

The merging of various chemometric techniques for data analysis and sample identification is described in Chapter 5. Post-consumer plastic samples were chosen for this key research phase. Unsupervised and supervised methods were used for data grouping purposes. Grouping analyses aided better understanding of the plastic samples' behaviors and were used to predict potential limitations for identification. Sample identification was accomplished using linear and nonparametric rank correlation methods. A number of spectral factors were considered in the identification assessment process.

In Chapter 6, the Raman system is coupled with the enhancement power of SERS. This merge was to increase the potential application breadth of the system. A simple SERS preparation technique using internal electrolysis of silver and gold on a copper substrate is described and appraised.

General conclusions from this dissertation work are discussed in Chapter 7. Recommendations for future studies and applications are also described.

CHAPTER 2 FUNDAMENTALS OF RAMAN SPECTROSCOPY

Introduction

When incident light interrogates a molecule, the excitation photons can be absorbed, transmitted, or scattered. The latter has importance for the fundamental Raman process. The Raman effect depends on a change in polarizability of a molecule as radiation interacts with that molecule (i.e., an exchange of energy between light and matter).^{36,37}

Light scattering can result from both elastic and inelastic collisions. Most light is scattered elastically, which produces no net change in energy and the molecule's polarizability is not altered. This type of scattered light has the same frequency as the excitation radiation and is termed Rayleigh scatter. The manner in which a small portion of the incident light interacts with a sample results in inelastic collisions and vibration of the analyte molecules. The frequency of the incident light is shifted and the molecule is left in an altered vibrational state. The magnitude of this frequency shift must be equivalent to the vibrational frequency of the molecule given that light energy is proportional to frequency. If the incident photons lose energy, there are spectral shifts to lower frequencies; and Raman Stokes bands are generated. Alternatively, Raman anti-Stokes bands are produced if the photons are scattered with increased frequencies. Spectra are plotted with scattered intensity as a function of wavenumber (cm^{-1}). All frequency shifts are calculated with respect to the excitation frequency, which is also the

Rayleigh scatter frequency. Because of this, Raman shifts are not excitation wavelength dependent. The general equation for Raman shift, $\Delta \bar{\nu}_o$, calculation is

$$\Delta \bar{\nu} = \bar{\nu}_o - \bar{\nu}_{data} = \left(\frac{1}{\lambda_o} \right) - \left(\frac{1}{\lambda_{data}} \right) \quad (2-1)$$

where $\bar{\nu}_o$ is the excitation wavenumber, $\bar{\nu}_{data}$ is the wavenumber corresponding to experimental data, λ_o and λ_{data} are the wavelengths in cm of the source light and data collected, respectively.

All three modes of scattering occur for Raman-active compounds, but not at equal intensities. Figure 2-1 shows a standard carbon tetrachloride (CCl_4) Raman spectrum. The Rayleigh line is the most intense, often by a factor of 10^6 to 10^8 . Raman bands are present on both sides of the Rayleigh peak. The Stokes bands correspond to negative wavenumbers and the anti-Stokes to positive, which is related to spectral shifts and energy changes. While these Raman shifts are symmetric, they differ in probability of occurrence leading to the disparity in Stokes and anti-Stokes peak intensities. Raman Stokes bands are typically used in analytical techniques and are plotted as a function of absolute wavenumbers.

The Raman effect is commonly described in terms of classical wave theory or quantum mechanics. The classical approach will be considered first, followed by a basic explanation of the quantum mechanical treatment. The discussions provided in the following sections are meant to present a general overview. A number of sources were consulted and used in formulating the model summaries.^{4,37-43} Note that from this point in the dissertation Raman spectroscopy refers to NIR Raman spectroscopy. For the presented research, the NIR region of the electromagnetic spectrum is of interest.

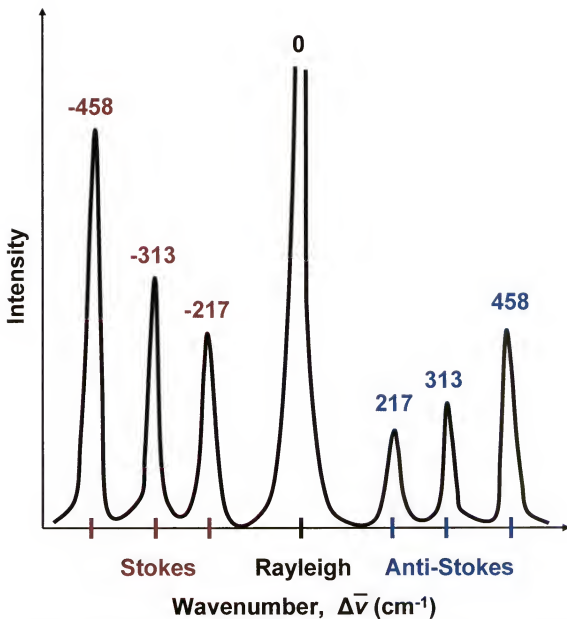


Figure 2-1. Representation of a typical CCl₄ Raman spectrum. (Not drawn to scale.)

Classical Wave Model

The classical wave approach is based on a tenet that the scattering molecule acts as a collection of atoms undergoing simple harmonic oscillations. A pictorial representation is shown in Figure 2-2. The incident radiation field, E , can be defined as

$$E = E_o \cos(2\pi\nu_o t) \quad (2-2)$$

where E_o is the amplitude of the wave, ν_o is the incident radiation frequency, and t is time. A dipole moment, μ , is induced when an analyte interacts with the oscillating electric field. This dipole moment results from the displacement of a molecule's electrons and temporary distortion of the associated electron cloud. There exists a proportional relationship between μ and E and is described by

$$\mu = \alpha E \quad (2-3)$$

where α represents a proportionality constant known as the polarizability of the molecule. Polarizability is the ease with which a molecule's electron cloud can be distorted in an electric field. This constant is molecule specific. Note that Equation (2-2) is a generalization and, if taken as is, only describes the dipole that has a vibrational frequency equal to the excitation frequency ($\nu_v = \nu_o$). Thus, Rayleigh scatter would be the sole scattering process considered. For a more comprehensive approach, Raman scatter should be included ($\nu_v \neq \nu_o$).

For Raman scattering, the polarizability of a molecule's bonds must vary as a function of internuclear distances.⁴⁰ If r_{eq} and r are defined as the internuclear distances at equilibrium and at any other point in time, respectively, then the Raman-required

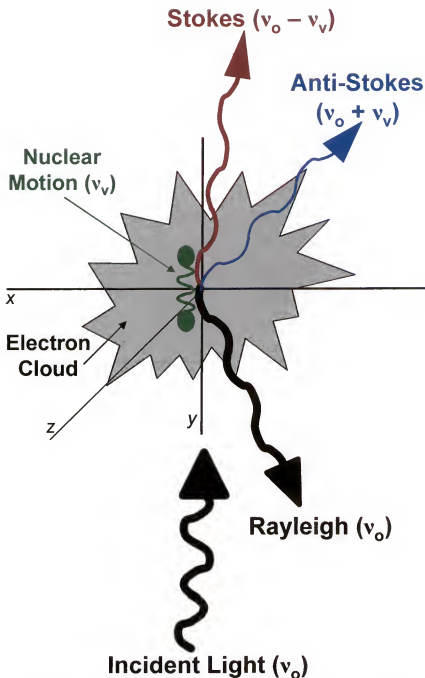


Figure 2-2. Classical wave model. Incident light at frequency ν_0 interacts with a molecule, setting it into vibrational motion. Scattered light is reemitted at the same frequency (Rayleigh), lower frequencies (Raman Stokes), and higher frequencies (Raman Anti-Stokes). Adapted from reference 44: Asher, S.A.; Munero, C.H.; Chi, Z. *Laser Focus World*. 1997, July, 99.

polarizability variation can be expressed as

$$\alpha = \alpha_o + (r - r_{eq}) \left(\frac{\partial \alpha}{\partial r} \right) \quad (2-4)$$

and internuclear separations are given by

$$r - r_{eq} = r_{\max} \cos(2\pi\nu_v t) \quad (2-5)$$

where α_o is the polarizability constant of r_{eq} , r_{\max} is the maximum internuclear distance with respect to the equilibrium position, and ν_v is vibrational frequency. Recognizing

that $\left(\frac{\partial \alpha}{\partial r} \right)_{r_{\max}}$ is the rate of change of polarizability relating to the equilibrium position,

the term can be redefined by a single variable, β , for simplification. A general

polarizability expression is obtained from the combination of Equations (2-4) and (2-5)

and from the substitution of β :

$$\alpha = \alpha_o + \beta \cos(2\pi\nu_v t) \quad (2-6)$$

Inserting Equations (2-2) and (2-6) into the relationship given by Equation (2-3) produces a more complete mathematical description of an induced dipole:

$$\mu = [\alpha_o E_o \cos(2\pi\nu_o t)] + [E_o \beta \cos(2\pi\nu_v t) \cos(2\pi\nu_o t)] \quad (2-7)$$

Applying the trigonometric identity:

$$\cos x \cos y = \frac{[\cos(x+y) + \cos(x-y)]}{2} \quad (2-8)$$

the following expression is produced, which accounts for Rayleigh and Raman scattering processes:

$$\mu = [\alpha_o E_o \cos(2\pi\nu_o t)] + \left[\frac{E_o}{2} \beta \cos[2\pi(\nu_o - \nu_v)t] \right] + \left[\frac{E_o}{2} \beta \cos[2\pi(\nu_o + \nu_v)t] \right]. \quad (2-9)$$

The initial term accounts for Rayleigh scattering, as demonstrated earlier with Equation (2-3). The second and third terms describe Raman Stokes ($\nu_o - \nu_v$) and anti-Stokes scattering ($\nu_o + \nu_v$), respectively. Information derived from Equation (2-9) provides insight into the Raman effect and its parameters. For example, laser intensity is proportional to polarization and scattering (Rayleigh and Raman) intensities.⁴ However, a classical approach is not complete. A shortcoming of the model, as it relates to scattering, is its inability to predict band intensities. Hence, using this model exclusively as a descriptor leads to the false conclusion that all three scattering modes are equally probable. A quantum mechanical approach can account for this discrepancy.

Quantum Mechanical Model

Where the classical wave model treats the scattering molecule as a collection of atoms undergoing simple harmonic oscillations, the quantum mechanical description is based on the idea that the vibrational energy of a molecule is quantized.⁴³ The resonance condition is a quintessential relationship in spectroscopy and is expressed as:

$$|\Delta E| = h\nu \quad (2-10)$$

where $|\Delta E|$ is the net energy difference in energy levels, h is Planck's constant, and ν is the emitted photon frequency. Through this equation, the absorbed and emitted photon frequencies (experimentally observed) are linked to energy changes in the interrogated molecule. However, the resonance condition does not apply to the Raman effect because it is neither an absorption nor emission process, but rather a scattering phenomenon.⁴¹ An analogous expression to Equation (2-10) can be derived for Raman spectroscopy. Due to conservation of energy, frequency shifts resulting from inelastic collisions are

related to the overall change in energy of the molecule. An expression for this relationship can be written as

$$\Delta E + h\Delta\nu = 0 \quad (2-11)$$

where ΔE and $h\Delta\nu$ are the net energy changes of the molecule and photons, respectively.

Figure 2-3 is an energy level diagram depicting different pathways for scattering. All molecules that undergo Rayleigh or Raman scattering are first excited to a virtual state from which relaxation occurs. A virtual state is not a true quantized energy level and can be better described as a very short lived distortion of the electron cloud by the oscillating electric field.⁴ Rayleigh scatter occurs when a molecule at a virtual state relaxes to the same energy level from which it originated. For Raman Stokes scattering, the molecule does not relax to the original energy level but to one of higher energy. This generates a positive ΔE and a negative $\Delta\nu$, as depicted in Figure 2-4a. A molecule that relaxes to an energy level positioned lower than the originating level undergoes Raman anti-Stokes scattering. For this scenario, ΔE is negative and $\Delta\nu$ positive, as shown in Figure 2-4b. Alluded to previously, Stokes shifts are more intense than the anti-Stokes shifts. This is a function of energy level populations with respect to the Boltzmann distribution. At room temperature, most molecules are essentially located in the lowest vibrational level in the electronic ground state. Since a molecule that experiences anti-Stokes scattering must return to an energy level lower than the original level, no molecules residing in the zero vibrational level can participate. This significantly decreases the probability of occurrence and reduces associated intensities. The ratio of

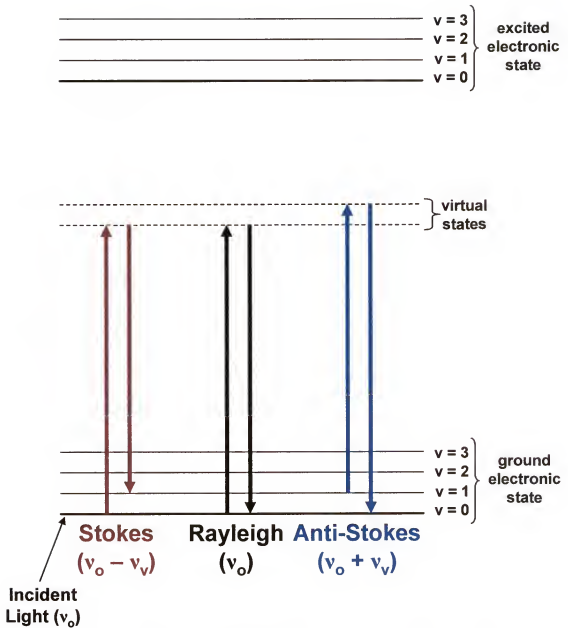
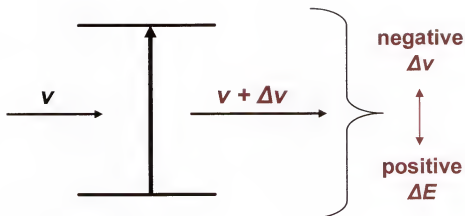


Figure 2-3. Energy level diagram showing the quantum mechanical origin of Rayleigh and Raman scattering.

(a)



(b)

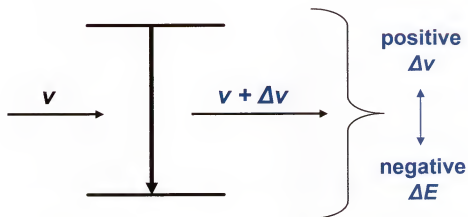


Figure 2-4. Forms of Raman scattering. (a) Raman Stokes band where molecular energy increases; and (b) Raman anti-Stokes band where molecular energy decreases. Adapted from reference 41: Woodbury, G. Physical Chemistry. Brooks/Cole Publishing Company: Pacific Grove, CA, 1997.

Raman Stokes and anti-Stokes band intensities can be calculated with respect to the Boltzmann distribution, indicating temperature dependence:

$$\frac{I_R(\nu_o + \nu_v)}{I_R(\nu_o - \nu_v)} = \frac{(\nu_o + \nu_v)^4}{(\nu_o - \nu_v)^4} \exp\left(\frac{-h\nu_v}{kT}\right) \quad (2-12)$$

where h is Planck's constant, k is Boltzmann's constant, and T is temperature.⁴

Selection Rules

The vibrational transition energy between any two consecutive levels should be constant for a harmonic oscillator. Thus, a transition from $\nu = 0 \rightarrow \nu = 1$ will equal the energy associated with a $\nu = 1 \rightarrow \nu = 2$ transition (where ν is a vibrational quantum number).⁴¹ Principals of quantum theory predict that the only transitions allowed are those for which the vibrational quantum number changes by unity, (i.e., $\Delta\nu = \pm 1, \pm 2, \text{etc.}$).⁴⁰ Based on vibrational level populations, the largest contribution to a Raman spectrum will be from the $\nu = 0 \rightarrow \nu = 1$ transition. Furthermore, a single peak should be detected for a given molecular vibration due to the equally spaced vibrational levels.^{40, 45}

In describing the motion of a molecule, three parts must be considered – translational motion, rotational motion, and vibrational motion. The first defines the motion of the entire molecule through space; the second component accounts for the rotational movement of the molecule around its center of gravity; and the third describes the motion of each atom in relation to other atoms comprising a molecule.^{40, 42} The total number of normal vibrational modes for a molecule can be calculated using the following relationships:

$$\text{linear molecules:} \quad 3N - 5 \quad (2-13)$$

$$\text{nonlinear molecules:} \quad 3N - 6 \quad (2-14)$$

where N is the number of atoms. The subtraction of 5 and 6 for linear and nonlinear molecules, respectively, accounts for the total degrees of freedom associated with translational and rotational molecular movements. While these equations predict the number of vibrational modes for a molecule, not all will produce distinct Raman bands. Two primary explanations account for this fact – symmetry and degeneracy.³⁸ Symmetry plays a significant role in the determination of Raman-active vibrations. For example, if a molecule has a center of symmetry, a certain mode in the molecule can only exhibit IR-activity or Raman-activity, but not both. This is known as the exclusion principle. Other selection rules that are governed by symmetry can be explained *via* group theory, which is beyond the scope of this dissertation. The second prime reason that not all normal modes result in a detectable band is related to the existence of degenerate vibrational modes. The degeneracy results from normal vibrations that have the same frequency, and thus they appear as a single peak.

Competing Spectroscopic Techniques

A wide array of spectroscopic techniques can be compared to Raman spectroscopy; however, it is more fruitful to consider only those techniques which are readily employed on similar applications for which Raman is used. In this section, a comparison will be made with IR absorption (FT-IR and NIR) and fluorescence spectroscopies. Table 2-1 provides a comparison of the aforementioned methods.

There are a number of analogous advantages between fluorescence and Raman with respect to sampling. However, the sensitivity of fluorescence is far superior to Raman. This is a result of larger fluorescence cross sections, which increases the probability of the phenomenon occurring and will be further discussed in Chapter 4. While

Table2-1. Some advantages and disadvantages of fluorescence, FT-IR absorption, NIR absorption, and Raman spectroscopic techniques. Adapted from references 4, 46, and 47.

| | Fluorescence | FT-IR Absorption | NIR Absorption | Raman |
|---------------|---|---|--|---|
| Advantages | <p>Easy sampling Noninvasive Water compatible Remote sampling, fibers Time resolved spectra</p> | <p>Good fingerprint Narrow bandwidths Libraries available</p> | <p>Easy sampling Noninvasive Water compatible Remote sampling, fibers Good penetration depth Time resolved spectra</p> | <p>Easy sampling Noninvasive Water compatible Remote sampling, fibers Good penetration depth Good fingerprint Narrow bandwidths</p> |
| Disadvantages | <p>Wide bandwidths Little spectral detail Sample heating</p> | <p>Sampling difficulties Water incompatible</p> | <p>Wide bandwidths Poor fingerprint Calibration complex</p> | <p>Low sensitivity Interferences</p> |

fluorescence leads to stronger signal intensities, there is little spectral detail available in the characteristic broad bands.

Raman is often compared with another prominent vibrational method, infrared (IR) absorption. Raman and IR absorption spectroscopies are often considered complementary techniques rather than competing. The selection rules and relative peak intensities differ yet, Raman frequency shifts and IR absorption peak frequencies are the same.³⁸ This direct correspondence is related to the quantized change in energy, ΔE , between two vibrational levels in the first electronic ground state of a molecule.⁴⁰ Generally, if a band is strong in a Raman spectrum it will be weak in an IR absorption spectrum and vice versa. The majority of IR absorption instruments used today are FT-based, hence FT-IR absorption was chosen for comparison purposes.

With increased interest in biological samples, a comparison between Raman and NIR absorption becomes important. While NIR absorption has distinct advantages over traditional FT-IR absorption for most biological samples, the advantages are less significant when compared to Raman spectroscopy. Both NIR vibrational techniques are water compatible. Easy, noninvasive, and remote samplings with good penetration depth are also common characteristics. Currently, the key advantage obtained by using NIR absorption, in lieu of Raman, is the ability to collect time resolved spectra. Generally, Raman spectroscopy combines important advantages available from FT-IR absorption and NIR absorption into a single technique.

One of the most significant barriers to the use of Raman spectroscopy is its inherently low signal intensities. Just as technological advancements aided the renewed

interest in this spectroscopic technique, future developments will continue to propel the Raman field forward.

CHAPTER 3 DESIGN OF LOW-END RAMAN SPECTROSCOPIC SYSTEM

Introduction

Selection and characterization of system components is a vital aspect in the development of a new system. A researcher considering the use of Raman spectroscopy must decide which of several instrument configurations is best for the intended applications, which is often dictated by sample requirements and specific research objectives.

There are several factors in the design of a Raman spectroscopic system that can significantly affect overall performance, S/N, measurement time, and sample radiation damage (if applicable). Such factors include spectrometer type, detector noise characteristics, resolution, sample type, collection geometry, and laser beam parameters.⁴⁸ McCreery has composed a criteria list for Raman spectrometer selection and an adaptation is shown in Table 3-1.⁴ This list of system considerations and accompanying questions can serve as a guideline in instrumental component selection.

The low-end system in this research was designed within the constraints of a number of requirements. While several Raman spectroscopic instruments are commercially available, they meet a different set of needs. These high-end systems generally possess excellent resolution, low detection limits, and relatively short measurement times. However, the instrument design complexity increases, ease of use decreases, and system cost rises for the high-end systems. The low-end Raman

Table 3-1. General considerations for Raman spectroscopic instrument selection. Modified from reference 4: McCreey, R.L. *Raman Spectroscopy for Chemical Analysis* in Chemical Analysis Series ed. by J.D. Winefordner, 157, John Wiley & Sons, Inc.: New York, 2000.

A. Laser Wavelength and Power

- What are the size, utility, and cooling requirements?
- Are low detection limits a priority?
- Will a fluorescence background need to be minimized?
- Are the samples photo-chemical and/or thermal sensitive?

B. Dispersive vs. Nondispersive Wavelength Analyzer

- What spectral range and resolution are desired?
- Which is most important – sensitivity or fluorescence suppression?
- What wavelength laser will be used?

C. Sampling Mode

- What types of samples will be analyzed (e.g. liquids, solids, biological)?
- Will samples be located near or a distance from the spectrometer?
- Is in vivo analysis desired?
- Is automated or on-line sampling required?

D. Data Analysis

- Is analysis primarily qualitative for identification purposes?
- Is analysis primarily quantitative? One or multiple components?
- Is real-time analysis required?
- Is a certain level of method sophistication desired?

E. Capital and Operating Costs

- Are there purchase price constraints?
- What will installation, utilities, and maintenance costs (per year)?
- Will a trained technician be required for operation?

spectroscopic system developed in this research was to comprise inexpensive and commercially available components, while possessing the potential for portability. Ease of use and fiber-optic sampling were also considerations. The instrument was intended for qualitative and identification purposes, and employment of simple data analysis techniques was sought. Lastly, a broad application base was desired. The long-range goal of the instrument was biological sample identification for biomedical diagnostic purposes, such as topical cancers (e.g. skin cancer) detection. Thus, all component selections were based upon the above listed system requirements and ultimate application goal.

A schematic of the low-end Raman system is shown in Figure 3-1. The instrument components resemble many other commercially available instruments; however, the component quality differs significantly, which leads to a number of sacrifices and challenges. The general flow for this system involves laser radiation delivered to the sample *via* a fiber optic cable, collection of scattered light *via* fiber optic cable, signal selection and detection by the spectrometer (equipped with a linear charge-coupled device array detector), and data processing by a personal desktop computer. The following sections will describe the major instrument components and their characterizations in relation to the low-end, inexpensive Raman spectroscopic system. Data analysis will be thoroughly discussed in Chapter 5.

Source

Background

Almost all Raman excitation sources used today are lasers. Prior to the invention of the laser, the source most commonly employed was the 435.8 nm line of a mercury

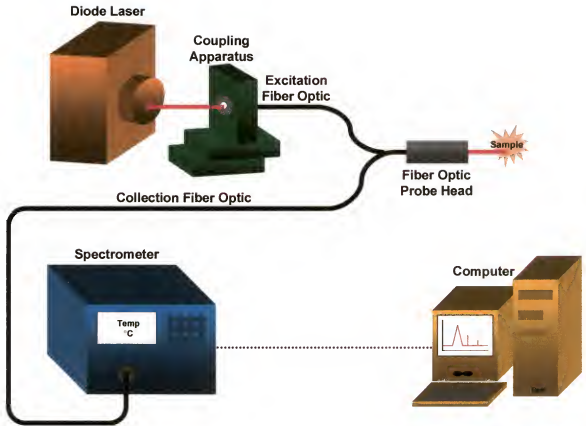


Figure Not Drawn to Scale.

Figure 3-1. General schematic of the inexpensive, low-end Raman spectroscopic system.

(Hg) arc lamp.¹ The first laser used for Raman excitation was a pulsed ruby laser in 1962 by Porto and Wood.⁴⁹ The next few years saw the introduction of continuous wave (CW) helium-neon (He-Ne) lasers to Raman setups. Since those early times, a wide variety of laser types and wavelengths have been used with Raman spectroscopy. Selection of the laser has far-reaching effects throughout the design of the instrument, limiting spectrometer, detector, and sampling optics options. Figure 3-2 displays wavelengths and available power ranges of commonly used commercial lasers in Raman spectroscopy. There are advantages and disadvantages to each excitation source that must be weighed against the general aim of the instrument during the selection process.

Various laser types

Ion Lasers. Ion lasers have found popularity in the Raman field due to high power output, variety of output wavelengths, and relatively long operating lifetimes. The argon (Ar^+) and krypton (Kr^+) ion lasers were the chief lasers used in Raman until the 1990s, when alternative laser sources that had lower associated costs and less power demands emerged as viable options.⁴ Inefficiency in the lasing process leads to the need for high electrical powers and water-cooling. These ion laser characteristics limit practicality and usefulness for routine Raman analysis. Air-cooled Ar^+ and Kr^+ lasers are available with lesser utility requirements for operation; however, laser output power is appreciably decreased.

Helium-Neon (He-Ne) Lasers. He-Ne lasers have become popular excitation sources for a number of commercially available Raman instruments. This is in part due to long operating lifetimes, low cost, excitation frequency precision, and adequately narrow output linewidths without additional accompaniments.⁴ The 632.8 nm He-Ne excitation wavelength has distinct advantages and disadvantages with regards to its use in

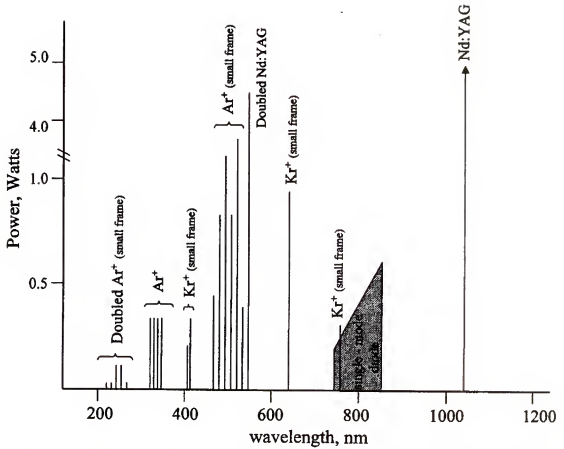


Figure 3-2. Common commercial lasers used for Raman spectroscopy. Wavelengths and available powers are shown.⁴

Raman spectroscopy. Such an excitation results in scattering wavelengths which span the most sensitive region of silicon CCD detectors, the most common detector for dispersive Raman instruments. However, if the samples of interest have significant fluorescence interferences, a wavelength shift into the near infrared (NIR) region is required and is not viable with this laser type. Additionally, He-Ne lasers are best used with samples that do not necessitate high laser output powers.

Neodymium-Yttrium Aluminum Garnet (Nd:YAG) lasers. Nd:YAG lasers are the most popular laser used in Raman spectroscopy. With the fundamental laser line at 1064 nm and the frequency-doubled line at 532 nm, Nd:YAG lasers have been used in both FT and dispersive Raman instruments. High lasing efficiency negates water-cooling needs and results in relatively high output powers. This laser, operating at the fundamental wavelength, has become the most extensively used source in FT-Raman instruments. The frequency-doubled wavelength is appropriate for samples that are not plagued by fluorescence interferences.

Titanium:sapphire (Ti:sapphire) lasers. Ti:sapphire lasers are a robust source for Raman applications benefiting from NIR excitation. This laser is tunable from approximately 690 nm to 1000 nm, which can be a significant advantage for certain Raman modes such as resonance Raman spectroscopy.³⁸ Ti:sapphire lasers have high output powers in comparison to other popular NIR lasers but, they are typically expensive compared to other laser types.

Diode lasers. Low cost, modest utility demand, design simplicity, ruggedness, and small size have made diode lasers attractive for Raman spectroscopic analysis. Common diode laser excitation wavelengths range from 650 nm to 900 nm, making these lasers

potentially excellent NIR sources. A number of drawbacks exist with diode laser use including broad gain curves, mode hopping, and output beam divergence.^{4,38} These drawbacks result in drifts in output power and frequency stabilization issues. Modifications can be made to minimize a number of these disadvantages.

Source Selection

Recognizing that the general research objective was to develop a Raman spectroscopic system that would be inexpensive, portable, user-friendly, and have a broad application base (particularly biomedical), a number of factors were considered in the selection of a commercially available source. Expense was given the greatest weight. Thus to best match the overall goals of the system, a 785 nm diode laser was chosen as the excitation source.

Diode lasers are based on semiconductor technologies. The basic idea behind diode laser operation is the production of radiation *via* recombination of electrons and holes at a *pn* junction.⁵⁰ See Figure 3-3 for a general diode laser illustration and Figure 3-4 for band diagrams. Electrons are excited (forward biasing) into the conduction band where hole-electron pairs are created. Eventually, the electrons relax and return to the valence band; in doing so, energy is released corresponding to the band-gap, E_g , energy.⁴⁰ If a sufficient density of the hole-electron pairs are created, the radiation can stimulate the recombination of these holes and electrons leading to the possibility of laser action.^{50,51}

The diode laser satisfies a number of the general system objectives. Most importantly, their mass production and commercial availability make them relatively inexpensive. This has largely been driven by the telecommunications industry. Diode lasers are also small and the housings often do not exceed the size of an adult hand. Such

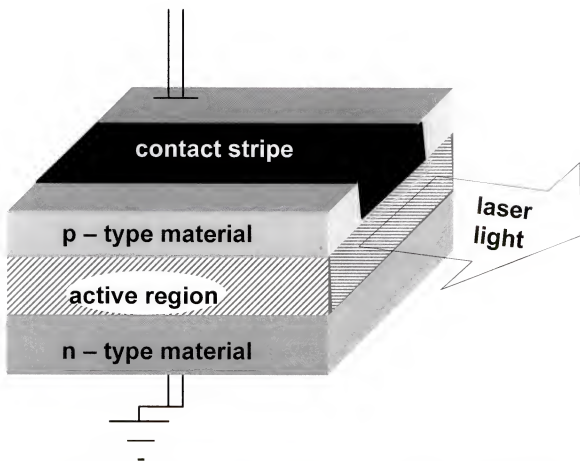


Figure 3-3. General depiction of a diode laser (stripe design). Modified from reference 50: Milonni, P. W.; Eberly, J. H. *Lasers*; John Wiley and Sons: New York, 1988.

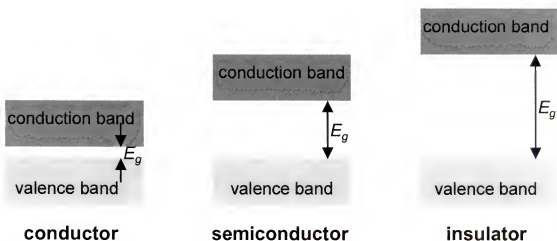


Figure 3-4. Band diagrams for three material types. Adapted from reference 40: Skoog, D. A.; Holler, F. J.; Nieman, T. A.; *Principals of Instrumental Analysis*, 5th Ed.; Harcourt Brace College Publishers: Philadelphia, 1998.

dimensions readily meet the requirement for instrument portability. Diode lasers are highly efficient, which minimizes power and cooling requirements and contributes to lower costs, ease of portability, and design simplicity. The excitation wavelength, 785 nm, was chosen because a shift into the NIR region of the electromagnetic spectrum reduces spectral interferences originating from fluorescence, which is often a significant disadvantage with biological samples. Fluorescence markedly decreases with longer excitation wavelengths. The lowest excited states of molecules, where fluorescence originates, have energies corresponding to visible wavelengths. These energies are higher in frequency than the NIR excitation energy, thus fluorescence is not readily excited by lower-energy NIR light.³⁷ There is a $1/\lambda^4$ signal dependence with the Raman scattering cross section and detection at longer wavelengths becomes more difficult. Thus, a laser wavelength should be selected so that fluorescence interference is minimized but not such that signal strength and detector noise are substantially affected.⁴ Since the Raman effect is a weak phenomenon, the excitation power must be great enough that the signal is detectable within a reasonable measurement time. Conversely, the excitation power that is delivered to sensitive samples must remain below damage thresholds, often referred to as the maximum permissible exposure (MPE) limit for biologicals. With the use of adequate laser powers, NIR light is nondestructive and can have penetration depths up to several centimeters.

Source Specifications

Diode lasers were acquired from Thorlabs, Inc. (Newton, NJ; Sanyo DL7140-201, 5.6 mm package). The nominal output power was 70 mW at a 785 nm excitation wavelength. Due to limitations of losses in alignments and transport through the fiber optic probe, only approximately half of the original power strikes the sample. All spectra

acquired with this low-end system were obtained with laser excitation powers ranging from 20 mW to 35 mW. Throughout this dissertation research, a number of diode lasers were employed with an average operating lifetime of 600 hr. Table 3-2 displays the manufacturer specifications for the particular diode laser used in this research. A typical laser profile is shown in Figure 3-5. For this dissertation work, the diode laser was operated around 40 °C and 130 mA, producing lasing wavelengths from 781 nm to 785 nm. The discrepancies in excitation wavelengths from individual diode lasers are attributed to manufacturing inconsistencies. Not surprisingly, these inconsistencies tend to increase with decreasing cost, which is indicative of lower quality.

Experimental Characterization

While lasers are common Raman excitation sources and serve as good sources of monochromatic light, fluctuations are inherent in the output signal and should be considered in system characterization. Short-term and long-term source fluctuations were considered for the chosen 785 nm diode laser. Three individual diode lasers were investigated, two of which had not been used previously (diode lasers B and C).

For short-term fluctuation analysis, the laser signal was monitored for approximately 35 min and the percent relative standard deviation (%RSD) was calculated. The experimental set-up is depicted in Figure 3-6. A total of 5 acquisitions for each diode laser was completed. Figure 3-7 shows the short-term signal fluctuations for three diode lasers (A, B, and C). All three were purchased from Thorlabs, Inc. and have identical manufacturer specifications. The diode laser that was previously used with the system (diode laser A) produced a %RSD of 5.4%; the other two new diodes had %RSD values of 2.9% and 1.5% (diode laser B and C, respectively). The low short-term laser fluctuations indicated that for given integration times of 35 min or less, little noise

Table 3-2. Diode laser manufacturer specifications for Sanyo DL7140-201 (Thorlabs, Inc.).⁵²

| | |
|---------------------------|-----------------|
| Wavelength | 785 \pm 10 nm |
| Maximum Power | 80 mW (CW) |
| Nominal Operating Power | 70 mW (CW) |
| Operating Temperature | -10 to 60 °C |
| Typical Threshold Current | 30 mA |
| Typical Operating Current | 100mA |
| Laser Package Size | 5.6 mm |

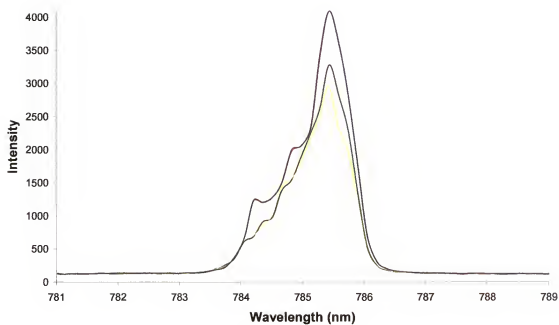


Figure 3-5. Typical laser profiles obtained with the inexpensive, low-end Raman system.

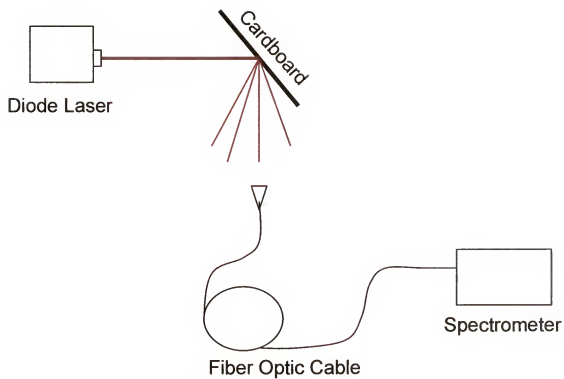


Figure 3-6. Experimental set-up for short-term and long-term laser signal fluctuation studies.

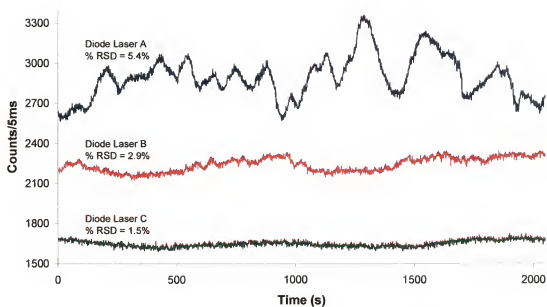


Figure 3-7. Diode laser short-term signal fluctuations (35 min analysis times).

would be contributed by the laser source. This is important for the analysis and determination of the system's limiting noise source, which is discussed in Chapter 4. Long-term laser fluctuations were also considered for laser characterization, which can provide insight about possible laser drifts during long-term data collecting sessions. In considering the long-term laser fluctuations, six consecutive 30 min data segments were graphically pieced together for a total analysis time of 3 hr, as shown in Figure 3-8. The experimental set-up was the same as depicted in Figure 3-6. The %RSD for diode lasers B and C were calculated at 3.1% and 4.5%, respectively. For both sources, the %RSD increased when short-term fluctuations and long-term fluctuations were compared. The observed drift was toward decreasing intensity, which indicated a slight laser drift that is independent of the Thorlabs DL7140-201 diode laser used.

Fiber Optic Probe

Background

Optical sampling schemes are an important aspect in Raman instrumental designs. They act as the transport pathway for excitation light from source to sample and scattered light from sample to spectrometer. Raman sampling modes can be divided into three general categories: conventional sampling, remote sampling, and microscopy.⁴ For the purposes of this research, remote sampling *via* fiber optics was explored. The use of fiber optic probes with Raman spectroscopic systems has been well established and a host of designs have been described.^{37,49,53-59} Nearly all Raman fiber optic probes operate in a backscatter style, meaning the light scattered 180° is collected and subsequently analyzed. The key variations in fiber optic probe design involve: (1) direction of laser excitation light from fiber to sample; (2) collection of Raman scattered light; and (3) if and how the probe is filtered.⁴⁹ The latter gives rise to the general classification of

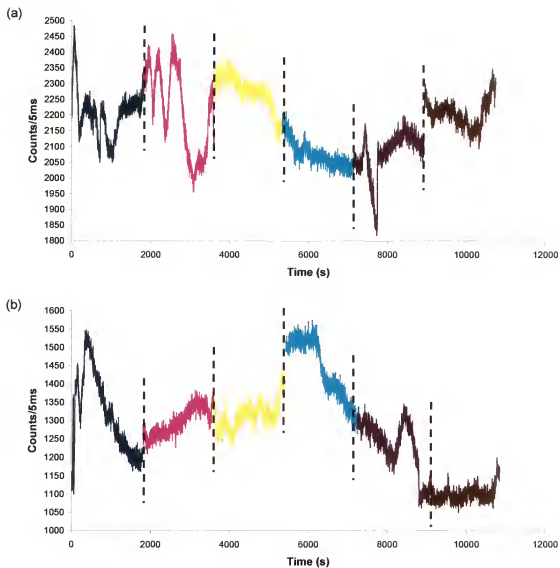


Figure 3-8. Diode laser long-term signal fluctuations. Six consecutive 30 min acquisitions merged for a total analysis time of 3 hr. (a) diode laser B; (b) diode laser C. The dashed lines delineate the six separate acquisitions.

Raman probes as either filtered or unfiltered.

Various fiber optic probe types

Unfiltered Raman probes. General characteristics of unfiltered probes include small size, low cost, and simple design. This was the first type of Raman fiber optic probe to be developed as reported by McCreery *et al.* in 1983.⁶⁰ The main drawback to unfiltered probes is their inability to minimize fiber background signals, which can obscure an analyte Raman spectrum.

The most commonly used unfiltered Raman fiber optic probe consists of a central excitation fiber and n number collection fibers peripherally positioned. This style has become known as the *n-around-1* geometry. The central excitation fiber delivers laser light to a sample and the surrounding fibers are responsible for scattered light collection and transport to spectrometer. The performance of this probe type is dependent upon the degree of overlap of the fibers' excitation and collection light cones.⁴⁹ To minimize the non-overlapping region and increase the *n-around-1* probe efficiency, various probe designs have incorporated angled fiber ends.^{54,55}

Filtered Raman probes. Filtered probes have more complex designs, larger sizes, and higher costs compared to unfiltered probes. Their key advantage is that they are capable of removing fiber background *via* filters. The degree of fiber background is spectrally demonstrated in Figure 3-9.

Filtered fiber optic probes can be categorized as either an in-line filtered probe or an integrated filtered probe. The former is similar to its unfiltered counterpart except for the in-line addition of such optical components as bandpass and notch filters. Integrated probes maintain the ability to filter fiber background, but the optics are confined to a

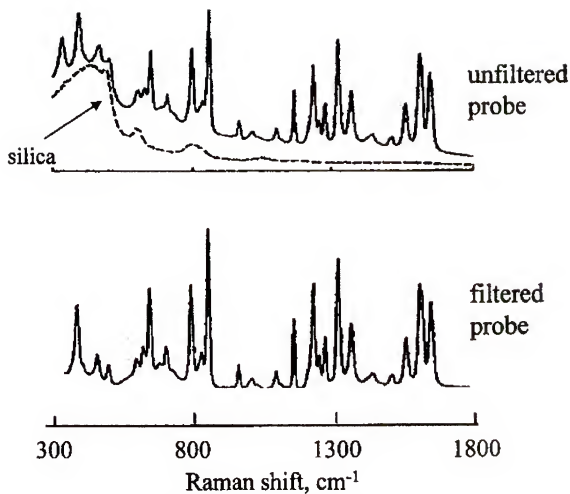


Figure 3-9. Raman spectra of 4-acetamidophenol (785 nm, Chromex spectrometer) to demonstrate the contribution of fiber background. Modified from reference 4. (a) unfiltered 18-around-1 probe; (b) integrated, filtered probe⁴

sampling probe head. While this is an advantage for remote sensing and application flexibility, probe modifications and internal alignments are not trivial. Integrated filter probes are also more efficient because their geometry provides complete overlap of excitation and collection light cones. A number of integrated filtered probes have been developed for Raman spectroscopic analyses.^{53,61-63}

Fiber Optic Probe Selection

In all probe designs, there is a mechanism for the delivery of excitation light and for the collection of scattered light from the sample. Since light is scattered in all directions (though not necessarily isotropically), the majority of modern probe designs collect scattered light with a backscattering arrangement. The overlap of excitation and collection light cones is beneficial to the collection efficiency, which translates into increased signal strength.

Another consideration in the selection of fiber optic probes is spectral background that originates from the fibers comprising the probe. This unwanted signal is known as fiber background. Light output from a fiber not only contains the reflected light from the sample, but also Raman bands originating from the silica fiber material. In some cases, fiber background can be subtracted from the spectrum; however, when the sample is a weak scatterer and/or there is a long fiber optic distance, the silica background can completely obscure the resulting spectrum.⁶¹

Considering the characteristics of different fiber optic sampling probe types and the overall objective for the low-end Raman spectroscopic instrument, an integrated filtered fiber optic probe was selected for the system. While this was not the simplest nor least costly option, the signal gains provided by the filtering offset the other disadvantages.

Fiber Optic Probe Specifications

The RamanProbe from InPhotonics, Inc. (Norwood, MA) was selected as the fiber optic probe assembly. A number of RamanProbe specifications are shown in Table 3-3 and a diagram of the probe sampling head is provided in Figure 3-10.

The laser excitation light (785 nm) enters the stainless steel probe head by way of a 90 μm diameter excitation fiber. The light first passes through a collimating lens and subsequently through a bandpass filter. The bandpass filter removes silica Raman bands produced by the fiber and transmits the pure laser light. The excitation light is then transmitted through a dichroic filter and focused outside the sampling head (5 mm focal point) *via* a lens. The laser light strikes the sample and the backscattered light enters the sampling head through the same focusing lens it previously exited and reflects off the dichroic filter. The scattered light collected from the sample passes through a long-pass filter as directed by an intermediate mirror. The long-pass filter assembly in the probe head transmits the Stokes scattered light and attenuates the Rayleigh band by a factor of 10^8 . The latter is another precautionary step to eliminate the observation of silica Raman bands from the fiber optic. The collimated light is then focused into a 200 μm collection fiber by another focusing lens and sent to the spectrometer. The backscattering sampling/collection geometry of the fiber optic probe provides optimum throughput due to a complete overlap between excitation and collection cones. A maximum of 300 mW can be passed into the optical fibers of the probe; therefore approximately 150 mW of power is theoretically the maximum laser power that can exit the sampling head and interact with a sample.

Table 3-3. Manufacturer specifications for RamanProbe model RP-785-05-01-SMA (InPhotonics, Inc.).⁶⁴

| | |
|------------------------------|-------------------|
| Typical Efficiency | 50% |
| Focal Length | 5.0 mm |
| External Focal Lens Diameter | 4.77 mm |
| Theoretical Spot Size | 90 μm |
| Practical Spot Size | 108 μm |
| Numerical Aperture | 0.40 |
| Approximate Depth of Field | 1.0 mm |

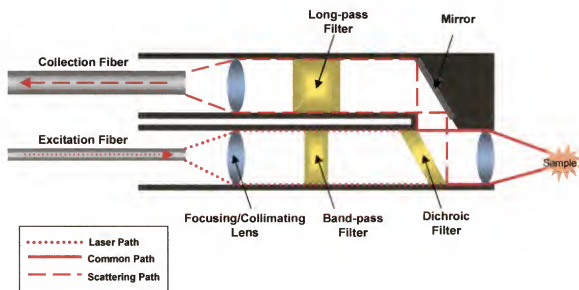


Figure 3-10. Schematic for the integrated, filtered fiber optic probe head. Adapted from reference 61: InPhotonics Technical Note #13: <http://www.inphotonics.com/technote13.pdf>.

Experimental Characterization

As previously mentioned, the fiber optic probe is a primary part of the Raman instrument and acts as the pathway for light transport through the system. The excitation fiber allows the laser light to reach the sample and the collection fiber sends the backscattered light to the detector. Three unique fiber optic probes were evaluated for implementation in the low-end Raman system.

The first probe assessed was a 1-around-1 probe (OceanOptics, Inc.; Dunedin, FL). This design consists of one excitation fiber and one collection fiber aligned side-by-side in the probe casing. The second probe considered was a 6-around-1 fiber optic bundle probe (OceanOptics, Inc.; Dunedin, FL). This bundle comprises a central excitation fiber optic with six surrounding collection fibers, following the traditional n-around-1 design. Since the efficiency of a fiber optic probe is highly dependent upon collection geometry, it is worth considering the overlap of the excitation and collection light cones. See Figure 3-11 for a pictorial representation of this overlap. Note there is a region of no cone overlap. This appears as a circular doughnut shape for the 6-around-1 probe, where the 1-around-1 is simply a cone. The area of no overlap can become critical if sample detection is preformed relatively close or flush with the probe head. Since the long-term goals of the developed Raman system would require close sample contact, another probe design was considered to maximize cone overlap.

The third fiber optic probe improved upon limitations of the previous designs. This third fiber optic probe, RamanProbe from InPhotonics, was described in detail in a previous section entitled "Fiber Optic Probe Specifications." Briefly, it comprises a series of optics which rejects Rayleigh light scatter and silica Raman bands while providing optimal collection geometry and efficiency due to total overlap between

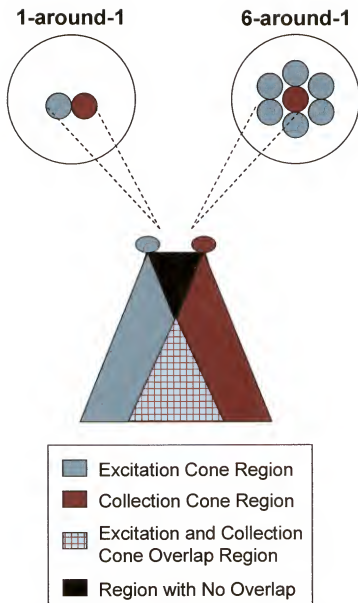


Figure 3-11. Representation of excitation light cone and collection light cone overlap for two popular n -around-1 unfiltered fiber optic probe designs.

excitation and collection light cones. A six fold increase in signal intensity was obtained using the RamanProbe when compared to the n-around-1 probes. Such an increase allowed an investigation of samples that are inherently weak scatterers (smaller Raman cross sections) while providing shorter integration times of those samples previously detected with the 1-around-1 and 6-around-1 fiber optic probes. The RamanProbe also produced spectra of CCl_4 and calcite with clean, distinct peaks *sans* laser tail interference. Refer to Figure 3-12 for a spectral comparison of the three evaluated fiber optic probes for a CCl_4 sample.

Laser-to-Fiber Coupling

It would be remiss to not mention the method used for coupling the laser beam to the excitation fiber optic cable of the probe. A series of translation stages and a ball lens constitute the coupling assembly. The stages afford several degrees of freedom for proper alignment. The ball lens is employed as a vehicle for laser light point focusing. It has been demonstrated that ball lens schemes are appropriate for focusing incident parallel light to a point which can then be aligned with optical fibers of varying diameters.⁶⁵⁻⁶⁷

Spectrometer

Background

Advancements in spectrometer technologies have significantly contributed to the progress in Raman spectroscopy. With the introduction of multiplex and multichannel spectrometers in the 1980s, routine analyses *via* Raman spectroscopy became a closer reality. Although the two spectrometer types have commonalities in that they reduce acquisition time and increase signal, they fundamentally differ in instrumental design and S/N effects.⁴ Today, the most prominent categories are generalized as Fourier

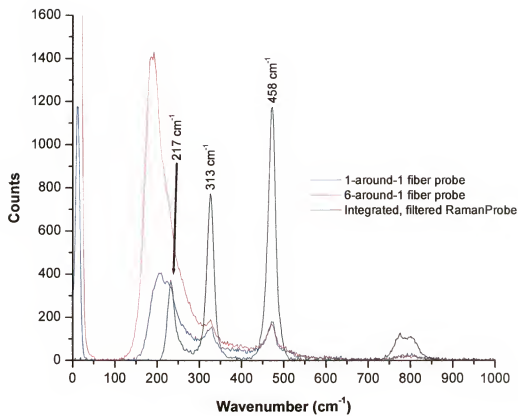


Figure 3-12. Spectral comparison of evaluated fiber optic probes using CCl₄.

transform (FT) Raman spectrometers (multiplex) and dispersive Raman spectrometers (multichannel), as shown in Figure 3-13. It is important to note for the purposes of this dissertation, the detector is considered a component of the spectrometer.

FT-Raman spectrometers are considered nondispersive, much like spectrometers based on filters (e.g., interference, acousto-optic, and liquid crystal). FT-based spectrometers modulate wavelengths so that each wavelength has a characteristic modulation frequency. The composite modulated signal is monitored by a single detector and demodulated by a Fourier transform algorithm.³⁸ For the case of dispersive Raman spectrometers, it is essential to disperse and analyze the scattered light collected from a sample. This involves the simultaneous monitoring of wavelengths and the subsequent wavelength differentiation. The latter is accomplished by way of spatial dispersion of the collected scattered light into a spectrum of the individual wavelengths. Most current dispersive spectrometers focus the signal onto a grating and the dispersed beam photons are then collected by CCD pixels.⁶⁸ With modern Raman instrumentation, the fundamental decision to use a FT spectrometer or a dispersive spectrometer becomes a choice of better fluorescence suppression or sensitivity, respectively.

Spectrometer Selection

Based on previous component selections, spectrometer options were reduced. To best accommodate previously described system criteria (e.g., low cost, portability, laser wavelength, etc.), a dispersive Raman spectrometer with a CCD detector was chosen.

With the general objective of the instrument in mind, the following observations were considered in the spectrometer selection process. The use of dispersive spectrometers has risen in popularity recently compared to FT-based spectrometers for NIR Raman analysis, particularly with biological samples. In the NIR region, FT-Raman

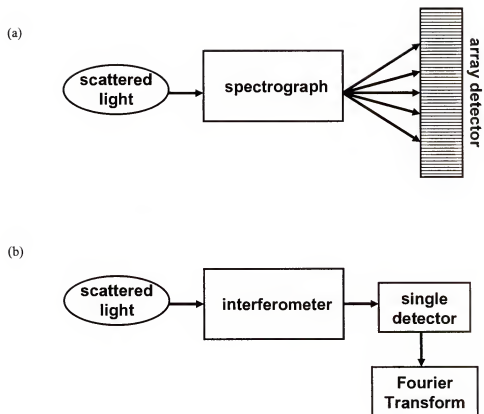


Figure 3-13. Block diagrams for general spectrometer types -- (a) multichannel; and (b) multiplex. Adapted from reference 4: McCreey, R.L. *Raman Spectroscopy for Chemical Analysis* in Chemical Analysis Series ed. by J.D. Winefordner, 157, John Wiley & Sons, Inc.: New York, 2000.

instruments usually produce a lower S/N due to reduced scattering ($1/\lambda^4$ dependence) of the sample and higher noise associated with NIR and IR detectors.^{6, 69} The multiplex advantage inherent with FT systems ceases to outweigh the aforementioned disadvantages within the NIR region for some sample analyses. At this point, there is a multiplex disadvantage meaning that S/N is adversely affected because each point in an interferogram is composed of signal from every wavelength.³⁹ Consequently, noise is spread over the entire spectrum. However, the multichannel approach measures the wavelengths simultaneously and reduces the total required acquisition time. The shorter analysis time decreases the possibility of conditions changing during an observation.⁴⁰ Additional advantages of a dispersive NIR Raman setup include: (1) the ability to use compact solid state semiconductor (diode) lasers for excitation; (2) optical fibers can be f-number matched with imaging spectrographs for better throughput; and (3) cooled CCD detectors can offer shot-noise limited detection in the NIR region.³⁷ The decision to use a CCD detector was made based upon instrumental constraints, availability, and current popularity. A compromise must be made between CCD detector performance and elimination of fluorescence spectral interference. Greater fluorescence signal suppression is evident at longer wavelengths; however, silicon-based CCD detector efficiency drops significantly with increasing wavelengths (see Figure 3-14). Excitation wavelengths in the 800 nm range are optimal for biological fluorescence minimization in conjunction with exploiting the advantages of CCD detector sensitivity.³⁷

The wide use of CCD detectors in spectroscopic applications began with their commercial availability in the early 1990s.⁴ Charge-coupled devices are based on

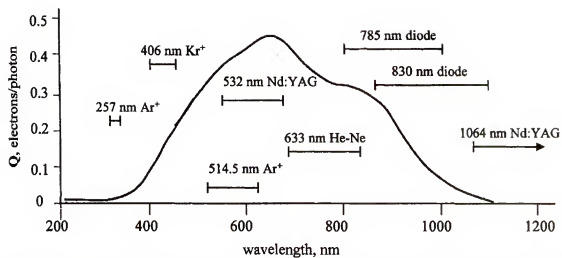


Figure 3-14. Typical efficiency curve for a front-illuminated silicon CCD detector with laser wavelengths superimposed.⁴

metal-oxide-semiconductor (MOS) technologies and have three primary functions: (1) photon collection and charge detection; (2) charge transfer; and (3) charge conversion.^{48,49} Essentially, x number of channels (i.e., pixels) containing individual photodiodes are positioned adjacent to one another. Photodetection occurs when a photon of sufficient energy generates an electron-hole pair in the photoactive material (most often silicon).^{4,50} The resulting photoelectrons are retained in potential wells which correspond to individual wavelengths. Charge accumulates until it is transferred to a shift register where it is read out and digitized for further processing by a computer.⁴⁹ The most commonly used CCD detector is a front-illuminated silicon CCD.

Spectrometer Specifications

The selected spectrometer was a thermoelectric temperature-regulated S2000 spectrometer from OceanOptics, Inc. (Dunedin, FL). The optical design is a crossed Czerny-Turner that has been reconfigured for a small optical bench footprint.⁷⁰ Refer to Table 3-4 for manufacturer specifications of the spectrometer unit. A few noteworthy components are addressed below.

The slit width of the spectrometer is fixed at 25 μm . The groove density of the grating is 1200 lines/mm with a blaze wavelength of 750 nm. The spectral range of the grating is approximately 250 nm, extending from 770 nm to 1030 nm (-160 cm^{-1} to 3050 cm^{-1} , centered at 785 nm). In Figure 3-15, the grating efficiency curve from the manufacturer is illustrated. As indicated in the table of specifications, a cylindrical lens is positioned after the grating. This lens focuses the dispersed light in the y-direction (vertically) before reaching the detector, designed to increase detector efficiency.

Table 3-4. Manufacturer specifications for temperature regulated S2000 spectrometer (OceanOptics, Inc.).⁷⁰

| | |
|---------------------------------------|--|
| <i>Physical Specifications</i> | |
| Overall Dimensions | 14 cm x 10 cm x 6 cm (LWH) |
| Fiber Optic Connector Type | SMA 905 to single strand with 0.22 NA |
| <i>Optics Specifications</i> | |
| Slit Width | 25 μm |
| Resolution | 0.3 – 10.0 nm |
| Focusing/Coupling Lens | cylindrical lens after grating |
| Grating Groove Density | 1200 lines/mm |
| Grating Spectral Range | 200 – 270 nm |
| Grating Blaze Wavelength | 750 nm |
| Grating Best Efficiency Range | 500 – 1100 nm |
| <i>Detector Specifications</i> | |
| Detector Type | linear silicon CCD array |
| CCD Elements | 2048 elements |
| CCD Element Dimensions | 12.5 μm x 200 μm (per element) |
| A/D Card | 1 MHz |
| Allowed Integration Time | 3 – 50 s |

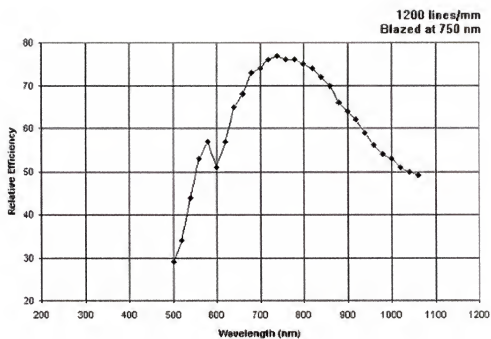


Figure 3-15. Spectrometer grating efficiency plot.⁷¹

The CCD detector used in the S2000 spectrometer is a front-illuminated silicon linear array consisting of 2048 pixels (Sony Electronics; San Jose, CA).⁷² It is temperature-controlled with a Peltier thermoelectric regulator which stabilizes to ± 0.1 °C. Temperature regulation is beneficial when a large amount of time between sample and reference measurements is present and when long integration times are employed. The latter applies to this research. The cooling element also aids in the reduction of baseline drift and dark noise.

Another specification to further mention is the 1 MHz analog-to-digital (A/D) card which provides integration times between 3 ms and 60 s. Such an integration window is not sufficient for a large portion of biological samples. This limitation was overcome by adding an electronic trigger box that delivered a 5 V signal, thereby increasing the integration window.

Experimental Characterization

Operating conditions

There are four main instrumental operating conditions that can be readily controlled in reference to the developed inexpensive Raman instrument. These are room light signal interference, diode laser operating current, diode laser operating temperature, and spectrometer operating temperature. Room light and spectrometer operating temperature are discussed below.

Suppression of stray light signals. Raman signal acquisition is quite sensitive to stray light. Figure 3-16 displays the emission spectrum of laboratory room light. Room light can cause spectral interference and mask smaller intensity peaks. A portion of the major Hg and Ar second order emission lines present in room light are displayed in the spectrum. To eliminate room light detection by the fiber optic probe, samples and the

probe head are placed in light-tight enclosures during the time of analysis. This was a successful approach and eliminated the need to acquire data in the dark.

Spectrometer operating temperature. The spectrometer operating temperature is another important parameter that can be experimentally controlled. Since the spectrometer is equipped with a Peltier thermoelectric regulator, thermal stability can be achieved (+/-0.1 °C over a range from 37 °C to 15 °C below ambient laboratory temperature). Generally, a CCD detector at lower temperatures will produce signals with reduced dark noise. Similar results were observed experimentally. The %RSD in pixel intensity across the spectrum decreased from 318% at 35.3°C to 29% at 11.0°C as shown in Figure 3-17. (RSD was calculated using pixel intensity average as signal and the standard deviation of the pixel average as noise.) Since the low temperature benefit appeared to plateau, 13.1°C was chosen as the nominal operating temperature. Over the same temperature range, dark spectra were acquired at 13 different temperature settings. The average counts (20 spectra) decreased with a decrease in temperature, as shown in Figure 3-18.

Spectrometer optical resolution

The optical resolution of a spectrometer is dictated by the grating groove density and the spectrometer slit width. The slit width-limited resolution, is given by twice the product of the reciprocal linear dispersion, R_d , and slit width, W , of the spectrometer:³⁹

$$\Delta\lambda_s = 2R_dW \quad (3-1)$$

The value for R_d is obtained from the inverse of the spectrometer linear dispersion, D_l . This variable defines the separation distance between two wavelengths in a focal plane.³⁹ The optical resolution calculation for the S2000 spectrometer is shown in the steps

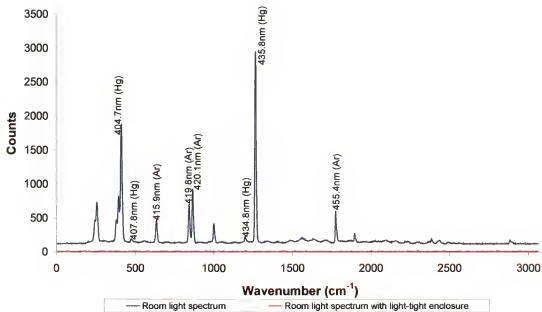


Figure 3-16. Room light emission spectrum with 2nd order Hg and Ar line assignments.

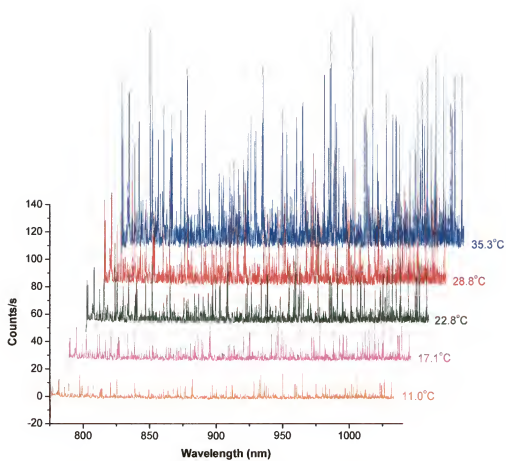


Figure 3-17. Effect of spectrometer operating temperature on dark spectra.

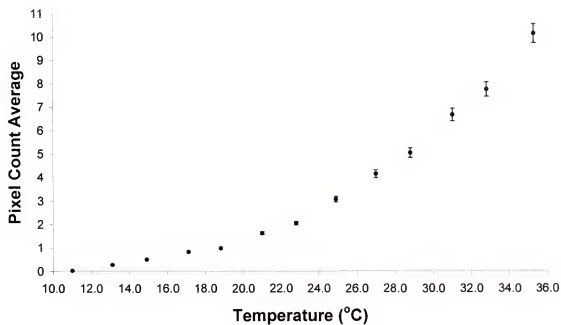


Figure 3-18. Dark count dependence on spectrometer operating temperature. Error bars indicate \pm average standard deviation for 5 replicates.

below. To calculate R_d , the following relationship is used:

$$R_d = \frac{1}{D_i} = \frac{\text{grating spectral range}}{\text{total number of pixels}} = \frac{260 \text{ nm}}{2048 \text{ pixels}} = 0.127 \frac{\text{nm}}{\text{pixel}} \quad (3-2)$$

More commonly, the units are expressed in nm/ μm and is converted by using the width of an individual pixel (14 μm):

$$R_d = \left(0.127 \frac{\text{nm}}{\text{pixel}} \right) \left(\frac{1 \text{ pixel}}{14 \mu\text{m}} \right) = 9.07 \times 10^{-3} \frac{\text{nm}}{\mu\text{m}} \quad (3-3)$$

Employing Equation (3-1), the optical resolution is calculated as

$$\Delta\lambda_s = 2R_d W = (2) \left(9.07 \times 10^{-3} \frac{\text{nm}}{\mu\text{m}} \right) (25 \mu\text{m}) = 0.4_s \text{ nm} . \quad (3-4)$$

Spectrometer response

The response of a spectrometer is not uniform across the analyzed spectral range; therefore, it is important to consider the spectrometer response when characterizing a system. This response provides insight about which wavelengths are favored in reference to sensitivity and if distant peaks can be accurately compared with peak intensities. The spectrometer response is profiled in a plot of measured counts/actual counts *versus* wavelength (or wavenumber) and is displayed in Figure 3-19. The response was a ratio of the experimental spectrometer detector counts from a calibrated W source to the certified calibration values ($\mu\text{W}/\text{cm}^2/\text{nm}$) for wavelengths from 800 nm to 1000 nm in 50 nm increments. The response of the spectrometer decreases with a shift further into the red region of the electromagnetic spectrum. Based on these findings, signals will be smaller in the longer wavelength region of the analysis window for the same number of incident photons compared to signals in the shorter wavelength area of the spectrometer analysis window. Additional aspects of the spectrometer will be

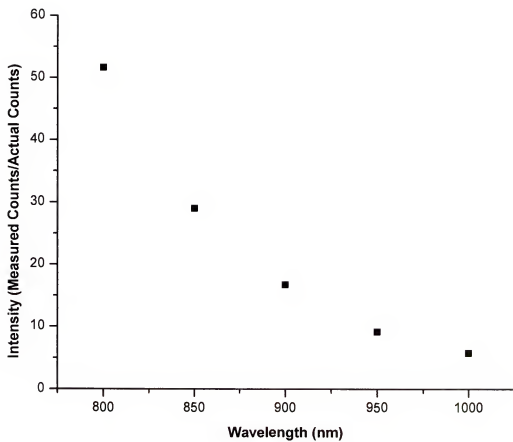


Figure 3-19. Experimentally determined spectrometer response.

discussed in Chapter 4.

Computer and Data Collection Software

Background

The primary functions of a computer and associated software with a Raman spectroscopic instrument include instrument control, in addition to, spectral data collection, preprocessing, and analysis.

Computer and Data Collection Software Specifications

The S2000 spectrometer was interfaced with a desktop personal computer (Dell; Round Rock, TX) employing a Windows 2000 (Microsoft; Redding, WA) operating system. OOIBase32 (OceanOptics, Inc.; Dunedin, FL) is a versatile spectrometer-controlling software package that allows one to monitor up to eight channels simultaneously, run in a mode that automatically subtracts a stored dark spectrum, and conduct time acquisition experiments. The integration time, number of spectral averages, and boxcar statistical treatment for smoothing are all options for spectra acquisition that can be set by the researcher. For the purposes of this work, most of the software features were not regularly used excluding integration time, dark spectrum storage and subtraction, and time acquisition experiments.

As mentioned previously, an electronic trigger box was incorporated in the setup to extend integration times (>50 s). The OOIBase32 software was operated in the synchronous trigger mode which permitted an external logic level to dictate the beginning and end of signal collection at the spectrometer.

A number of programs were employed for data manipulation and analysis. They include the following: Excel XP (Microsoft; Redding, WA), Origin 6.0 (OriginLab

Corporation; Northampton, MA), Visual Basic 6.0 (Microsoft; Redding, WA), and MATLAB 6 (The MathWorks, Inc.; Natick, MA).

Experimental Characterization

The analysis of solids and solvents that are good scatterers allow selection of integration times that are often less than 50 s. However some target samples in this research, such as plastics and biological samples, require longer integrations times for adequate detectable signal. There are limitations with the OOIBase32 operating software as well as the A/D converter that restrict integration times longer than 50 s in normal operating mode. In order to address this, two courses of action were evaluated.

The first method used a summation of lower integration time spectra, thus theoretically obtaining (*via* mathematical means) a spectrum with signal comparable to that of a longer integration time. To test if this was a valid assumption with the inexpensive Raman system, 10 spectra of CCl_4 with a 1 s integration time were acquired, summed, and compared to a spectrum of CCl_4 with a 10 s integration time. Figure 3-20 displays the resultant spectra. S/N ratios were evaluated and the addition of the spectra resulted in a significant drop in S/N. A more detailed discussion of system noise will be addressed in Chapter 4.

The second option was the addition of a trigger box that sends a 5 V pulse indicating the start and end of an acquisition. With this addition, the integration time is theoretically unlimited. However, the practical integration time limit is a function of system noise and saturation capacity of the detector. Lower integration time spectra taken in the normal mode and acquired in the synchronous mode (trigger box) are comparable. Hence, application of the trigger box to achieve longer integration times is deemed sufficient.

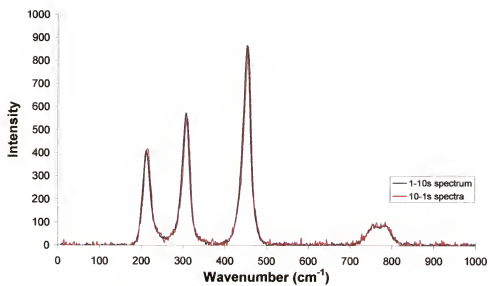


Figure 3-20. Evaluation of spectral addition.

Concluding Remarks

In this phase of research, a low-end Raman spectroscopic system was compiled from a number of commercial components. There was a desire to produce an instrument that is low-cost, potentially portable, and meets the needs for a variety of applications. The main constituents of the instrument include a 785 nm diode laser, filtered integrated fiber optic probe, and a dispersive grating spectrometer with CCD detector. A cost analysis is shown in Table 3-5 and indicates the total expense at approximately \$14,500. A typical commercial Raman instrument ranges from \$60,000 to \$150,000+. With a cut in price, component quality is often sacrificed and the challenge becomes acquiring spectra that are adequate for identification purposes. The next chapter continues to characterize and optimize the system by considering various aspects of performance.

Table 3-5. Instrument cost analysis (after market).

| | |
|-------------------|------------------|
| Diode Laser | \$ 2,000 |
| Fiber Optic Probe | \$ 5,000 |
| Spectrometer | \$ 3,500 |
| TEC | \$ 1,000 |
| Power Supply | \$ 1,000 |
| Computer | \$ 1,000 |
| Miscellaneous | \$ 1,000 |
| Total | \$ 14,500 |

CHAPTER 4 PERFORMANCE OF LOW-END RAMAN SPECTROSCOPIC SYSTEM

Introduction

In the quest to better understand the system for optimization purposes, various aspects of instrument performance were investigated. These studies encompassed a wide range of factors. The first main section contains information on peak intensities, typical system spectra, and limits of detection. A number of detailed noise considerations are presented in the consequent main section.

Signal and Performance Considerations

Raman spectra are a function of analyte and background signals. The analyte signal is a result of the inelastic scatter of photons by the analyte. Background signals form the continuum background present in spectra and have elements of fluorescence bands, detector dark noise, fixed pattern noise, and Rayleigh scatter. Under ideal conditions, the background is suppressed while the analyte signal is maximized. Comparison of theoretical and experimental peak intensities, spectra and S/N values for various compounds, and limits of detection were studied and presented below.

Peak Intensity Theoretical Calculation

Beginning stages of system evaluation involved theoretical signal intensity calculations based on the parameters of the spectroscopic system. Such an approach provided a better understanding of the losses in the system and aided in optimization. CCl_4 was chosen as the analyte for these calculations due to characteristic strong Raman bands. Since Raman spectroscopy has only relatively recently experienced a resurgence

in interest and applicability, many aspects have yet to be standardized. This coupled with the fact that Raman system components vary greatly, there is no universal equation with defined terms for theoretical signal intensity computations. The following relationship was used to determine the theoretical peak intensity (counts s^{-1}):

$$I = n_{sc} \sigma \Omega l PF T EQ \quad (4-1)$$

where, n_{sc} is the number density of scatterers (cm^{-3})

σ accounts for the cross section of scatterer ($cm^2 sr^{-1}$)

Ω is the solid angle of collection (sr)

l is the path length (cm)

PF is the source photon flux (photons s^{-1})

T is the transmittance from sample to spectrometer (dimensionless)

EQ is the efficiency of the spectrometer and quantum efficiency of detector (counts $photon^{-1}$)

Conditions mimicking experimental ones were utilized – 785 nm excitation wavelength and 22 mW laser power. This enabled a direct comparison between CCl_4 calculated and experimental intensity values. The following sub-sections cover the various elements of Equation (4-1).

Number density

The number density of scatterers, n_{sc} , describes the number of analyte molecules in a given volume. It is expressed as:

$$n_{sc} = \frac{\rho_{CCl_4}}{MW_{CCl_4}} N_A \quad (4-2)$$

where, ρ_{CCl_4} is the density of CCl_4 ($g cm^{-3}$)

MW_{CCl_4} is the molecular weight of CCl_4 (g mol^{-1})

N_A is Avogadro's number ($\text{molecules mol}^{-1}$)

The number density was calculated as $6.61 \times 10^{21} \text{ molecules cm}^{-3}$.

Scatterer cross section

Cross sections are areas of probability for photon and analyte interaction. Larger values indicate a greater potential for interaction. Raman cross sections are typically small, ranging from 10^{-29} to $10^{-32} \text{ cm}^2 \text{ sr}^{-1}$, and are wavelength dependent. An experimentally determined cross section value for CCl_4 at 283 nm was reported as $1.7 \times 10^{-29} \text{ (cm}^2 \text{ sr}^{-1})$.⁷³ Taking into account a $1/\lambda^4$ dependence, the CCl_4 cross section for 785 nm is scaled by the expression:

$$\sigma_{785} = \frac{\sigma_{283} (283)^4}{(785)^4} \quad (4-3)$$

where, σ_{283} and σ_{785} are cross sections at wavelengths 283 nm and 785 nm, respectively.

The cross section used in the theoretical intensity calculation was $2.87 \times 10^{-31} \text{ cm}^2 \text{ sr}^{-1}$.

Solid angle

Calculations of the solid angle are related to the fiber optic probe lens radius and focal length, which can be accounted for in the variable θ (see section "Limit of Detection"). The angle of collection, Ω , is given by:

$$\Omega = \frac{1}{1 + \frac{1}{\tan^2 \theta}} \quad (4-4)$$

The solid angle for the low-end spectroscopic system was determined to be 0.48 sr.

Path length

The distance over which the radiation interacts with an analyte is the path length, l . Sample depth of the fiber optic probe is 1 mm and the sample cuvette is 1 cm in width. Since CCl_4 is a highly efficient Raman scatterer and a colorless liquid, the width of the cuvette was used as the path length. If the path length was limited by probe depth, then the numerical aperture and operating focal distance would need to be considered.

Photon flux

The average flow of electrons generated by photons reaching the detector constitutes photon flux, PF .^{32,36} It is calculated using:

$$PF = \frac{E\lambda}{hc} \quad (4-5)$$

where, E is the excitation laser energy (W)

λ is the excitation wavelength (cm)

h is Planck's constant (J s)

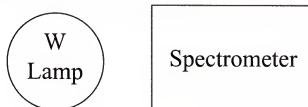
c is the speed of light (cm s^{-1})

The photon flux for the inexpensive Raman instrument was 8.69×10^{16} photons s^{-1} .

Transmittance

The transmission of light from sample to spectrometer is an important parameter. Determination of this value was facilitated by a plot of transmittance as a function of wavelength. Figure 4-1 shows an experimental schematic diagram and Figure 4-2 displays a corresponding plot. Using a tungsten (W) lamp, response curves were obtained for direct incident radiation and radiation delivered by the fiber optic probe. Over a large wavelength range, the transmission was approximately 0.9, thus this was the value chosen for T .

I_0 Data:



I Data:

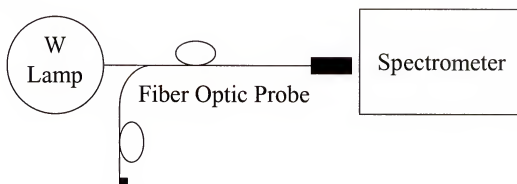


Figure 4-1. Experiment set-up for light transmission study ($T = I/I_0$) through the probe head.

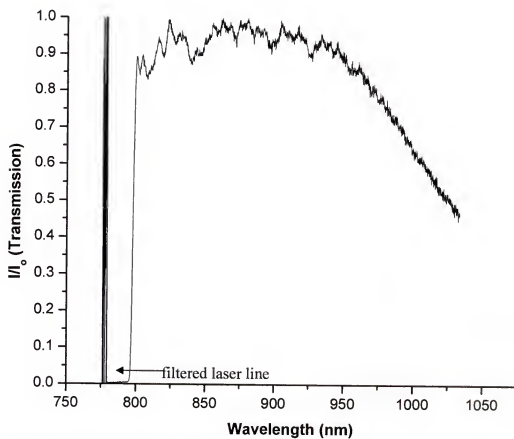


Figure 4-2. Transmission from sample to spectrometer.

Efficiencies

The efficiency of spectrometer and quantum efficiency of detector are key factors in signal intensity and are accounted for in the EQ term of Equation (4-1). To experimentally determine this value, a series of neutral density filters were employed as described in Sommer *et al.* and shown in Figure 4-3.⁷⁴ A plot of counts output (counts s⁻¹) versus count rate (photons s⁻¹) was constructed and the slope of the data was calculated. This slope served as the EQ term in counts/photon and is shown in Figure 4-4. The x-values, count rate, were calculated by the following equation:

$$\text{Photon Count Rate} = \frac{P_{\text{laser}}}{h\nu} T \quad (4-6)$$

where, P_{laser} is the laser power (W)

h is Planck's constant (J s)

ν is laser frequency (s⁻¹)

T is transmission of neutral density filter (dimensionless)

For the y-axis, all spectral data were normalized to 1 s integration time. For each neutral density filter, the data (counts) associated with 785 nm (5 pixels) were averaged and this value served as the counts output. The slope for the data was 2×10^{-7} counts photon⁻¹. A confirmation of this experimental value was provided by a plot of photons count⁻¹ versus wavelength employing a calibrated W lamp source. A 2-term polynomial function was fit to the data points ($R^2 = 0.9992$) and the photons count⁻¹ for 785 nm were calculated from the resultant binomial equation, as shown in Figure 4-5. Based upon an extrapolation, the EQ term should be approximately 5.8×10^{-7} counts photon⁻¹ which is close to the previously determined value of 2×10^{-7} counts photon⁻¹. The EQ term accounts for grating efficiency, reflectivity of the CCD surface, and quantum efficiency

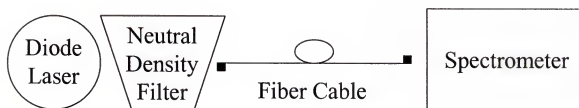


Figure 4-3. Experimental design for EQ term.

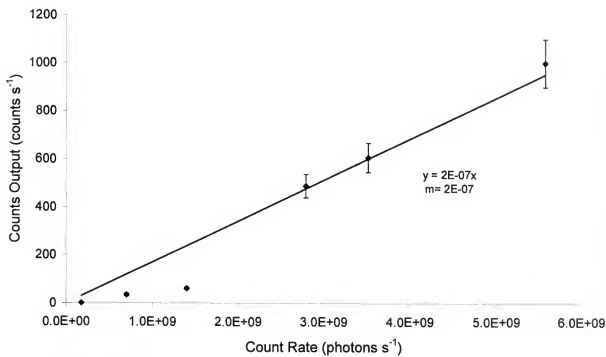


Figure 4-4. Experimental determination of EQ term. Error bars indicate \pm average standard deviation for 3 replicates.

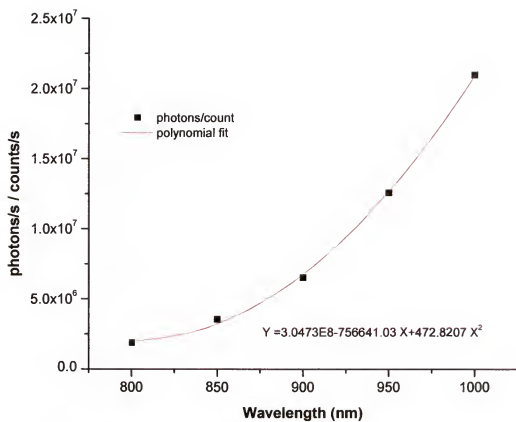


Figure 4-5. Photons/count for signal over spectrometer range.

of the detector.

Calculation results

When the theoretical intensity of Raman scattering for CCl_4 is calculated using Equation (4-1), an approximate value of 14.4 counts s^{-1} is obtained. Experimentally, the intensity is approximately 100 counts s^{-1} , demonstrating that the experimental findings are within an order of magnitude when compared to the theoretical value. Discrepancy could potentially be attributed to the calculation of the scatterer Raman cross section. For this computation, a classical $\bar{\nu}^4$ dependence was used. This general dependence was derived from the treatment of scattering as an oscillating induced dipole with intensity expressed in watts.⁴ However, modern Raman spectrometers are based on photon counting which leads to a somewhat different dependence. This dependence is best considered by means of quantum mechanics which treats cross sections as probability statements.⁴⁸ The result is that the Raman intensity scales with $\bar{\nu}_0(\bar{\nu}_0 - \bar{\nu}_j)^3$ rather than $(\bar{\nu}_0 - \bar{\nu}_j)^4$.⁴ Nevertheless, the peak intensity calculation was a good reference for assessment of achievable signal.

Spectra and S/N Values

A number of solvent spectra were obtained with the inexpensive instrument as part of system characterization. These solvents included chloroform, toluene, acetonitrile, acetone, methanol, ethanol, and 2-propanol. A solid sample, calcite, was also interrogated. For all analytes, characteristic peaks were well-defined and produced shifts corresponding to those in literature.⁷⁵ Raman spectra of chloroform, toluene, and calcite are presented in Figure 4-6. It is important to note that variations in the diode laser manufacturing and its operating conditions led to changes in the excitation wavelength by

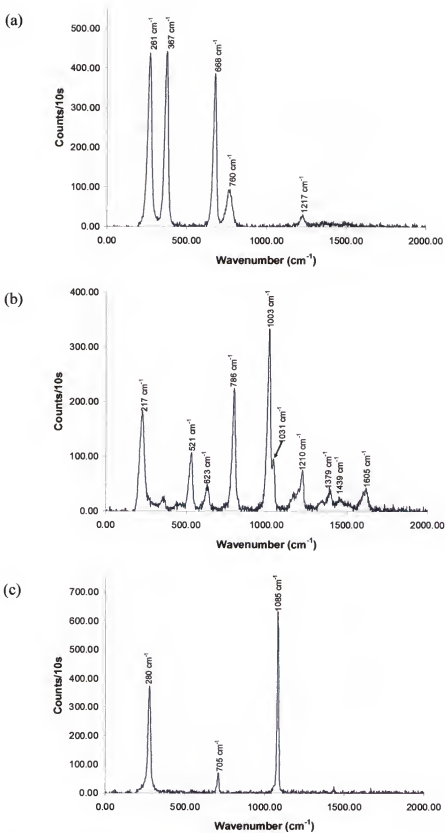


Figure 4-6. Typical Raman spectra acquired with low-end instrument: (a) chloroform; (b) toluene; (c) calcite.

as much as ± 10 nm and needs to be accounted for in wavenumber assignments.

For the purposes of S/N considerations, the signal was defined as the average peak intensity value and noise as the standard deviation of the peak intensity.⁴ Representative S/N values were: 90 for carbon tetrachloride; 62 for chloroform; 48 for toluene; and 89 for calcite. No significant improvement in S/N was observed with an increased number of averaged acquisitions. A more detailed discussion of signal and noise relationships for the low-end system is provided later.

Limit of Detection (LOD)

Determination of detection limits is a fundamental aspect in instrument assessment. For the low-end Raman spectroscopic system, both relative and absolute LODs were calculated. A methanol/ethanol solvent mixture was used to construct a calibration curve and to determine the calibration sensitivity. Figure 4-7 shows overlapping solvent spectra. The dominant methanol and ethanol peaks at 1036 cm^{-1} and 883 cm^{-1} , respectively, were monitored for calibration studies. The resulting calibration curve in terms of signal intensity and molarity is provided in Figure 4-8. A slope of 5.3 counts/molarity was associated with the solvent mixture, which is the calibration sensitivity (m).

The standard definition of LOD was employed for relative computations:

$$LOD = \frac{3\sigma_{bk}}{m} \quad (4-7)$$

where, σ_{bk} is the blank noise (counts)

m is calibration sensitivity or slope of calibration curve (counts/molarity)

Based on the evaluation of 50 blank spectra, the σ_{bk} value was determined to be 0.31 counts. Using Equation (4-7), the concentration LOD is 0.18 M. However, this value is

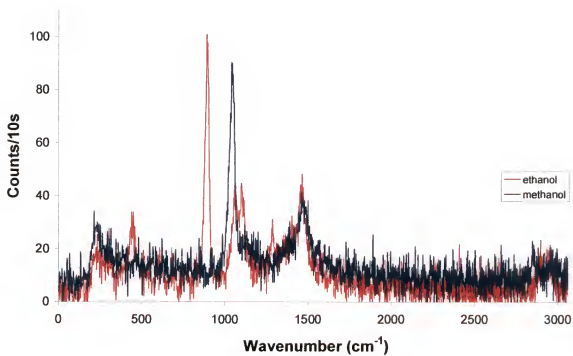


Figure 4-7. Superimposed methanol and ethanol Raman spectra.

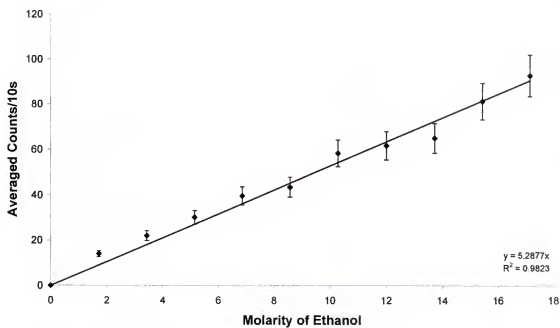


Figure 4-8. Calibration curve with methanol/ethanol solvent mixtures. Error bars indicate \pm average standard deviation for 3 replicates.

indicative of the methanol/ethanol samples and cannot be applied universally.

To calculate an absolute LOD that is solvent system independent, Avogadro's number and the volume probed by the interrogating laser radiation need to be considered. A number of the probe's external focusing lens characteristics (e.g., F/n , numerical aperture, and operating range) are accounted for in the volume calculation. The probed volume, V_{probe} , was assumed to be cylindrical in shape as demonstrated in Figure 4-9a. A basic relationship between the laser spot size and operating distance was employed in volume computations:

$$V_{probe} = \pi r^2 l \quad (4-9)$$

where, r is the laser spot radius

l is operating distance of the focusing lens

The cone of light accepted by the collection fiber is the numerical aperture (NA) which is integral in determining operating distance. A standard equation for NA is given by:

$$NA = \frac{\eta \cos \theta_0}{2 F/n} \quad (4-10)$$

where, η is the index of refraction for silica fiber

θ_0 is the focal point angle

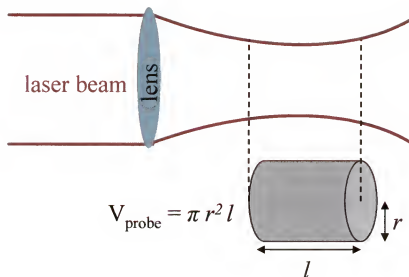
F/n is the F-number of the lens

The F-number is determined by:

$$F/n = \frac{b}{2a} \tan \theta_0 \quad (4-11)$$

where a and b are triangle side lengths as defined in Figure 4-9b. F/n for the lens is 0.5 and the NA is 1.1. This NA value is similar to a good microscope objective with a tight

(a)



(b)

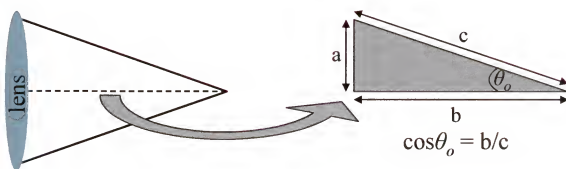


Figure 4-9. Illustration of: (a) cylindrical probed volume; (b) geometric features of light cone.

focus. Based on the *Handbook of Optics*, a typical operating range for such lenses is 0.01 cm.⁷⁶ Applying this value for l and 5.4×10^{-4} cm for r in Equation (4-9), the probe volume is 9.2×10^{-7} ml.

The general relationship for absolute LOD calculations is:

$$LOD_{absolute} = (LOD)(V_{probe})(N_a) \quad (4-12)$$

Normal Raman scattering with the inexpensive instrument produces an absolute LOD of 1.0×10^{14} molecules. Neither the relative nor absolute detection limits are stellar; however, this is to be expected due to poor optical throughput and low detector quantum efficiency. One method to lower detection limits is to utilize signal enhancement techniques. The application of surface-enhanced Raman scattering is discussed in Chapter 6.

Noise Considerations

A number of experimental observations prompted a more detailed deliberation of system noises. For example it was noted, in the section entitled "Spectra and S/N Values," that no S/N improvement resulted from an increase in spectral acquisitions. Furthermore, in Chapter 3, the addition of spectra was shown to significantly decrease S/N. Insight for these situations can be gained by further system characterizations; a better understanding of the dominating noise sources aids in instrumental optimization and data treatment.

Fixed Pattern Noise (FPN)

When a plot of dark counts versus acquisition number was considered, the average count and standard deviation values remained the same. Visual comparison of dark spectra acquired at identical integration times supported this finding. Figure 4-10 shows

two dark spectra acquired with a 10 s integration time. The overlay of these two spectra demonstrates that they are nearly identical, which opposes the characteristic randomness of noise. If the difference of two dark spectra are plotted and compared with another difference spectrum, then randomness is observed with the overlay (see Figure 4-11). The portion of the dark spectrum that was removed by subtraction is fixed pattern noise (FPN). FPN is an artifact of the CCD detector and is a function of individual pixel sensitivities. When an uniform number of photons strike different pixels on an array, identical signal intensities should theoretically be produced. However, the response of each pixel varies leading to a fixed ratio. A descriptive cartoon is presented in Figure 4-12.

FPN can often dominate spectra acquired with lesser quality (i.e., inexpensive) detectors. To determine the integration times that are FPN dominated, a series of dark spectra at various integration times ranging from 0.5 s to 120 s were obtained. Spectra of similar integration times were correlated and the coefficients were plotted as a function of integration time. The resulting plot is shown in Figures 4-13. With correlation values approaching 1, it is concluded that FPN begins to dominate spectra between 3 s and 5 s. (Refer to Chapter 5 for a discussion on correlation methods.)

Fixed pattern noise can dominate and effectively mask the random error of a system; however, FPN is linear with integration time and can be corrected for in spectra. Removal methods for FPN reported in the literature consist of master dark subtraction and signal regulation by electronic circuitry.^{74,77} For the purposes of this research, a mathematical treatment was preferred to retain design simplicity and low cost. In the master dark subtraction method, the difference between an analyte spectrum of interest

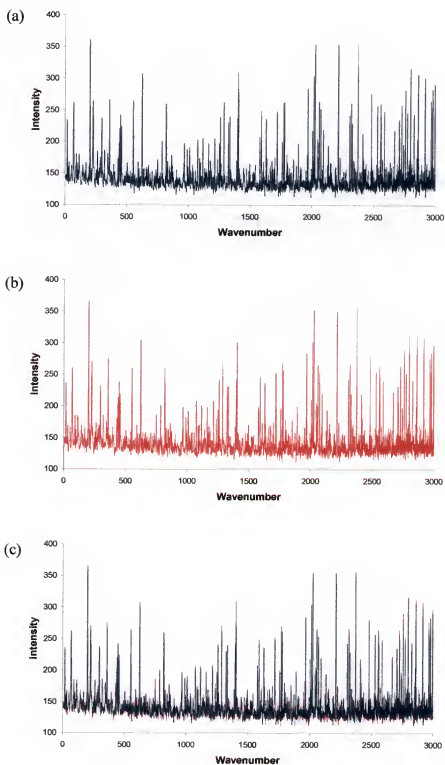


Figure 4-10. Visualization of FPN: (a) and (b) dark spectra acquired with similar experimental conditions; (c) dark spectra superimposed.

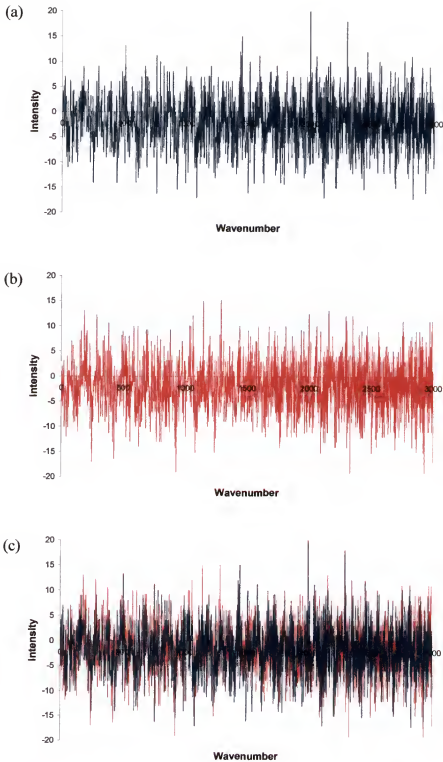


Figure 4-11. Visualization of dark spectra without FPN: (a) and (b) dark difference spectra acquired with similar experimental conditions; (c) dark difference spectra superimposed.

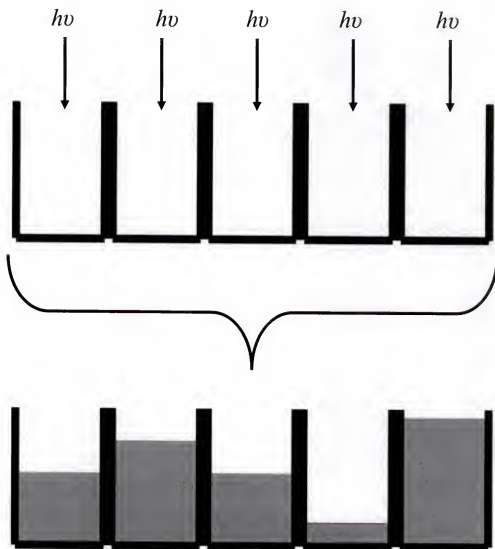


Figure 4-12. Illustration of FPN. Each pixel in an array has a unique sensitivity. Therefore, when an equal number of photons strike, each pixel produces a different signal.

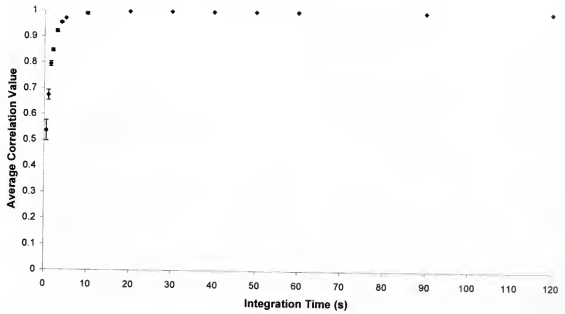


Figure 4-13. Correlation of dark spectra (with FPN) as a function of integration time. Error bars indicate \pm average standard deviation for 5 replicates.

and the master FPN spectrum is obtained. The latter is an average of 100 dark spectra. This approach is not feasible for simple and routine analyses with the low-end system because (1) master dark spectra creation is time consuming; (2) updated master spectra should be made frequently during data acquisition; and (3) master spectra are not independent of integration time.

A straightforward 1-to-1 subtraction method was evaluated for FPN removal. This scheme was facilitated by the OOIBase32 operating software – a dark spectrum was stored and automatically subtracted from subsequent analyte spectra. Figure 4-14 demonstrates this with a series of averaged acrylic spectra. As the integration time increased, the effectiveness of 1-to-1 subtraction decreased. Adverse effects (e.g., difference spikes) were observed at integration times as early as 50 s for some samples.

Most samples would require minute integration times with the low-end system; thus, an alternative FPN removal method was devised. The general approach entailed scaling a fixed ratio to an analyte spectrum and afterwards removing the FPN contribution. This fixed ratio is characteristic of the individual pixel sensitivities, making the ratio unique to the detector. The developed FPN removal algorithm is detailed in Figure 4-15. Proof-of-concept evaluation was based on spectral comparison and is shown in Figure 4-16. CCl₄ at 10 s was chosen for the analysis foundation because 1-to-1 subtraction is adequate. The two methods, 1-to-1 subtraction and FPN removal

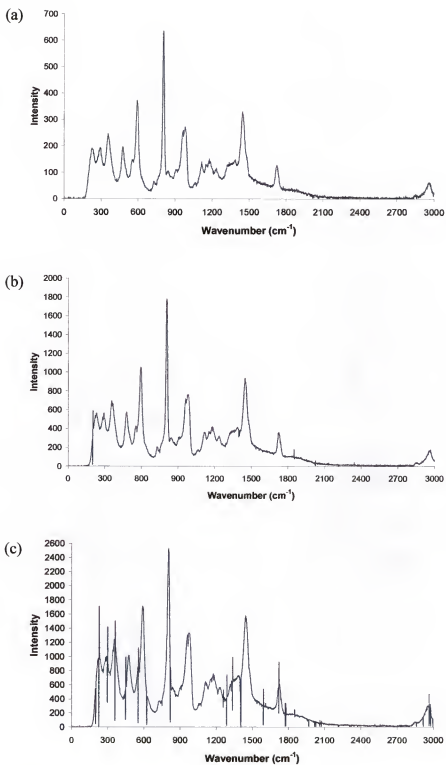


Figure 4-14. Acrylic Raman spectra with 1-to-1 subtraction: (a) 1 min integration; (b) 3 min integration; (c) 5 min integration.

Using an averaged dark spectrum:

- ➡ Select a reference pixel with intensity x (x_{ref})
- ➡ Produce a list of ratios indicative of FPN contribution (χ_i)

$$\chi_{i \text{ (i: 1? 2048)}} = \frac{\text{data } x_i}{\text{data } x_{ref}}$$

Using an analyte spectrum:

- ➡ Select pixel which corresponds to x_{ref} (y_{ref})
- ➡ Scale FPN ratios to analyte spectrum of interest (α_i)
This new set of numbers represents the amount to be deducted from analyte spectrum and is considered the FPN contribution.

$$\text{data } y_{ref} * \chi_{i \text{ (i: 1? 2048)}} = \alpha_i$$

- ➡ Corrected analyte spectrum intensities (ϕ_i)

$$\text{data } y_i - \alpha_i = \phi_i$$
- ➡ Plot ϕ_i vs. wavenumber to obtain a "FPN suppressed" analyte spectrum

Figure 4-15. FPN removal algorithm.

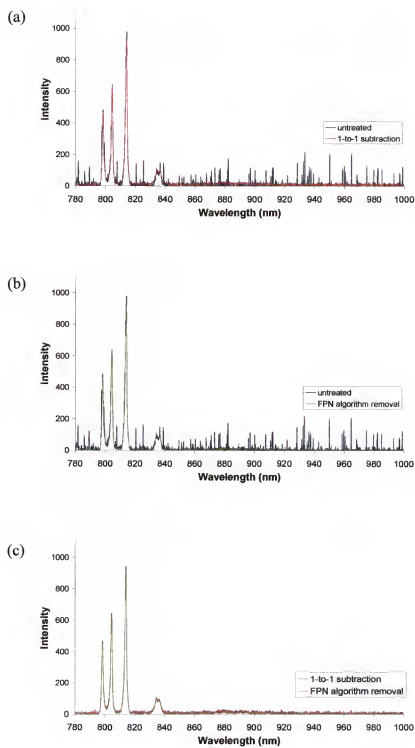


Figure 4-16. Spectral comparison of two FPN removal methods for CCl_4 .

algorithm, produced comparable spectra. Several reference pixels were assessed. It is important to note that reference selection is not trivial; it is paramount that a pixel is chosen which contains no other noise signals than FPN. Figure 4-17 displays an algorithm corrected spectrum of polyethylene terephthalate (PET). Advantages of FPN removal algorithm method include: (1) no integration time dependence; (2) ratios only need updating when the spectrometer is recalibrated; and (3) large potential for computer automation leading to operation simplicity.

Limiting Noise Source

Since FPN is a detector artifact and not a true noise, it cannot be classified as the limiting noise source for the low-end instrument. However, the identification and removal of FPN allows further noise characterization studies. Simultaneous monitoring of pixels corresponding to dark, background, and primary CCl_4 peak intensities afforded the opportunity to investigate instrument behavior as a function of time (see Figure 4-18). It appeared that the solvent peak pixels demonstrated the largest amount of fluctuation. As relative peak intensities increased, there was an increase in fluctuation magnitude indicated by signal noise, σ_s : peak1 (0.98 counts) < peak 2 (1.3 counts) < peak 3 (3.4 counts). This pattern was the initial indication that the system was limited by signal flicker noise. A series of other studies were conducted to confidently determine the limiting noise source.

Assuming all noises are independent of each other, a general noise expression is given by:

$$\sigma_{total} = \sqrt{\sigma_{s_s}^2 + \sigma_{s_f}^2 + \sigma_{B_s}^2 + \sigma_{B_f}^2 + \sigma_{det}^2} \quad (4-13)$$

where, σ_{s_s} is analyte signal shot noise (counts)

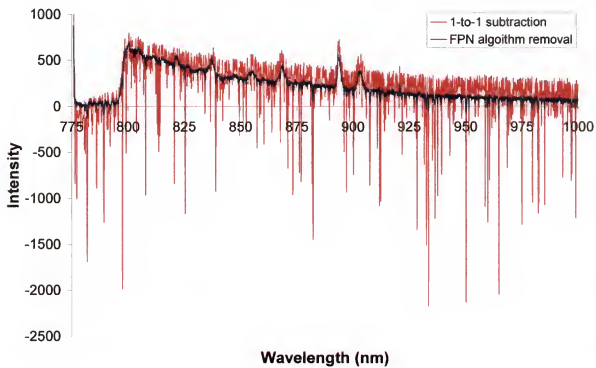


Figure 4-17. Spectral comparison of two FPN removal methods for PET.

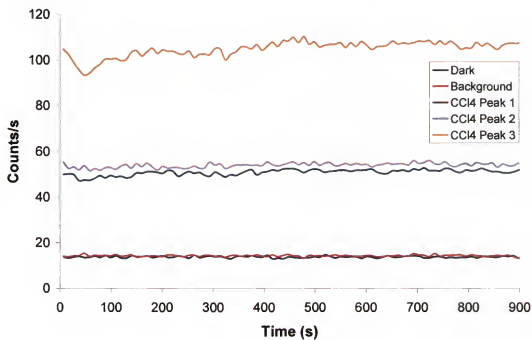


Figure 4-18. Signal as a function of time for dark, background, and CCl_4 primary peaks.

σ_{S_f} is analyte signal flicker noise (counts)

σ_{B_s} is background signal shot noise (counts)

σ_{B_f} is background flicker noise (counts)

σ_{det} is detector dark and readout noise (counts)

Based on Equation (4-13), there are five potential noise limiting cases. In the following sub-sections, each will be considered with respect to the inexpensive Raman instrument.

Signal and background shot noise

Scattered photons arrive at the spectrometer in a random fashion. The average and standard deviation values resulting from the counting of these photons is governed by the Poisson probability distribution function.³⁹ Poisson statistics provides the mathematical basis for shot noise. When any random event is counted, the standard deviation equals the square root of the number of events counted.⁴ Signal shot noise is expressed as:

$$\sigma_{S_s} = \sqrt{S} \quad (4-14)$$

where S is analyte signal (counts).

Background signal consists of all detected photons from radiation/sample interaction other than analyte Raman photons of interest. Fluorescence, stray light, and Rayleigh scatter contribute to background signal. As with signal shot noise, background shot noise is fundamental and follows a Poisson distribution. The expression is similar to Equation (4-14) and is given by:

$$\sigma_{B_s} = \sqrt{B} \quad (4-15)$$

where B is background signal (counts).

The shot noise limit is an inherent limitation of spectroscopy. If the system is shot noise limited, increasing the number of acquisitions will improve S/N with square root dependence. Important to note, even with a “perfect” spectrometer, shot noise cannot be completely eliminated since it is a fundamental noise.³⁸

Signal and background flicker noise

Often signal and background fluctuations exceed shot noise level. This excess is a nonfundamental noise, known as flicker or 1/f noise. It is characterized by a magnitude that is inversely proportional to the observed signal frequency.⁴⁰ The prime source of flicker noise in Raman spectroscopy is source intensity fluctuations. Changes in the laser output results in proportional variations in Raman scattering and the measured signal.⁴ Source fluctuations can cause both analyte signal and background flicker noise. Signal flicker noise is denoted as:

$$\sigma_{s_f} = \xi S \quad (4-16)$$

and background flicker is expressed by:

$$\sigma_{B_f} = \chi B \quad (4-17)$$

where ξ and χ are flicker factors for analyte signal and background, respectively.

Signal and background flicker factors can be equivalent or different depending upon the flicker origination; thus, separate symbols are often employed. Unlike shot noise, flicker noise can be completely eliminated from a system. Additionally, S/N is not affected by increasing number of acquisitions nor integration time.

Detector noise

For the purposes of this discussion, general detector noise is the combination of detector dark noise, σ_{dk} , and readout noise, σ_r . The latter is the standard deviation

resulting from conversion of stored electrons to current. This transition is controlled by an analog-to-digital converter. Dark noise accounts for the random generation of electrons, which are chiefly a product of thermal generation.³⁹ Thus, dark noise is strongly temperature dependent. Refer to Figures 3-17 and 3-18 for the system's dark count dependence on spectrometer operating temperature.

Detector noise behaves in a random manner; therefore, it is treated as a type of shot noise and expressed in term of a Poisson relationship:

$$\sigma_{\text{det}} = \sqrt{\sigma_{\text{dk}}^2 + \sigma_r^2} \quad (4-16)$$

where σ_{dk} , is often defined as the product of electron generation rate, ϕ_{dk} , and integration time, t .⁴⁸ General detector noise is demarcated from background noise by means of source intensity dependence. The background signal depends on laser intensity, but the detector signal does not.

Limiting noise source determination

A number of approaches can be taken to experimentally determine the limiting noise source. Several methods were used in this research for final conclusion validation. The principal goal was to determine if the low-end system was limited by shot or flicker noise. Demarcation characteristics of these noise types were drawn upon for the system analysis (i.e., S/N values can be improved by increasing the number of spectral averages and integration time). CCl_4 was used for the limiting noise source studies.

When S/N values were evaluated as a function of acquisition number, no significant improvement was observed. As shown in Figure 4-19, the quantities remain statistically similar. Without an improvement proportional to the square root of acquisition number, shot noise cannot be the limiting source indicated in this study.

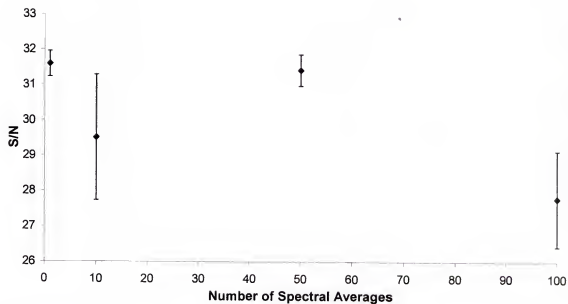


Figure 4-19. S/N values as a function of acquisition number. Error bars indicate \pm average standard deviation for 3 replicates.

At a given integration time, the relationship between different spectral peaks and their associated RSD values provides dominant noise information. For each of the three CCl_4 peaks, RSDs were calculated and compared. It was found that equivalent values were produced. Since flicker noise is proportional to signal intensity, it is expected that the ratios are constant. In this case, the RSD value is directly related to the flicker factor:

$$RSD_{s_f} = \frac{\xi S}{S} = \xi \quad (4-17)$$

This is likewise applicable to background flicker noise.

The Raman signal is linear with integration time. In a plot of intensity versus integration time, an expected linear pattern is noted for all three primary peaks of CCl_4 (see Figure 4-20). If flicker noise dominates the spectra, a plot of RSD values as a function of integration times should be horizontal. This is for the same reasons as in the previous study – RSD is the flicker factor. Moderately constant values were calculated and are demonstrated in Figure 4-21.

The last consideration in determining the limiting source was classic noise cases defined by the slopes of $\log S/N$ versus $\log S$ plots. The general log/log scenarios are outlined in Figure 4-22. Each of the primary CCl_4 peaks was evaluated and the graphical results are presented in Figure 4-23. The three peaks produced a slope of approximately 0, indicating limitation by flicker noise. All noise studies indicate flicker noise as the limiting noise source for the low-end Raman instrument. To determine if the flicker noise originates in analyte signal or background is nontrivial. It is hypothesized that the majority is analyte signal flicker resulting from laser fluctuations.

Concluding Remarks

A broader and deeper knowledge of the low-end instrument has been attained by evaluating a number of performance factors. It is clear that the system is capable of producing Raman spectra of a variety of liquid and solid samples. The next step is to assess its usefulness in sample identification.

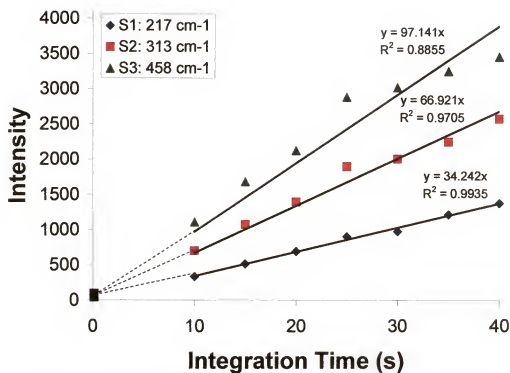


Figure 4-20. Analyte signal intensity as a function of integration time for CCl₄ primary peaks.

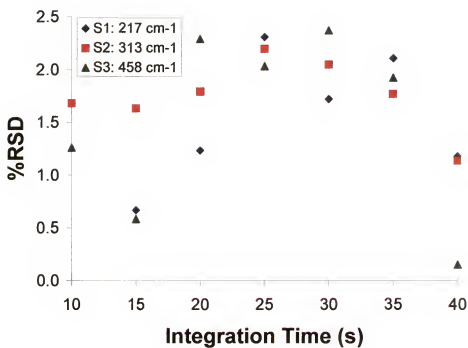


Figure 4-21. Relative standard deviation as a function of integration time for CCl₄ primary peaks.

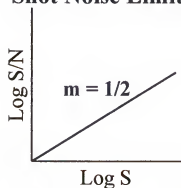
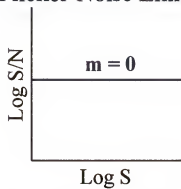
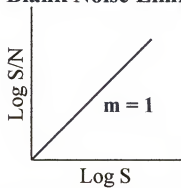
Shot Noise Limited**Flicker Noise Limited****Blank Noise Limited**

Figure 4-22. General noise scenarios for log/log plots.

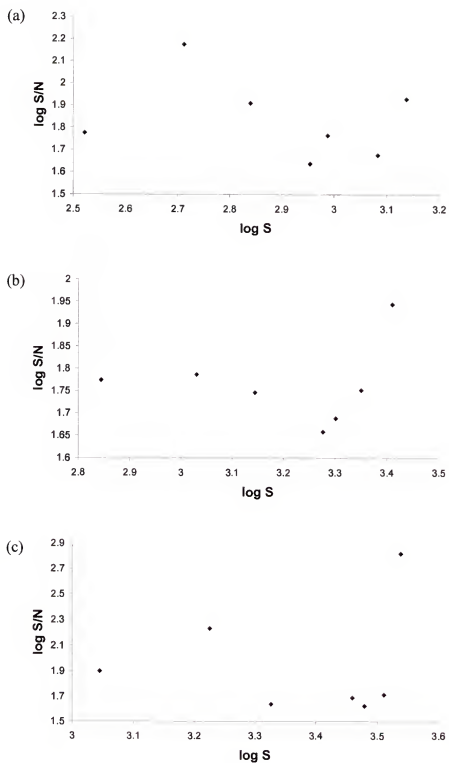


Figure 4-23. Log/log plots for CCl_4 : (a) peak 1 at 217 cm^{-1} ; (b) peak 2 at 313 cm^{-1} ; (c) peak 3 at 458 cm^{-1} .

CHAPTER 5 DATA ANALYSIS FOR LOW-END RAMAN SPECTROSCOPIC SYSTEM

Introduction

Due to marked technological and instrumental advancements over the past few decades, modern analytical techniques are generating vast amounts of data at unprecedented rates. How to adequately assimilate the mass amount of information is rapidly becoming a priority across the analytical chemistry discipline.⁷⁸ The primary objective is to extract the maximum amount of useful information but, not compromise the data integrity in the mathematical manipulation process. The field of chemometrics is evolving to address these critical data processing issues.

Chemometrics is loosely defined as the process of deriving chemical information from data.⁴⁹ Mathematical, statistical, and other methods of logic are used to determine the properties of substances that would otherwise be difficult, or nearly impossible, to measure by direct means.⁷⁸ The range of chemometric techniques available is wide and continues to grow, particularly with regards to specific applications. General background information is provided and followed by detailed discussions concerning sample grouping and identification analyses with respect to the low-end Raman spectroscopic system.

Background Information

Chemometric treatment of data can be considered a visual rearrangement. The instrument provides all the puzzle pieces and mathematical operations place these pieces together. However, there is more than one way to assemble the puzzle, just as there are

multiple ways to interpret data. This is why a variety of techniques are available and more are in development. The methods employed are often chosen on the basis of application, analytical method, and intended information. There is no method that acts as a panacea for all situations.

There are several areas of chemometrics including: experimental design, signal processing, pattern recognition, modeling, databanks and libraries, knowledge processing, and quality control. Each of these sub-disciplines contains their own set of methods for data analysis. For the purposes of this research, pattern recognition is further considered.

Pattern recognition seeks similarities and regularities present in data.⁷⁹ The mode of pattern recognition is twofold – grouping of samples and sample classification. Grouping considers how samples are defined in relation to one another while the goal of classification is to identify individual samples with corresponding groups. Pattern recognition methods are further delineated as unsupervised or supervised. Unsupervised techniques determine relationships between samples without prior knowledge about the relationship. Conversely, supervised techniques take into account sample grouping information to establish models from which classifications can be made. A combination of unsupervised and supervised methods are investigated, as well as, sample grouping and classification. Samples and experimental conditions are detailed in the next section.

Samples and General Experimental Parameters

For data analysis optimization, post-consumer plastic materials were employed. The motivation to use such samples was the result of several factors. First, Raman spectroscopy has previously been used for the identification of post-consumer plastics. It was demonstrated by Allen *et al.* that Raman spectra contain a wealth of sharp, resolved

peaks which are valuable in the unique identification of plastic samples.⁸⁰ Even though the study incorporated a high-end commercial instrument with visible excitation, a general spectral comparison base was available. The second reason for the use of plastic samples was relative spectral simplicity. Simultaneously though, post-consumer plastic samples presented a wealth of diversity with respect to density, thickness, and color. The blending of spectral simplicity and variation was a key consideration. Maintaining a certain level of simplicity afforded the opportunity to focus on other potential critical identification factors (e.g., variations between samples of the same category). Third, extensive correlation analysis has been conducted with laser-induced breakdown spectroscopy (LIBS) including plastic samples.⁸¹⁻⁸⁴ While the spectroscopic principals differ between LIBS and Raman, the end result – the analysis of spectra and their correlation to a library of predetermined standards – is identical. Knowledge gleaned from other correlation studies are beneficial and act as an identification comparison base. Lastly, post-consumer plastic samples are readily available and sample handling is not cumbersome. In general, post-consumer plastic samples were identified as a good intermediary between solvents used for instrument characterization and complex biological samples of long-range interest.

Samples representing different post-consumer plastic types were used and sorted based on their printed recycling code located on the product bottom side. These codes were established in the late 1980s by the Society of Plastics Industry for standardization purposes.⁸⁵ See Figure 5-1 for an overview of categories. Each number represents a commonly used household plastic: 1 is polyethylene terephthalate (PET); 2 is high-density polyethylene (HDPE); 3 is polyvinyl chloride (PVC); 4 is low-density



Figure 5-1. Post-consumer plastic categories and product examples. Adapted from reference 85: website: <http://www.domme.ntu.ac.uk/people/alotfi/personal/recycle/plastic.html>

polyethylene (LDPE); 5 is polypropylene (PP); 6 is polystyrene (PS); and 7 is a mixture of co-layered polymers. Only materials from categories 1 through 6 were used in the research and they were designated as P1 to P6, respectively. For each category, there were three unique samples and Table 5-1 displays the sample products and colors.

Three complete sets of data were acquired. The original set consisted of 50 spectra per unique sample (900 total spectra). Eight months later, two additional sets were collected each consisting of 20 spectra per unique sample (720 total spectra). The latter compilations were only applied to identification analysis. Figure 5-2 provides a visual representation of samples and categories. The original collection was acquired with 20 mW laser power and the other two sets with 30 mW. A 1 min integration time was used for all plastic spectra and was governed by a manually operated external trigger. An adjustable metal ring on the end of the fiber optic probe head was fixed at the probe focal distance (5 mm). Plastic samples were placed flush to the ring ensuring reproducible sample placement. Figure 5-3 shows representative post-consumer plastics Raman spectra acquired with the low-end instrument.

Sample Grouping Analysis

By considering grouping analysis prior to identification, information concerning the samples can be gained. This information usually translates to a clearer understanding of the samples' classification behaviors and predictions can be made concerning potential areas of identification difficulty. Additionally, the grouping analysis affords a better general understanding of instrumental capabilities. Three methods were employed in the sample grouping analysis studies: hierarchical cluster analysis, principal component analysis, and linear discriminate analysis. Each is described below; a number of sources were consulted and used in forming the fundamental summaries.⁸⁶⁻⁹¹

Table 5-1. Post-consumer plastic samples used in identification analysis.

| | | | Sample | Product | Color |
|--------|------------------|----|--------|------------------------------|-----------|
| P 1 | P E T | 1 | A | Twister bottle | Colorless |
| | | 2 | B | Honey mustard squeeze bottle | Colorless |
| | | 3 | C | Paint tray | Yellow |
| P 2 | H D P E | 4 | A | Crystal Light container | Frosted |
| | | 5 | B | Pert shampoo bottle | Green |
| | | 6 | C | Bubble gum container | White |
| P 3 | P V C | 7 | A | Refrigerator bottle | Colorless |
| | | 8 | B | Spray bottle | Blue |
| | | 9 | C | Light switch mount | Colorless |
| P 4 | L D P E | 10 | A | Glue squeeze bottle | Frosted |
| | | 11 | B | Mustard squeeze bottle | Yellow |
| | | 12 | C | Suntan lotion squeeze bottle | White |
| P 5 | P P | 13 | A | Glad container | Colorless |
| | | 14 | B | Organizer box | Frosted |
| | | 15 | C | Flower pot | White |
| P 6 | P S | 16 | A | Meat tray | White |
| | | 17 | B | Meat tray | Blue |
| | | 18 | C | Meat tray | Yellow |

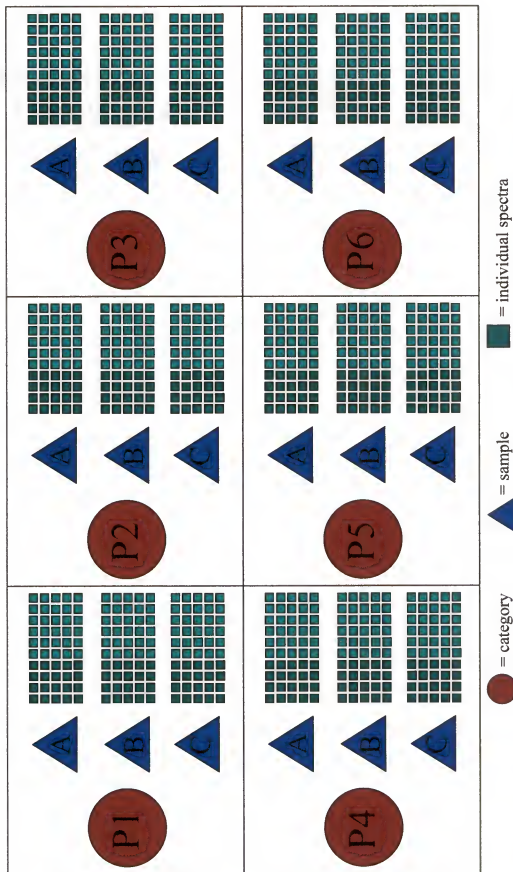


Figure 5-2. Visualization of categories and samples. The darker green blocks indicate the 20 individual spectra acquired in the 2 latter data sets. All green blocks represent the 50 spectra collected for the original data set.

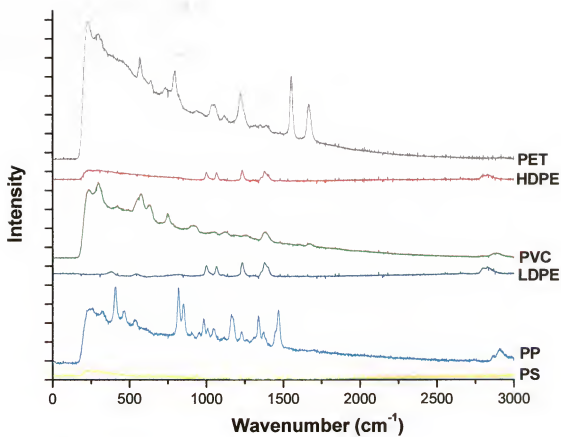


Figure 5-3. Representative Raman spectra of post-consumer plastic samples.

Hierarchical Cluster Analysis (HCA)

HCA seeks natural classifications in data sets. It is a well-established and simple method which was first developed by biologists for numerical taxonomy purposes. In chemistry today, HCA is used primarily to acquire initial information on unknown analyte groups. It is simply an unsupervised chemometric visual tool for sample grouping.

Fundamentals

The basic assumption that HCA is based upon is that measurements collected for related samples are similar. Thus, projected in space, the distance between similar samples is smaller than that of unrelated objects. A main disadvantage of HCA is that it commonly uses distance measures that do not consider correlation between variables.

HCA is a stepwise process. The first stage involves selection and application of a distance measure. This dictates how the distance between two entities is calculated, thus how similarity is defined. Several recognizable measures of distance exist including Euclidean, city block, Mahalanobis, and Minkowski. With similarities calculated, the information is linked together in an aggregated manner governed by a linkage method. Examples of linkages are single (nearest neighbor), complete (furthest neighbor), average, and centroid. Distance and linkage calculations are continued until all objects have been associated with one main group. At each step, the most similar two objects are paired. The results of HCA are often displayed in a dendrogram format (see Figure 5-4). As the distance in objects and linkages increases, the similarity between clusters decreases.

A number of the above distance measures and linkages were used in a variety of combinations for HCA analysis of plastics. Euclidean distance and centroid linkage are

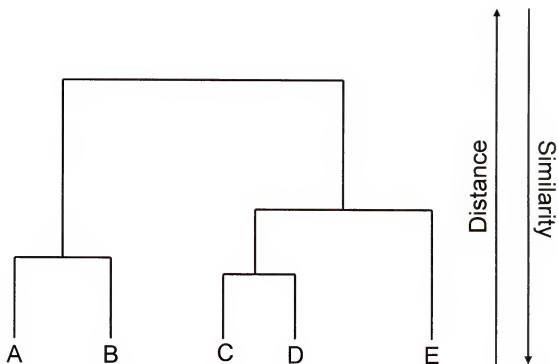


Figure 5-4. Illustrative example of a HCA dendrogram.

used in the examples presented. The geometric distance between two objects is the Euclidean distance. It is the most commonly used measure of distance. An illustration with a mathematical relationship is provided in Figure 5-5. The centroid is the average of a cluster in 3-dimensional space. Pictorial representation and equation are shown in Figure 5-6.

Application to plastics grouping

A comparison of dendrograms representing clusters for untreated and dark eliminated spectra is displayed in Figure 5-7. Ideally, six distinct clusters, composed of three similar objects each, would exist. This would account for the six plastic categories and the three unique samples in each category. For untreated spectra, the majority of samples were classified together (10 out of 18 samples). The other 8 samples were distributed among 4 groups. Twelve groups emerged for dark eliminated plastic spectra with 1 or 2 samples in each. Neither clustering scenario is ideal. There is not enough natural distribution for untreated spectra; however, dark eliminated spectra led to too much fragmentation.

Principal Component Analysis (PCA)

PCA is a form of variable reduction which reduces the dimensionality of a given data set. It is the most commonly employed multivariate chemometric technique. Like HCA, PCA is an unsupervised technique. As opposed to HCA, however, the PCA method begins with the whole group and breaks samples into categories.

Fundamentals

In PCA, the original data matrix is redefined as the product of two smaller matrices, known as the scores and loadings matrices. The original data can then be described in terms of principal components (PCs), which are linear combinations of the

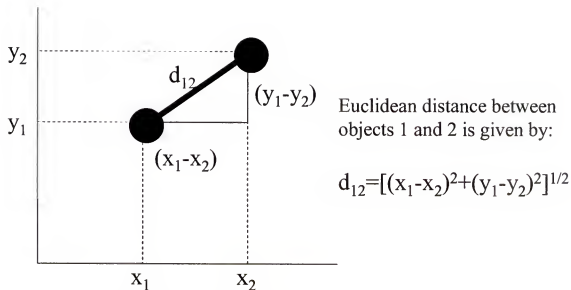


Figure 5-5. Euclidean distance measure for HCA. Adapted from references 87 and 90: Otto, M. *Chemometrics: Statistics and Computer Application in Analytical Chemistry*; Wiley-VCH: Weinheim, 1999 and Beebe, K.R.; Pell, R.J.; Seasholtz, M.B.; *Chemometrics: A Practical Guide*; Wiley & Sons, Inc.: New York, 1998.

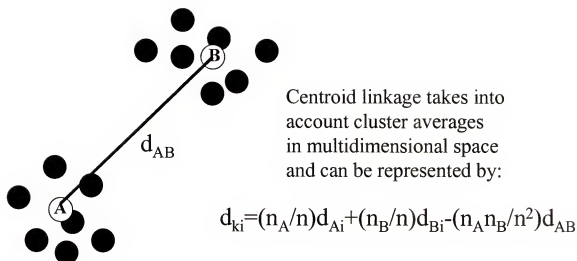


Figure 5-6. Centroid linkage for HCA. Adapted from references 87 and 90: Otto, M. *Chemometrics: Statistics and Computer Application in Analytical Chemistry*; Wiley-VCH: Weinheim, 1999 and Beebe, K.R.; Pell, R.J.; Seasholtz, M.B.; *Chemometrics: A Practical Guide*; Wiley & Sons, Inc.: New York, 1998.

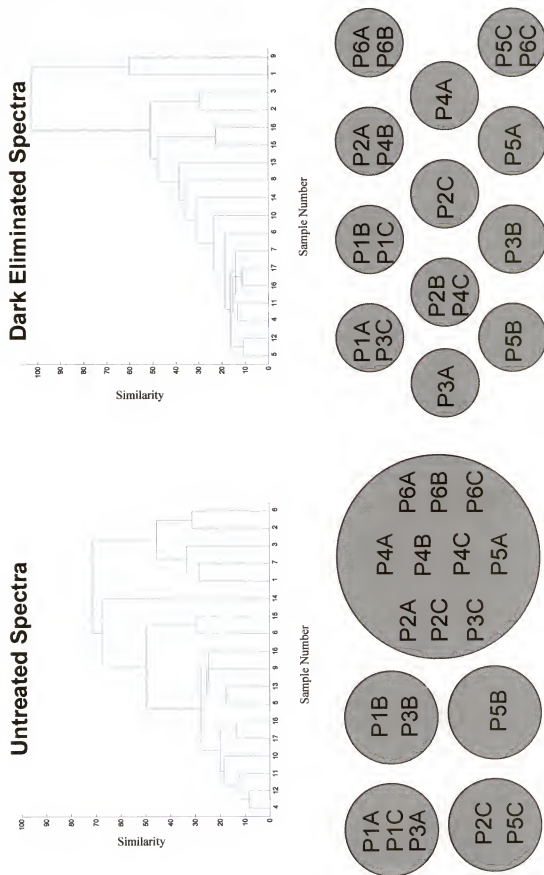


Figure 5-7. HCA dendrograms for untreated and dark eliminated plastic spectra.

variables. Usually the first few PCs contain the majority of spectral information and are quantized by eigenvalues resulting from variance calculations. Oftentimes, the grouping is visualized by plotting the first 2 or 3 principal components against each other.

Application to plastics grouping

To evaluate plastic sample (untreated) grouping with PCA, the first two PCs were plotted for each of the six categories. Figure 5-8 shows a series of each of the six plastics and there average visual distribution. The first 2 PCs account for at least 90% of the spectral variations. The information in these 6 plots is superimposed in Figure 5-9 to gain a better visual perspective of the natural groupings. The plastic categories are not well separated which indicates that sample identification has the potential of not working effectively. Variations within the plastic categories are visualized in Figure 5-10.

Linear Discriminant Analysis (LDA)

LDA is a supervised technique and is a more formal method of determining boundaries between classes. It seeks linear functions which maximize the variance between classes and minimize within class. The visual tool for LDA is scores plots. The use of PCA to reduce dimensionality is often employed prior to LDA.

Fundamentals

For a generalized approach to LDA, consider a data matrix X containing n objects, p feature variables, and a total of g different groups:

$$\left(\begin{array}{cccc} x_{11} & x_{12} & \cdots & x_{1p} \\ x_{21} & x_{22} & \cdots & x_{2p} \\ x_{31} & x_{32} & \cdots & x_{3p} \\ x_{41} & x_{42} & \cdots & x_{4p} \\ \vdots & & & \\ x_{j1} & x_{j2} & \cdots & x_{jp} \\ x_{n1} & x_{n2} & \cdots & x_{np} \end{array} \right\} \begin{array}{l} g_1 \\ g_2 \\ \\ g_{n_j} \end{array} \quad (5-1)$$

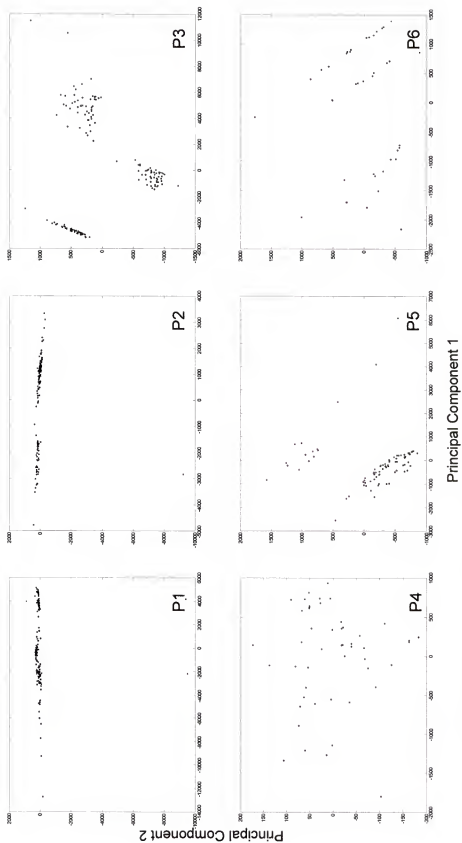


Figure 5-8. PCA plots showing average spread for each plastic category.

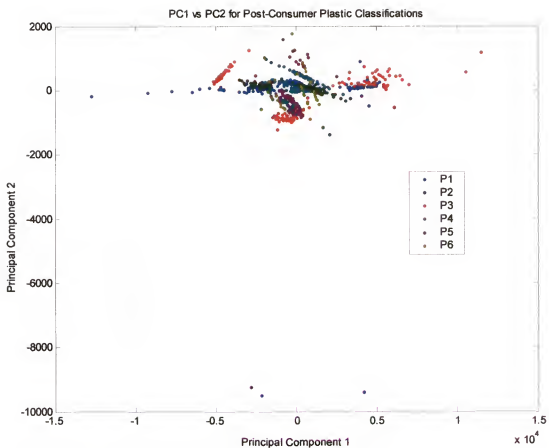


Figure S-9. PCA plot for plastic category comparison.

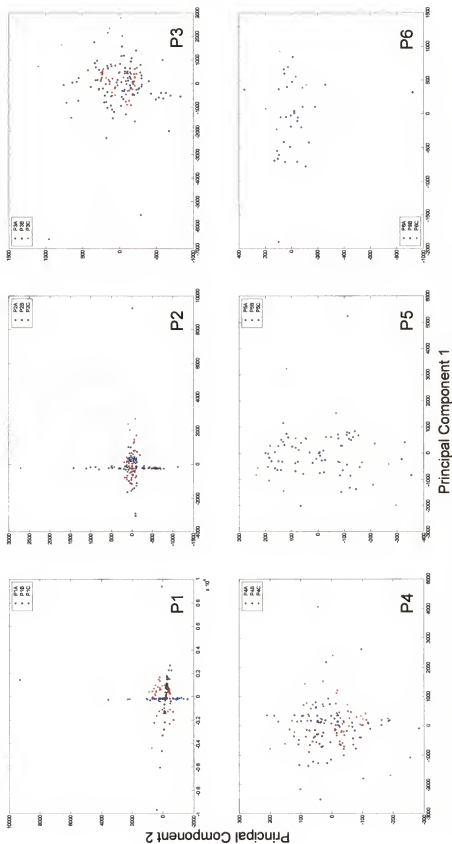


Figure 5-10. PCA plots displaying spread between samples of the same plastic category.

Weights of linear discriminate functions are found as eigenvectors of the matrix denoted as

$$G^{-1} H w = \lambda w \quad (5-2)$$

where G matrix is derived from the covariance matrix of the different groups of g

H matrix describes the spread of group means in relation to the grand average

λ represents eigenvalues

w represents eigenvectors

Based on the largest eigenvalue (λ_1), the eigenvector (w_1) produces the first linear discriminate function (LDF) and can be summarized as

$$s_1 = w_{11}x_1 + w_{12}x_2 + \dots + w_{1p}x_p \quad (5-3)$$

With residual x-data, another eigenvalue is generated using λ_2 from which a second linear discriminate function is obtained. With a set of well-defined functions, unknown data can be inserted into the LDFs for classification.

Application to plastics grouping

Often PCA is required prior to LDA to reduce the dimensionality of the data because there are matrix size restrictions in LDA. To determine the number of principal components needed to be retained for linear discrimination, scree plots were considered. The needed component number is derived from the leveling-off in the plot of eigenvalues *versus* PCs. See Figure 5-11 for a series of scree plots that correspond to the various plastic categories. From the inspection of points corresponding to where the slope begins to level, it was decided to retain 8 PCs for LDA. The resulting scores plot is shown in Figure 5-12, which demonstrated good separation between a number of categories.

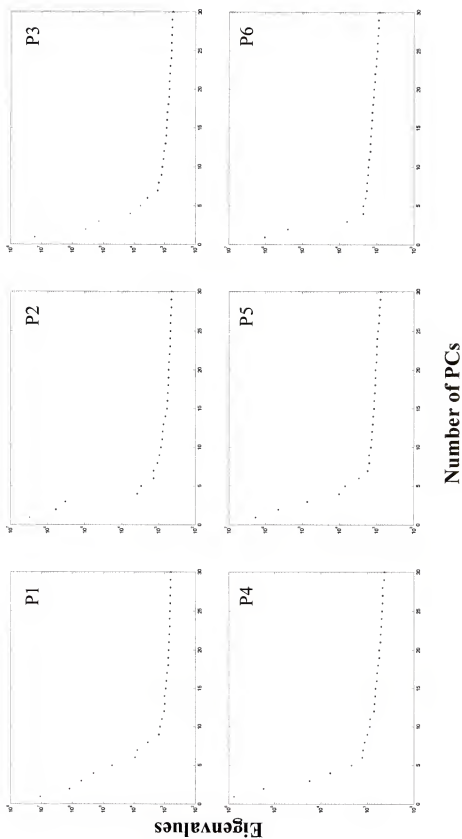


Figure 5-11. Scree plots to determine the number of PCs to retain for LDA analysis.

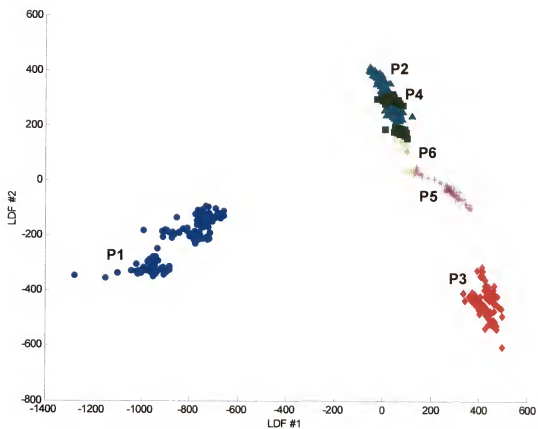


Figure 5-12. LDA scores plots displaying plastic category grouping. 8 PCs were retained.

Grouping Analysis Conclusions

It can be concluded from the three methods of grouping analysis that the post-consumer plastics provide both simplicity and challenge for identification. The best grouping was obtained with LDA. PET and PVC (P1 and P3) each separate into their respective categories nicely. However the success of the other categories is mixed. The largest potential identification difficulty lies with HDPE and LDPE (P2 and P4). With P2 and P4 sample differences arising from crystallinity ratios, subtle spectral disparities need to be detected for adequate separation and identification.⁸⁰

Sample Identification Analysis

The primary objective of identification analysis is sample classification. From these studies information can be extracted concerning essential factors governing identification, effectiveness of various data pre-treatment methods, and feasibility of classifying samples with confidence. Identification via correlation methods is the main focus for the data analysis phase of research. The fundamental discussion of linear and nonparametric correlations is intended to present a general overview of the techniques. A number of sources were consulted and used in forming the summary.^{86-90,92}

Correlation Methods

Considering some of the instrumental limitations such as poor optical throughput and low detector quantum efficiency, it becomes apparent that data treatment methods need to compensate for these system shortcomings and others. There are a number of powerful chemometric identification tools that could be joined with the low-end Raman instrument. The methods span a wide range of complexities with respect to programming, interpretation, and ease of use. The impetus in selecting an identification technique is to find one that produces adequate results but, does not exceed the minimum

level of complexity required. Correlation methods are relatively simple and enough statistical material (2048 data points) is provided to permit their use for sample identification.

Fundamentals

Linear correlation measures the association between variables. The linear correlation coefficient, r , is expressed by the following equation:

$$r = \frac{\sum_i (x_i - \bar{x})(y_i - \bar{y})}{\sum_i (x_i - \bar{x})^2 \sum_i (y_i - \bar{y})^2} \quad (5-4)$$

where \bar{x} is the mean of the x_i values

\bar{y} is the mean of the y_i values.

The correlation coefficient is also known as Pearson's r . The value of r lies between -1 and 1, where 1 indicates a complete positive correlation and -1 symbolizes a complete negative correlation. As the correlation coefficient approaches 0, it becomes more difficult to find similarities between the variables which decreases the chance of using one variable to predict another. The linear correlation function does not take into account the individual distributions of x and y . The unknown distributions make r an inferior statistic with respect to determining statistical significance of the observed correlation. In experimental terms, linear correlation is not a robust technique for spectra exhibiting intensity fluctuations.

Nonparametric (or rank) correlation is similar to linear correlation, but takes into account the individual distributions of x and y . This is achieved by ranking each x_i and y_i value with respect to the other x_i and y_i values, respectively. The equation for

nonparametric correlation is the same as in Equation (5-4) except the values of x and y are replaced by their corresponding ranks, R and S . The resulting expression is given by

$$\rho = \frac{\sum_i (R_i - \bar{R})(S_i - \bar{S})}{\sqrt{\sum_i (R_i - \bar{R})^2 \sum_i (S_i - \bar{S})^2}} \quad (5-5)$$

where ρ is the rank correlation coefficient (or Spearman's ρ)

R_i is the rank x_i values

\bar{R} is the mean of R_i values

S_i is the rank of y_i

\bar{S} is the mean of S_i values

The ranks are numbers 1, 2, 3, . . . , N, where N is the total number of data points. For the CCD detector used, each pixel produces a data point, so N=2048. The rank numbers replace the true values of x and y in accordance with their magnitudes. For example, the most intense pixel in the spectrum will be assigned a value of 2048, the least intense pixel assigned a rank of 1, and the correlation is drawn from a perfectly known distribution.

Application of correlation methods to plastics identification

The initial stage of identification analysis with correlation methods used solvent samples: carbon tetrachloride, methanol, ethanol, toluene, benzene, and acetonitrile. The solvent spectra had significant visual differences, but served as software validation. As expected, all samples were identified correctly. Post-consumer plastic samples became the focus for identification analysis.

Analyte spectra were correlated with an averaged plastic sample library. Each of the three acquired data sets had its respective library. Identifications were made in a relative manner; samples were assigned to the classification that had the largest

correlation value in comparison to the other library members. A number of factors were investigated with respect to influence on correlation and sample identification. Untreated (raw) spectra served as a comparison foundation for positive identification percentages. The factors evaluated include spectral in-class variation, dark elimination, averaging, window for correlation, and shifts. Each is presented below.

In-class variation effects. Spectral differences between samples of the same group are known as in-class variations. These sample deviations can lead to poor correlation, which makes positive identification difficult. Take Figure 5-13 as an illustrative example. There are three diamonds of different colors, and the goal is to identify each in the same group -- diamond. If the three samples are sufficiently similar with respect to the other classification groups, then the probability of a positive identification is great. However, if a relatively large amount of variation exists among the diamond samples, then the potential for misidentification increases. Extraneous factors are given identification priority; hence in the example, the yellow diamond is falsely classified with a yellow circle. Generally, an increase in sample chemical complexity is accompanied with a greater amount of spectral in-class variation.

The spectral differences between samples of the same plastic category are visually significant (see Figure 5-14). Accompanying box plots indicate the experimental spread. The collective positive identification percentage for untreated plastic spectra was approximately 50%. The low value was attributed to in-class variations arising primarily from discrepancies in the amount of spectral background.

Raman spectroscopy can undoubtedly benefit from the use of a robust background correction procedure. The origin of Raman continuum background is not fully

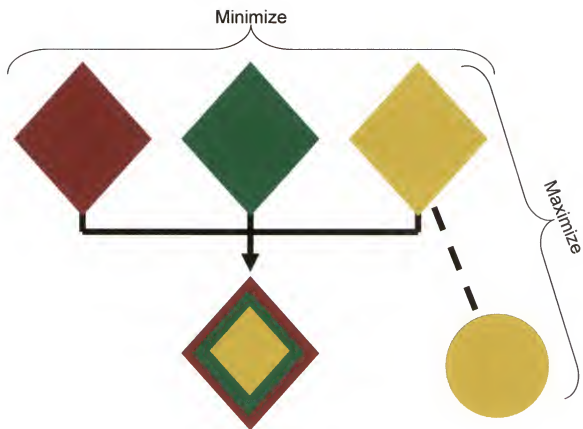


Figure 5-13. Illustration of in-class variations.

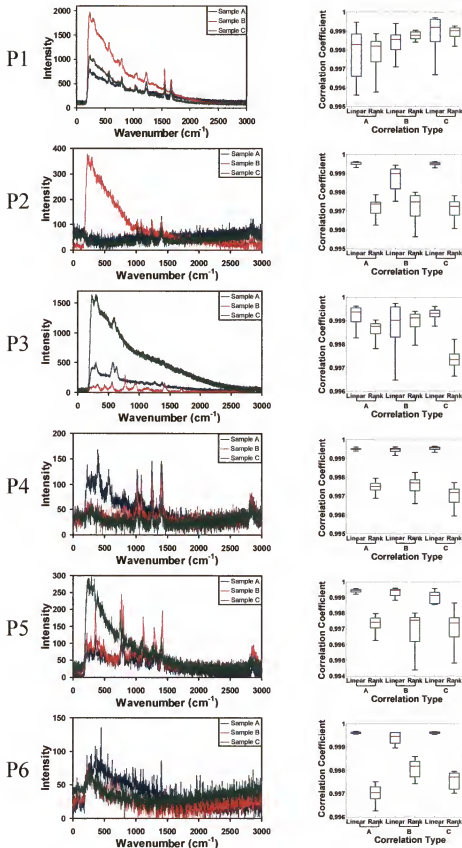


Figure 5-14. Representative Raman spectra of each plastic sample. In-class variations are visually notable. Box plots show spread of data. Dark has been removed from spectra for visualization purposes.

understood. Anomalous broad bands in Raman spectra are often clearly attributed to the fluorescence of the sample matrix of the analyte itself. However, others believe there is a non-fluorescent nature to Raman background due to some independent physical phenomenon.⁹³ Additionally, contributions from source (laser) fluctuations, detector noise, fixed pattern noise, and Rayleigh scatter need to be considered. Regardless of origin, background signals often obscure Raman signals, making spectral analysis, identification, and quantitation difficult.

A number of background corrective measures have been previously proposed for Raman spectra. One of the most common methods employed is the fitting of a single polynomial function to the data set with subsequent subtraction from the original spectra. This approach has often not produced optimum results for high-background samples due to the complexity of the spectra.⁹⁴ Another common approach that has been used with Raman spectra is segmentation of raw spectra and fitting polynomials to the individual sections. This can result in better polynomial fitting; however, in the recombination process, the possibility exists of introducing nonlinear behavior to the resultant spectra.⁹⁴ The in-house background correction algorithm developed and applied in this research uses a piecewise approach in conjunction with single polynomial function fitting. Details are provided in Figure 5-15.

The general algorithm goal was the approximation of continuum background over a wide (several hundred nm) spectral range. It is heuristic in nature and validity was established through successful practical application. While ideally the algorithm could be used with any instrument containing an array detector, it was originally developed for

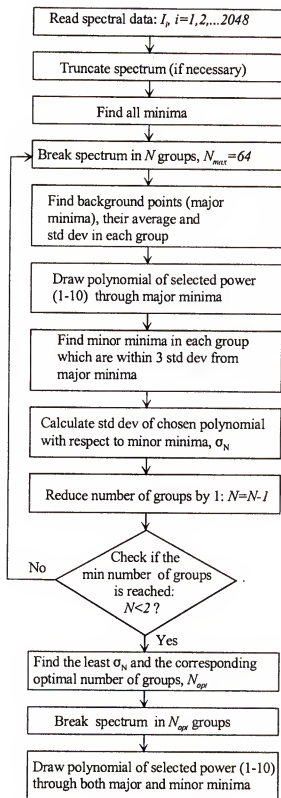


Figure 5-15. Background correction algorithm. Adapted from reference 95.

non-gated LIBS. Potential benefits for Raman were foreseen and the algorithm was evaluated with the low-end system.

Background corrected spectra for the six plastic categories are shown in Figures 5-16. Taking a closer look at P1 in Figure 5-17, minimization of in-class variation is visually evident. The average correlation coefficient values for the three unique samples increased (0.98 to 0.9990) while the standard deviations decreased (0.01 to 0.0004). Analogous trends were observed for all plastic categories.

Tables 5-2 to 5-5 display correlation coefficients for untreated and background corrected spectra for linear and rank correlations. Figure 5-18 presents bar graphs with positive identification percentages for visual comparison.

Spectral averaging effects. The effect of spectral averaging on correlation analysis was evaluated. The majority of presented analyses were completed by correlating an averaged analyte spectrum to a library composed of averaged spectra. However, for experimental flexibility and time efficiency, the ideal situation involves the comparison of a single spectrum with an averaged library. Figure 5-19 is a pictorial representation of the two correlation scenarios. The results of an average/average correlation were compared to the results of a single/average correlation to determine the presence and extent of analyte spectral averaging effects. Bar graphs representing the positive identifications are shown in Figure 5-20. The overall positive identification percentages for correlation of single/average plastic samples were unaffected. Thus, it was concluded that no latent variable is detectable with respect to analyte spectral averaging and correlation with an averaged library.

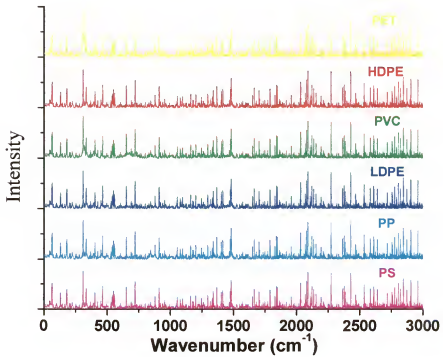
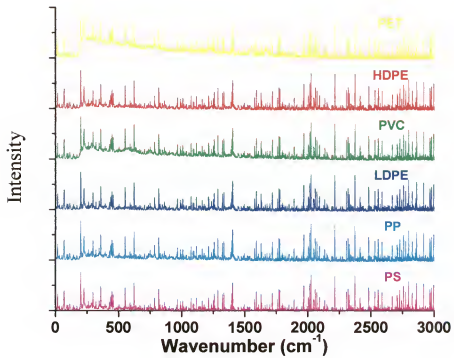


Figure 5-16. Representative Raman spectra for plastic categories:
(top) untreated spectra; (bottom) background corrected

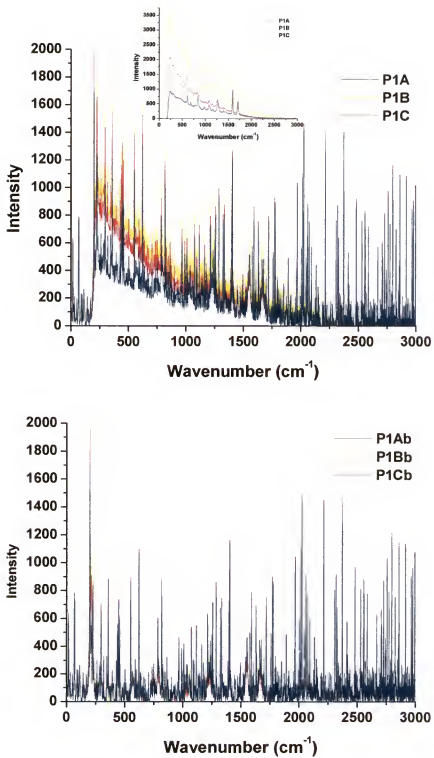


Figure 5-17. Representative Raman spectra for PET (P1) samples: (top) untreated spectra with dark eliminated inlay; (bottom) background corrected spectra.

Table 5-2. Linear correlation values for untreated spectra.

| | Plastic Categories | | | | | |
|-----------|--------------------|--------|--------|--------|--------|--------|
| | 1 | 2 | 3 | 4 | 5 | 6 |
| 1a | 0.9700 | 0.8900 | 0.9822 | 0.8613 | 0.9152 | 0.8835 |
| 1b | 0.9917 | 0.6930 | 0.9163 | 0.6433 | 0.7368 | 0.6828 |
| 1c | 0.9973 | 0.7629 | 0.9505 | 0.7164 | 0.8004 | 0.7544 |
| 2a | 0.7022 | 0.9927 | 0.8632 | 0.9986 | 0.9807 | 0.9927 |
| 2b | 0.8882 | 0.9766 | 0.9760 | 0.9577 | 0.9834 | 0.9731 |
| 2c | 0.7069 | 0.9937 | 0.8666 | 0.9988 | 0.9820 | 0.9940 |
| 3a | 0.9436 | 0.9175 | 0.9956 | 0.8894 | 0.9359 | 0.9121 |
| 3b | 0.9914 | 0.7793 | 0.9635 | 0.7346 | 0.8167 | 0.7707 |
| 3c | 0.7852 | 0.9919 | 0.9198 | 0.9886 | 0.9936 | 0.9916 |
| 4a | 0.7278 | 0.9953 | 0.8803 | 0.9997 | 0.9861 | 0.9937 |
| 4b | 0.7780 | 0.9983 | 0.9140 | 0.9973 | 0.9938 | 0.9954 |
| 4c | 0.6939 | 0.9915 | 0.8575 | 0.9975 | 0.9786 | 0.9927 |
| 5a | 0.7841 | 0.9965 | 0.9189 | 0.9939 | 0.9975 | 0.9961 |
| 5b | 0.7640 | 0.9901 | 0.9032 | 0.9904 | 0.9947 | 0.9891 |
| 5c | 0.8801 | 0.9801 | 0.9724 | 0.9636 | 0.9902 | 0.9777 |
| 6a | 0.6936 | 0.9907 | 0.8573 | 0.9956 | 0.9778 | 0.9933 |
| 6b | 0.8515 | 0.9899 | 0.9586 | 0.9769 | 0.9938 | 0.9893 |
| 6c | 0.7449 | 0.9975 | 0.8930 | 0.9973 | 0.9895 | 0.9992 |

Table 5-3. Linear correlation values for background corrected spectra.

| | | Plastic Categories | | | | | |
|-----------------|----|--------------------|--------|--------|--------|--------|--------|
| | | 1 | 2 | 3 | 4 | 5 | 6 |
| Plastic Samples | 1a | 0.9994 | 0.9285 | 0.9757 | 0.9782 | 0.9757 | 0.9780 |
| | 1b | 0.9991 | 0.9733 | 0.9718 | 0.9728 | 0.9701 | 0.9723 |
| | 1c | 0.9986 | 0.9881 | 0.9864 | 0.9876 | 0.9860 | 0.9880 |
| | 2a | 0.9805 | 0.9999 | 0.9947 | 0.9998 | 0.9971 | 0.9987 |
| | 2b | 0.9811 | 0.9997 | 0.9958 | 0.9991 | 0.9968 | 0.9990 |
| | 2c | 0.9808 | 0.9999 | 0.9949 | 0.9998 | 0.9973 | 0.9990 |
| | 3a | 0.9688 | 0.9835 | 0.9944 | 0.9825 | 0.9789 | 0.9834 |
| | 3b | 0.9801 | 0.9963 | 0.9989 | 0.9952 | 0.9933 | 0.9966 |
| | 3c | 0.9746 | 0.9925 | 0.9928 | 0.9922 | 0.9945 | 0.9926 |
| | 4a | 0.9805 | 0.9998 | 0.9945 | 1.0000 | 0.9969 | 0.9982 |
| | 4b | 0.9799 | 0.9990 | 0.9937 | 0.9997 | 0.9959 | 0.9968 |
| | 4c | 0.9806 | 0.9998 | 0.9952 | 0.9995 | 0.9975 | 0.9995 |
| | 5a | 0.9794 | 0.9984 | 0.9945 | 0.9978 | 0.9996 | 0.9988 |
| | 5b | 0.9732 | 0.9921 | 0.9884 | 0.9922 | 0.9983 | 0.9918 |
| | 5c | 0.9794 | 0.9985 | 0.9946 | 0.9979 | 0.9993 | 0.9988 |
| | 6a | 0.9805 | 0.9990 | 0.9951 | 0.9983 | 0.9973 | 0.9999 |
| | 6b | 0.9800 | 0.9988 | 0.9956 | 0.9979 | 0.9972 | 0.9998 |
| | 6c | 0.9805 | 0.9990 | 0.9952 | 0.9982 | 0.9974 | 0.9999 |

Table 5-4. Rank correlation values for untreated spectra.

| | | Plastic Categories | | | | | |
|-----------------|----|--------------------|--------|--------|--------|--------|--------|
| | | 1 | 2 | 3 | 4 | 5 | 6 |
| Plastic Samples | 1a | 0.9931 | 0.8429 | 0.9800 | 0.7931 | 0.8921 | 0.8333 |
| | 1b | 0.9963 | 0.7506 | 0.9602 | 0.6882 | 0.8175 | 0.7380 |
| | 1c | 0.9989 | 0.8075 | 0.9804 | 0.7505 | 0.8669 | 0.7971 |
| | 2a | 0.6837 | 0.9778 | 0.7927 | 0.9949 | 0.9437 | 0.9734 |
| | 2b | 0.9020 | 0.9694 | 0.9635 | 0.9329 | 0.9801 | 0.9616 |
| | 2c | 0.6843 | 0.9799 | 0.7941 | 0.9948 | 0.9453 | 0.9773 |
| | 3a | 0.9645 | 0.9038 | 0.9972 | 0.8586 | 0.9439 | 0.8942 |
| | 3b | 0.9890 | 0.7765 | 0.9746 | 0.7146 | 0.8413 | 0.7640 |
| | 3c | 0.8103 | 0.9779 | 0.8990 | 0.9680 | 0.9818 | 0.9774 |
| | 4a | 0.7296 | 0.9849 | 0.8304 | 0.9986 | 0.9599 | 0.9750 |
| | 4b | 0.8031 | 0.9939 | 0.8908 | 0.9918 | 0.9818 | 0.9821 |
| | 4c | 0.6612 | 0.9727 | 0.7743 | 0.9890 | 0.9348 | 0.9734 |
| | 5a | 0.8394 | 0.9859 | 0.9192 | 0.9730 | 0.9945 | 0.9841 |
| | 5b | 0.7877 | 0.9719 | 0.8778 | 0.9725 | 0.9856 | 0.9672 |
| | 5c | 0.8990 | 0.9695 | 0.9626 | 0.9369 | 0.9897 | 0.9658 |
| | 6a | 0.6594 | 0.9680 | 0.7724 | 0.9782 | 0.9315 | 0.9773 |
| | 6b | 0.8767 | 0.9789 | 0.9472 | 0.9483 | 0.9876 | 0.9802 |
| | 6c | 0.7482 | 0.9904 | 0.8478 | 0.9867 | 0.9687 | 0.9972 |

Table 5-5. Rank correlation values for background corrected spectra.

| | Plastic Categories | | | | | |
|-----------|--------------------|--------|--------|--------|--------|--------|
| | 1 | 2 | 3 | 4 | 5 | 6 |
| 1a | 0.9971 | 0.9349 | 0.9243 | 0.9323 | 0.9192 | 0.9345 |
| 1b | 0.9981 | 0.9216 | 0.9169 | 0.9174 | 0.9038 | 0.9171 |
| 1c | 0.9973 | 0.9430 | 0.9355 | 0.9397 | 0.9303 | 0.9417 |
| 2a | 0.9317 | 0.9993 | 0.9678 | 0.9990 | 0.9792 | 0.9880 |
| 2b | 0.9359 | 0.9977 | 0.9763 | 0.9936 | 0.9765 | 0.9905 |
| 2c | 0.9332 | 0.9993 | 0.9697 | 0.9988 | 0.9805 | 0.9903 |
| 3a | 0.9040 | 0.9464 | 0.9842 | 0.9401 | 0.9237 | 0.9452 |
| 3b | 0.9331 | 0.9769 | 0.9916 | 0.9694 | 0.9588 | 0.9780 |
| 3c | 0.9028 | 0.9561 | 0.9646 | 0.9537 | 0.9622 | 0.9591 |
| 4a | 0.9310 | 0.9984 | 0.9664 | 1.0000 | 0.9772 | 0.9850 |
| 4b | 0.9274 | 0.9942 | 0.9629 | 0.9981 | 0.9717 | 0.9775 |
| 4c | 0.9326 | 0.9987 | 0.9713 | 0.9968 | 0.9817 | 0.9938 |
| 5a | 0.9237 | 0.9845 | 0.9662 | 0.9810 | 0.9981 | 0.9883 |
| 5b | 0.8954 | 0.9561 | 0.9376 | 0.9562 | 0.9921 | 0.9562 |
| 5c | 0.9275 | 0.9866 | 0.9675 | 0.9827 | 0.9954 | 0.9901 |
| 6a | 0.9332 | 0.9907 | 0.9710 | 0.9859 | 0.9819 | 0.9988 |
| 6b | 0.9280 | 0.9874 | 0.9728 | 0.9810 | 0.9789 | 0.9981 |
| 6c | 0.9326 | 0.9903 | 0.9713 | 0.9853 | 0.9820 | 0.9991 |

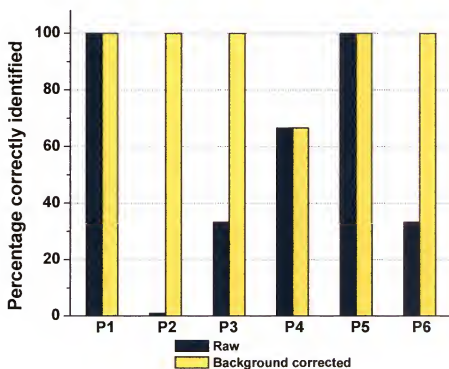
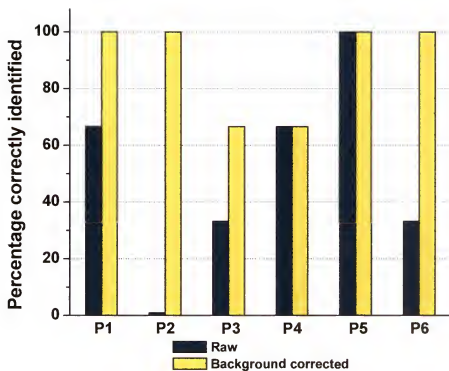


Figure 5-18. Comparison of positive identification percentages for untreated (raw) and background corrected spectra: (top) linear correlation; (bottom) rank correlation.

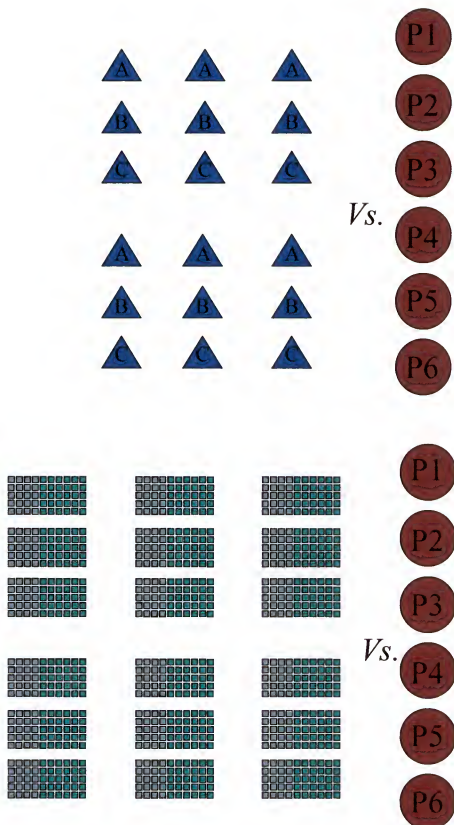


Figure 5-19. Correlation scenarios: (top) average/average; (bottom) single/average.

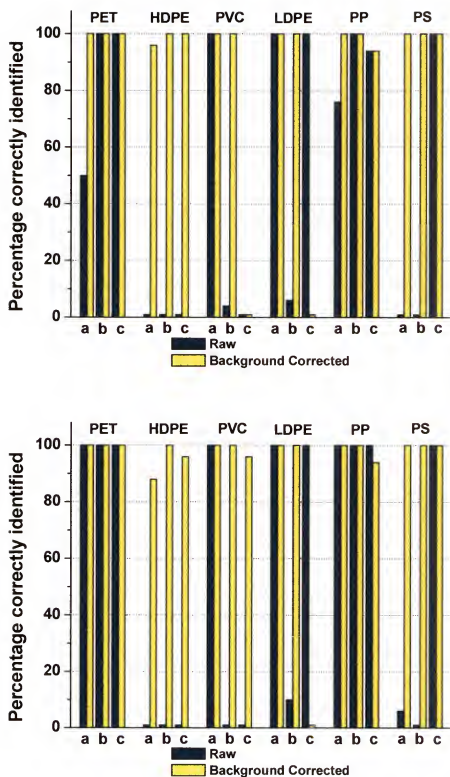


Figure 5-20. Comparison of positive identification percentages for untreated (raw) and background corrected spectra: (top) linear correlation; (bottom) rank correlation. Individual samples were correlated with averaged libraries.

Dark effects. At a 1 min integration time, fixed pattern noise (FPN) was the dominating noise factor present in the plastic spectra. A comparison of identification results for untreated and dark eliminated spectra was used to determine if FPN removal significantly improved sample correlation. The comparison is graphically displayed in Figure 5-21. Additionally, a comparison was drawn between background corrected with and without dark elimination. Figure 5-22 presents the respective positive identification percentages. No significant advantage was determined with FPN removal, indicating that the artifact is a fixed proportionality present in all collected spectra. If the FPN fluctuated in a non-linear fashion, it would have most likely been detected with linear correlation and compensated for with rank correlation. While the removal of dark did not change the overall positive identification percentages, the differences in correlation values did significantly differ. Identification was relative – the library member associated with the highest correlation value was selected as the identified sample category. The classification did not take into account the absolute correlation value nor the difference magnitude between the first and second library hits. Tables 5-6 through 5-9 display linear and rank correlation values for dark eliminated (with and without background subtraction) spectra. The ability to better separate correlation values and draw a larger distinction between library members should prove advantageous for more spectrally complex samples.

Spectral window effects. A common pre-treatment technique for spectral comparisons is reducing the spectral window, centering on characteristic peaks of the samples. Such treatment often increases correlation values because the extraneous portions of the spectra are no longer considered. Approximately 300 pixels from the left

Table 5-6. Linear correlation values for dark eliminated spectra.

| | 1 | 2 | 3 | 4 | 5 | 6 |
|----|--------|--------|--------|--------|--------|--------|
| 1a | 0.9792 | 0.9003 | 0.9487 | 0.8127 | 0.8828 | 0.9196 |
| 1b | 0.9963 | 0.9346 | 0.9719 | 0.8130 | 0.8999 | 0.9640 |
| 1c | 0.9883 | 0.9151 | 0.9444 | 0.7868 | 0.8730 | 0.9478 |
| 2a | 0.7034 | 0.8890 | 0.7313 | 0.9684 | 0.7645 | 0.7011 |
| 2b | 0.6965 | 0.8811 | 0.7155 | 0.9573 | 0.7530 | 0.6917 |
| 2c | 0.6965 | 0.8811 | 0.7155 | 0.9573 | 0.7530 | 0.6917 |
| 3a | 0.9672 | 0.9305 | 0.9845 | 0.8166 | 0.9013 | 0.9669 |
| 3b | 0.8664 | 0.8529 | 0.9255 | 0.7819 | 0.9014 | 0.8846 |
| 3c | 0.9659 | 0.9324 | 0.9929 | 0.8245 | 0.9173 | 0.9619 |
| 4a | 0.7678 | 0.9208 | 0.7926 | 0.9894 | 0.8241 | 0.7631 |
| 4b | 0.9157 | 0.9783 | 0.9301 | 0.9561 | 0.9069 | 0.9124 |
| 4c | 0.5446 | 0.7723 | 0.5607 | 0.9076 | 0.6204 | 0.5401 |
| 5a | 0.8733 | 0.8760 | 0.9274 | 0.8279 | 0.9713 | 0.8822 |
| 5b | 0.7398 | 0.7829 | 0.7930 | 0.7839 | 0.9532 | 0.7621 |
| 5c | 0.9635 | 0.9396 | 0.9715 | 0.8327 | 0.9513 | 0.9657 |
| 6a | 0.7706 | 0.7333 | 0.7891 | 0.6595 | 0.7552 | 0.8594 |
| 6b | 0.9434 | 0.9124 | 0.9578 | 0.8056 | 0.8950 | 0.9831 |
| 6c | 0.9551 | 0.9174 | 0.9630 | 0.8013 | 0.8995 | 0.9842 |

Table 5-7. Rank correlation values for dark eliminated spectra.

| | 1 | 2 | 3 | 4 | 5 | 6 |
|----|--------|--------|--------|--------|--------|--------|
| 1a | 0.9951 | 0.8908 | 0.9695 | 0.8007 | 0.8823 | 0.8973 |
| 1b | 0.9947 | 0.9005 | 0.9770 | 0.8112 | 0.8989 | 0.9104 |
| 1c | 0.8961 | 0.8681 | 0.8887 | 0.8396 | 0.8936 | 0.8672 |
| 2a | 0.7860 | 0.9573 | 0.8105 | 0.9449 | 0.9107 | 0.8028 |
| 2b | 0.6728 | 0.8637 | 0.7091 | 0.8746 | 0.8105 | 0.7150 |
| 2c | 0.6728 | 0.8637 | 0.7091 | 0.8746 | 0.8105 | 0.7150 |
| 3a | 0.9609 | 0.9111 | 0.9766 | 0.8408 | 0.9162 | 0.9047 |
| 3b | 0.8889 | 0.8766 | 0.9369 | 0.8432 | 0.9228 | 0.8721 |
| 3c | 0.9829 | 0.9086 | 0.9872 | 0.8225 | 0.9024 | 0.9095 |
| 4a | 0.7950 | 0.9436 | 0.8255 | 0.9741 | 0.9193 | 0.8001 |
| 4b | 0.8331 | 0.9382 | 0.8518 | 0.9538 | 0.9196 | 0.8425 |
| 4c | 0.5837 | 0.7824 | 0.6235 | 0.8802 | 0.7547 | 0.6276 |
| 5a | 0.9292 | 0.9457 | 0.9558 | 0.8920 | 0.9732 | 0.8866 |
| 5b | 0.8157 | 0.9236 | 0.8564 | 0.9196 | 0.9776 | 0.8225 |
| 5c | 0.9102 | 0.9266 | 0.9192 | 0.8834 | 0.9624 | 0.8841 |
| 6a | 0.7674 | 0.7447 | 0.7786 | 0.7086 | 0.7543 | 0.8533 |
| 6b | 0.8639 | 0.8427 | 0.8739 | 0.7895 | 0.8382 | 0.9374 |
| 6c | 0.8938 | 0.8617 | 0.8941 | 0.8101 | 0.8700 | 0.9415 |

Table 5-8. Linear correlation values for dark eliminated and background subtracted spectra.

| | 1 | 2 | 3 | 4 | 5 | 6 |
|-----------|--------|--------|--------|--------|--------|--------|
| 1a | 0.9872 | 0.1614 | 0.1343 | 0.0541 | 0.0579 | 0.0459 |
| 1b | 0.8567 | 0.2670 | 0.2900 | 0.1526 | 0.2262 | 0.1130 |
| 1c | 0.9603 | 0.1448 | 0.1674 | 0.0490 | 0.1196 | 0.0496 |
| 2a | 0.1345 | 0.9753 | 0.1299 | 0.4452 | 0.2410 | 0.0253 |
| 2b | 0.1567 | 0.9170 | 0.1948 | 0.2596 | 0.2766 | 0.0674 |
| 2c | 0.1567 | 0.9170 | 0.1948 | 0.2596 | 0.2766 | 0.0674 |
| 3a | 0.1268 | 0.1164 | 0.4545 | 0.0531 | 0.0476 | 0.1078 |
| 3b | 0.0883 | 0.1428 | 0.9063 | 0.0033 | 0.5225 | 0.1555 |
| 3c | 0.0411 | 0.0155 | 0.0040 | 0.8541 | 0.0900 | 0.1650 |
| 4a | 0.1537 | 0.9298 | 0.1461 | 0.4658 | 0.2807 | 0.0305 |
| 4b | 0.1798 | 0.8593 | 0.2311 | 0.3613 | 0.2892 | 0.0484 |
| 4c | 0.1276 | 0.9324 | 0.1566 | 0.4790 | 0.2435 | 0.0103 |
| 5a | 0.1134 | 0.2117 | 0.4368 | 0.1500 | 0.8445 | 0.1470 |
| 5b | 0.0569 | 0.2662 | 0.4023 | 0.0668 | 0.9856 | 0.1008 |
| 5c | 0.0899 | 0.2884 | 0.4042 | 0.0573 | 0.8884 | 0.1552 |
| 6a | 0.0795 | 0.0274 | 0.1668 | 0.2400 | 0.0893 | 0.6978 |
| 6b | 0.3780 | 0.7480 | 0.9890 | 0.1246 | 0.0419 | 0.6713 |
| 6c | 0.0270 | 0.0009 | 0.1512 | 0.2694 | 0.0744 | 0.6578 |

Table 5-9. Rank correlation values for dark eliminated and background subtracted spectra.

| | 1 | 2 | 3 | 4 | 5 | 6 |
|-----------|--------|--------|--------|--------|--------|--------|
| 1a | 0.9156 | 0.2373 | 0.3405 | 0.1495 | 0.2706 | 0.1140 |
| 1b | 0.9702 | 0.1771 | 0.1589 | 0.0424 | 0.0490 | 0.0412 |
| 1c | 0.8665 | 0.1998 | 0.2416 | 0.1242 | 0.2555 | 0.0745 |
| 2a | 0.1462 | 0.7824 | 0.0393 | 0.2805 | 0.3506 | 0.0773 |
| 2b | 0.1631 | 0.6129 | 0.1376 | 0.3212 | 0.2166 | 0.0405 |
| 2c | 0.1631 | 0.6129 | 0.1376 | 0.3212 | 0.2166 | 0.0405 |
| 3a | 0.1555 | 0.1577 | 0.4207 | 0.0899 | 0.0614 | 0.0723 |
| 3b | 0.0805 | 0.0074 | 0.6539 | 0.0591 | 0.3151 | 0.0765 |
| 3c | 0.2200 | 0.1913 | 0.4364 | 0.3832 | 0.0902 | 0.0004 |
| 4a | 0.1856 | 0.4648 | 0.1335 | 0.6123 | 0.2873 | 0.0786 |
| 4b | 0.2603 | 0.5770 | 0.0641 | 0.3813 | 0.3114 | 0.0876 |
| 4c | 0.0632 | 0.4692 | 0.0894 | 0.4957 | 0.2820 | 0.0005 |
| 5a | 0.1734 | 0.2485 | 0.3398 | 0.1681 | 0.6584 | 0.0866 |
| 5b | 0.2082 | 0.3444 | 0.3173 | 0.0758 | 0.9182 | 0.1198 |
| 5c | 0.3414 | 0.2733 | 0.2667 | 0.0731 | 0.7581 | 0.1574 |
| 6a | 0.0729 | 0.0108 | 0.0353 | 0.0068 | 0.0337 | 0.5246 |
| 6b | 0.0217 | 0.0484 | 0.0823 | 0.0234 | 0.0317 | 0.6333 |
| 6c | 0.1532 | 0.0953 | 0.0523 | 0.0616 | 0.1853 | 0.5569 |

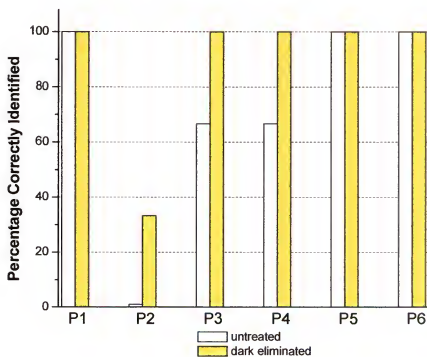
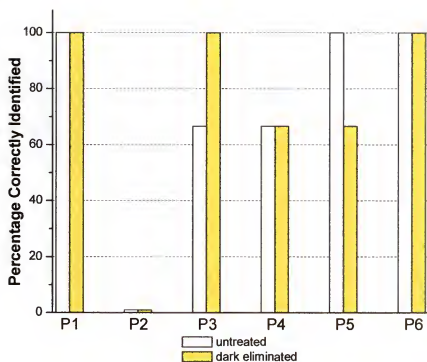


Figure 5-21. Comparison of positive identification percentages for untreated and dark eliminated spectra: (top) linear correlation; (bottom) rank correlation.

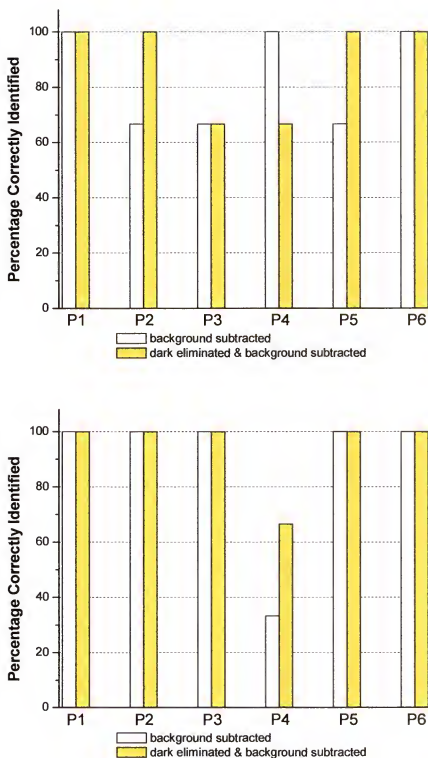


Figure 5-22. Comparison of positive identification percentages for background corrected and background corrected/dark eliminated spectra: (top) linear correlation; (bottom) rank correlation.

and 950 from the right were truncated, leaving about 800 pixels for correlation. Considering only background corrected plastic spectra, the positive identifications increased resulting in near 100% correlation efficiency.

Spectral shift effects. Since identifications are based on relative correlation values, it was originally thought that spectral shifts would not be a significant factor. With a shift, the correlation values would decrease, but so would all the others proportionally. When spectra from a newer data set were correlated to the original library, it was concluded that such assumptions were invalid. Averaging of the three different libraries did not alleviate the problem; averaging resulted in feature broadening, which was counterproductive for proper identifications. There are difficulties in mathematically shifting the spectra for good feature overlap. The spectrometer type used is based on discrete pixels and their corresponding wavelengths. However, wavenumbers are not linearly proportional. For example, a 5 pixel range in one area of the detector accounts for 10 wavenumbers while another 5 pixel segment encompasses 25 wavenumbers. A spectral shift correction algorithm was developed (see Figure 5-23) and tested on a proof-of-concept basis.

Identification Analysis Conclusions

Identification of samples using correlation analysis and the low-end Raman spectroscopic instrument is possible. Several spectral features were investigated during this phase of research. It was concluded that in-class variations are the most significant and influential factor in sample identification. On average, positive identification percentages increased from 50% (untreated) to 90% (background correction).

1. Select a spectrum which will serve as a reference.
2. Calculate/determine which pixel corresponds to the excitation wavelength and denote as λ_{L1} .
3. Calculate discrete wavelength values at all pixels greater than the pixel corresponding to λ_{L1} and denotes as $\lambda_{L1+1}, \lambda_{L1+2}, \dots, \lambda_{L1+n}$.
4. Calculate $\Delta\lambda$ values such that:

$$\Delta\lambda_1 = \lambda_{L1+1} - \lambda_{L1}$$

$$\Delta\lambda_2 = \lambda_{L1+2} - \lambda_{L1}$$

$$\vdots$$

$$\Delta\lambda_n = \lambda_{L1+n} - \lambda_{L1}$$

5. Select another spectrum for which excitation wavelengths differ such that $\lambda_{L1} \neq \lambda_{L2}$.
6. Calculate $1/\lambda_{L2}$.
7. Calculate λ values by:

$$\lambda_{L2+1} = \frac{\lambda_{L2}}{1 - \lambda_{L2} * shift_1}$$

$$\vdots$$

$$\lambda_{L2+n} = \frac{\lambda_{L2}}{1 - \lambda_{L2} * shift_n}$$

recognizing that:

$$shift = \frac{1}{\lambda_{L2}} - \frac{1}{\lambda_{L2+n}}$$

$$shift = \frac{1}{\lambda_{L2}} - \frac{1}{ax^2 + bx + c}$$

$$\Downarrow$$

$$ax^2 + bx + c = \frac{\lambda_{L2}}{1 - \lambda_{L2} * shift},$$

$$\text{where } \lambda_{L2+n} = ax^2 + bx + c$$

8. Find pixels corresponding to $\lambda_{L2+1}, \lambda_{L2+2}, \dots, \lambda_{L2+n}$.
9. Find closest pixels to x calculated in step 8 (from both sides) so that $x_p \leq x \leq x_{p+1}$.
10. Use linear interpolation between I_p and I_{p+1} which are the intensities corresponding to x_p and x_{p+1} , respectively, to determine x intensity value.
11. Repeat for all remaining wavelengths.
12. Displayed interpolated intensities as a function of a new pixel number.
13. Conduct correlation analysis.

Figure 5-23. Spectral shift correction algorithm.

Concluding Remarks

Even though the sample focus of this research phase was placed on post-consumer plastics, the goal of the work was the development of a general Raman system – instrumentation and data analysis that is applicable to a wide range of studies. The results were promising in that good identification percentages were obtained when correlation was combined with data pre-treatment (e.g., background correction). The pervasive question throughout the research is “How low can the system go in cost/quality and still be able to produce spectra capable of routine identifications?” One way to push the limit is to couple the existing instrument and data practices with a signal enhancement method.

CHAPTER 6

SURFACE-ENHANCED RAMAN SCATTERING SPECTROSCOPY WITH LOW-END RAMAN SPECTROSCOPIC INSTRUMENT

Introduction

Interest in coupling an enhancement technique with the inexpensive Raman instrument was instigated by relatively high detection limits observed with normal Raman. Surface-enhanced Raman scattering (SERS) was selected as the means of enhancement. A brief description of fundamentals, materials, preparation methods, and applications is provided prior to experimental discussions.

General Background

Raman spectroscopy produces information-rich spectra; however, the phenomenon is plagued by small scattering cross sections resulting in weak signals. Even though the technique is often superior with respect to the level of structural detail provided, other spectroscopic methods have been routinely employed. This is largely driven by low Raman signal intensities and associated analysis complications. In the 1970s, a variation of normal Raman scattering was discovered, which enabled the acquisition of characteristic Raman spectral detail with increased detection capabilities (i.e., improved signal intensities).⁹⁶⁻⁹⁸ The alternative technique became known as surface-enhanced Raman scattering (SERS) spectroscopy.

Surface-enhanced Raman scattering is the most widely used Raman enhancement technique available to date. It is often associated with signal enhancements ranging from 10^2 to 10^{11} .⁹⁶ Analogous to normal Raman, SERS interrogates the molecular vibrations

related to the inelastic scattering of incident radiation. The difference lies in the adsorption of analyte molecules on rough metallic surfaces.³⁸ Metal particles are central to the augmented SERS intensities. Figure 6-1 presents an illustrative comparison of normal Raman and SERS. As discussed in Chapter 2, normal Raman intensities are proportional to source (laser) power, scattering cross section, and the number of molecules in the interrogated volume. In SERS spectroscopy, the signal intensities are related to similar factors. However, the effective cross section is defined by the adsorbed molecule, which increases the magnitude and probability of Raman scattering. Also, the lower population of the probed volume, determined by the number of molecules involved in the SERS process,⁹⁸ results in lower detection limits.

The exact explanation for SERS enhancement is debated; yet, experts in the field generally agree that more than one effect contributes to the increased signals.^{4,38,96} Enhancement mechanisms are commonly categorized as chemical or electromagnetic in origin. The chemical enhancement effect is analyte specific and generally associated with metal and analyte electronic wavefunction overlap leading to charge-transfer processes.⁹⁸ The effect is short ranged (0.1-0.5 nm) and is estimated to produce enhancement factors of 10 to 100.^{38,96} The primary source of electromagnetic field enhancement is the excitation of surface plasmons by incident radiation.⁹⁸ Under certain conditions, energy carried by photons is transferred to packets of electrons, called plasmons, on a metal surface. These localized electrons oscillate along the incident field and produce an enhanced local electric field.⁴ In contrast to chemical effects, field effects generate enhancement factors up to 10^8 , are analyte independent, and span relatively long distances.^{38,96} Fundamental studies are on-going to better define and

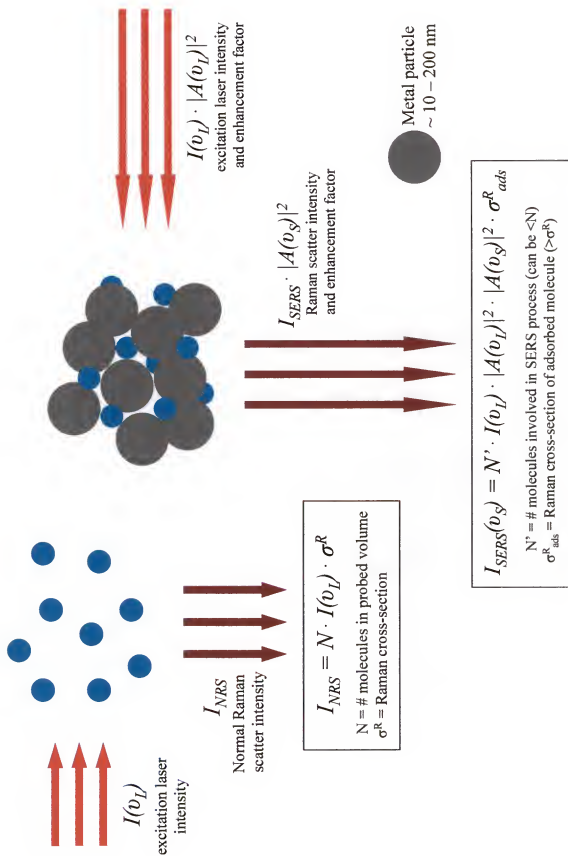


Figure 6-1. Illustrative comparison of normal Raman and SERS. Adapted from reference 98: Kniepp, K.; Kniepp, H.; Itzkan, I. *Chemical Reviews*. **1999**, *99*, 2957.

characterize enhancement mechanisms related to SERS. Regardless of the theoretical derivation of SERS enhancements, a number of different types of metal substrates have been successfully employed over the past three decades. SERS substrates are divided into three general categories: noble metals (e.g., Ag, Au, Cu), free-electron-like metals (e.g., Al, Na, K), and transition metals (e.g., Ni, Pd, Pt).³⁸ The metal surfaces are modified/roughened by several methods including electrochemical, photochemical, evaporation, sputtering, lithography, chemical etching, mechanical polishing, chemical reduction, suspension, and laser ablation.³⁸ Each approach has an unique set of advantages and disadvantages. In deciding which approach to adopt, aspects such as excitation wavelength, production reproducibility, and intended applications are often weighed. The applications are as varied as the preparation methods. A large portion of current SERS research focuses on biomedical and environmental interests.^{96,97,99}

Simple SERS Substrate Preparation and Use with Low-End System

Selection of the substrate preparation method was governed by the general research goal and system criteria detailed in Chapter 1. A methodology for the production of simple Ag SERS substrates was reported in 2002 by Nie and Feng.⁹⁹ The primary modification mechanism was internal electrolysis of Ag^+ onto Cu foil. The design simplicity, ease of preparation, materials availability, and low cost were all attractive features of this method. The basic preparation procedures are illustrated in Figure 6-2. It should be noted that copper foil was used as the substrate base in the aforementioned published study, but copper circuit board was employed in this dissertation research. Pieces of copper circuit board were cleaned with a 0.1 M H_2SO_4 solution. After washing with deionized water and drying with house air, the circuit board chips were placed in an

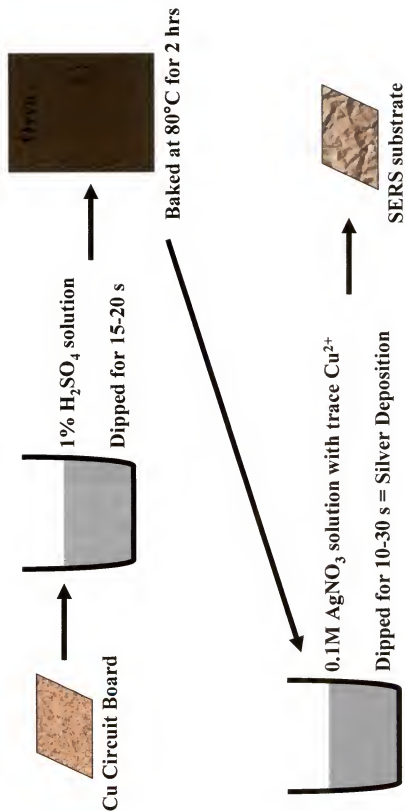


Figure 6-2. Steps for simple Ag SERS substrate preparation as outlined in reference 99; Nie, S.; Feng, Z. *Applied Spectroscopy*. **2002**, *56*, 300.

oven for 2 h at 80 °C. The baking deactivated the chip surface by forming a thin layer of oxide, which aids in retarding the silver plating rate. When the circuit board pieces had cooled, they were dipped into a solution of AgNO_3 where internal electrolysis occurred. Upon removing from the solution, the modified substrates were rinsed and dried. The lifetimes of the substrates were greatly reduced following silver deposition; thus, immediate use followed this preparation stage. Initial studies focused on Ag SERS substrate creation and subsequent evaluation with respect to enhancement, reproducibility, and detection limits. Au SERS substrate production was attempted using similar procedures described for Ag.

A series of scanning electron microscope (SEM) images at assorted stages of SERS substrate preparation are displayed in Figure 6-3. Visual differences were noted and attributed to successful surface modification. Ideal metal particle size for SERS has been reported within a range from 10 nm to 200 nm. Figure 6-4 displays a simple Ag SERS substrate and indicates that the Ag particles produced on the Cu circuit board fell within the ideal size window.

Rhodamine 6G (R6G), para-aminobenzoic acid (PABA), and 2,2'-bipyridine (bpy) were employed in the substrate evaluation phase of research because they have characteristic SERS spectra and have been commonly used in SERS optimization studies. Figure 6-5 displays R6G and PABA SERS spectra obtained with the low-end system. For both, the enhanced spectra are shown with the spectrum from unmodified circuit board. As indicated in the plots, the simple Ag SERS substrates were successful in producing enhanced analyte signals. The plating of Ag onto the Cu circuit board was not a uniform process. Variations in the surface produced different levels of signal

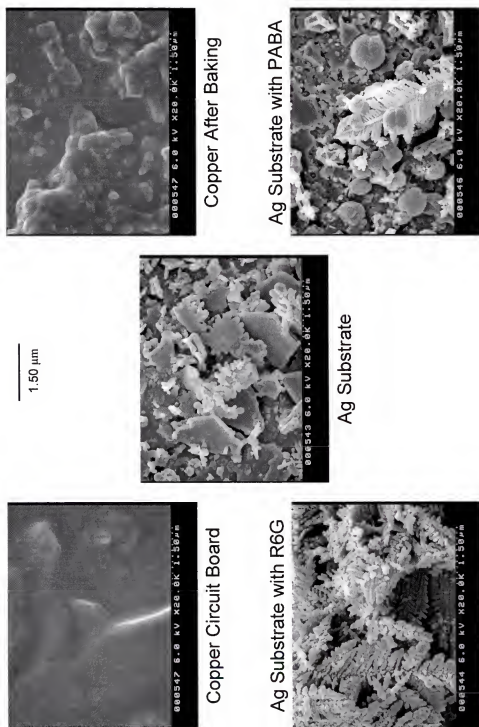


Figure 6-3. SEM images of various substrate preparation stages with 20.0 K magnification. Images acquired by Qian Li.

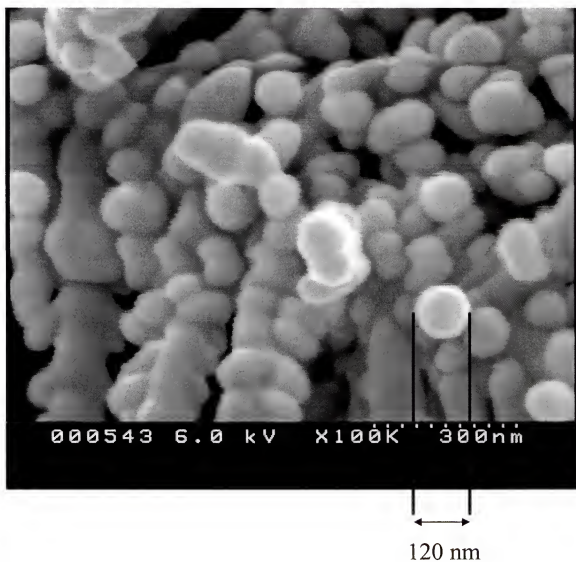


Figure 6-4. SEM image of simple Ag SERS substrate with 100 K magnification. The individual metal particle sizes produced are ideal for SERS. Image acquired by Qian Li.

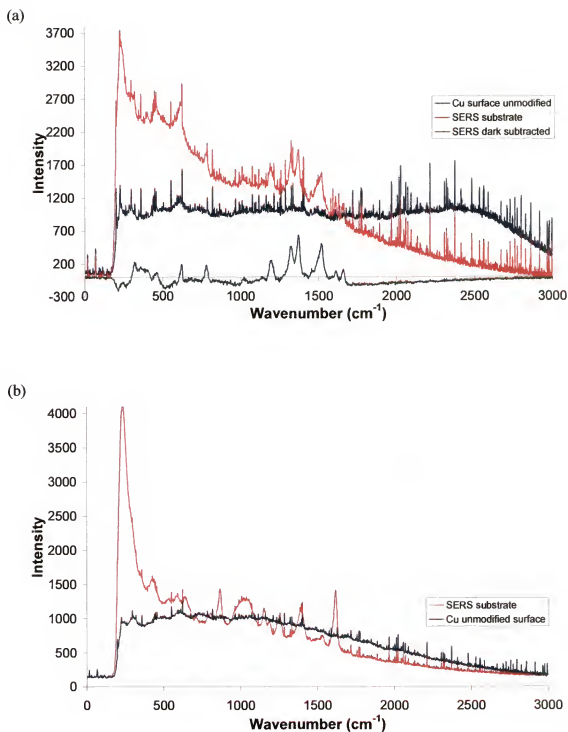


Figure 6-5. Typical SERS spectra obtained with low-end instrument and simple Ag substrates: (a) R6G; (b) PABA.

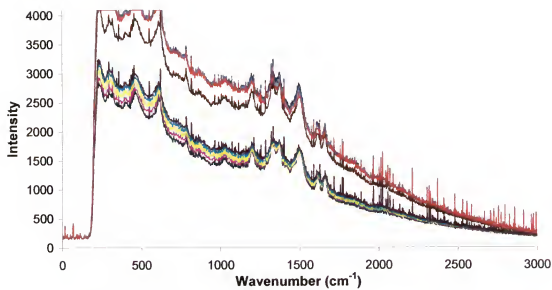


Figure 6-6. Several SERS spectra of R6G at different locations on the substrate.

enhancement across the chip. The resulting spectral deviations are shown in Figure 6-6. Even though the enhancement magnitude differed, it is important to note that the Ag substrates consistently demonstrated increased intensities.

The main impetus for coupling SERS to the low-end system was to achieve lower limits of detection. For comparative purposes, the method used by Nie and Feng to approximate the LOD was found using the following relationship:

$$LOD_{SERS} = M * V_{spotted} \quad (6-1)$$

where, M is analyte molarity ($\mu\text{mol}/\mu\text{L}$)

$V_{spotted}$ is the amount of analyte placed on substrate (μL)

The estimated LOD_{SERS} for the inexpensive instrument was 100 nmol, which is comparable to 1 nmol reported in the Nie study.⁹⁹ Refer to Figure 6-7 for a corresponding bpy (1 μL of 0.1 M) spectrum. Assuming that SERS is completely a surface technique, the region probed by the laser is equivalent to the laser spot size area. Calculations resulted in an absolute LOD of 9 pmol, which is equivalent to 5.4×10^{12} molecules. When the latter value was compared to the absolute detection limit for normal Raman (9.8×10^{16} molecules), an approximate enhancement factor of 2×10^4 was revealed.

Following the success of the simple Ag SERS substrates in conjunction with the low-end system, there was interest in producing simple Au substrates in a similar fashion. The absorption maximum of Ag colloids is around 600 nm and 800 nm for Au; hence, Au should generate larger enhancements in the NIR region when compared to Ag.^{96,97} The first attempt to create Au SERS substrates followed the Ag methodology. The approach, however, did not produce substrates exhibiting any signal enhancement. As with Ag, the

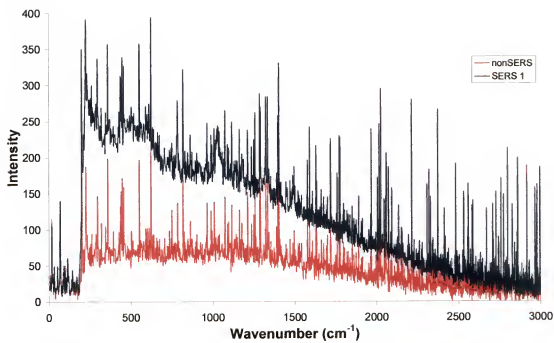


Figure 6-7. SERS Raman spectrum of 0.1 M bpy.

reduction potentials indicated that Au^+ could be reduced by Cu; but, these potentials do not contain information about reaction rates. By eliminating the deactivation (baking) step and increasing the amount of time the Cu circuit board was placed in a Au solution (30 min), enhanced Raman signals were obtained. Figure 6-8 shows a R6G spectrum off of a Au modified chip. Unlike the Ag SERS substrates, the consistent production of good Au substrates was not achieved.

Concluding Remarks

A simple SERS substrate preparation method by means of Ag^+ reduction on the Cu circuit board was evaluated with the low-end Raman instrument. As hoped, the system LOD was significantly reduced, which makes the instrument more useful for a greater variety of qualitative applications. A similar investigation was completed for Au. Enhancement signals were recorded but, there was little reliability in the production process. Lastly, to follow the penny-pinching approach of this research, pennies were evaluated as SERS substrate (Ag modification). Refer to Figure 6-9 for a penny SERS spectrum. The replacement of Cu circuit board with Cu pennies (pre and post 1982), worked well and did not compromise the ability to produce active SERS substrates. Much potential lies in the production of simple and inexpensive SERS substrates. For the purposes of this research, the substrates enabled the production of enhanced signals and lower limits of detection while allowing the project to remain within the original criteria.

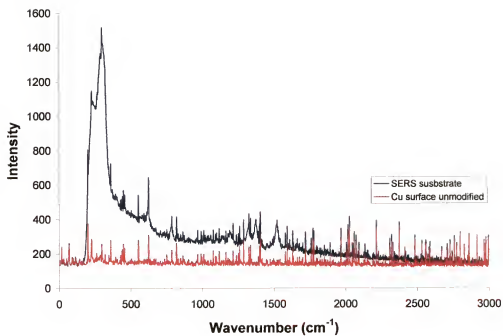


Figure 6-8. R6G SERS spectrum obtained with low-end instrument and simple Au substrate.

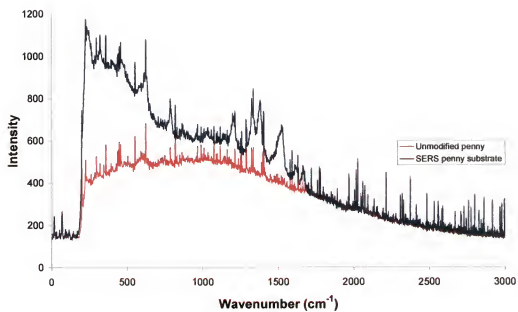


Figure 6-9. R6G SERS spectrum produced from a modified penny substrate.

CHAPTER 7 CONCLUDING REMARKS AND FUTURE WORK

Conclusions

The research described in this dissertation evolved around the development of a low-end Raman spectroscopic system for sample identification purposes. Design criteria stipulated low cost, portability, broad application base, fiber optic sampling, commercially available components, simple data analysis, and ease of use. The work can be divided into three research phases: (1) instrumental design and characterization; (2) data analysis; and (3) signal enhancement.

In the first phase of research, a dispersive Raman instrument was designed within the aforementioned constraints. The general set-up consisted of a diode laser, fiber optic probe, and a grating spectrometer with CCD detector. A number of characterization and optimization studies were conducted, which provided valuable information concerning instrument operation (e.g., laser profiles, spectrometer response, and detector artifacts). System noise was investigated and the limiting source was determined to be flicker noise. Detection limits, concentration and absolute, were also calculated.

The second research phase encompassed a variety of data analysis matters. Using post-consumer plastic samples, grouping and identification analyses were performed. The establishment of sample grouping patterns prior to identification helped to pinpoint samples and categories of potential difficulty. Correlation methods were employed for identification purposes. The effects of several spectral features were examined and it was

concluded that differences in continuum background, leading to in-class variations, was the most significant identification factor.

Prompted by the relatively high detection limits obtained in the initial phase of research, a Raman enhancement technique was coupled to the low-end system. The focus of the third phase was preparation and evaluation of a simple SERS substrate. Silver and gold modification *via* internal electrolysis was attempted on copper circuit boards. Both exhibited enhanced Raman signals, but the gold was difficult to reproduce consistently. Absolute LOD values for normal Raman and SERS were compared, which indicated an approximate signal enhancement of 2×10^4 .

Figure 7-1 provides an illustrative summary of research. Substantial progress was made with respect to general research goals and the foundation for a variety of subsequent projects has been established.

Future Research Directions

Interest in Raman spectroscopy as an analytical tool has resulted in much emphasis being placed on expanding the application base. Combining Raman with chemometric analysis is a rapidly expanding area of research, which is making its way into industry and government sectors. Furthermore, the popularity of SERS has likewise grown and is used even in single molecule detection studies. The potential for future Raman research seems endless.

Based on the research presented in this dissertation, there is a variety of directions to be followed. These paths can be divided into four categories: (1) instrumentation; (2) data analysis; (3) SERS substrate development; and (4) applications.

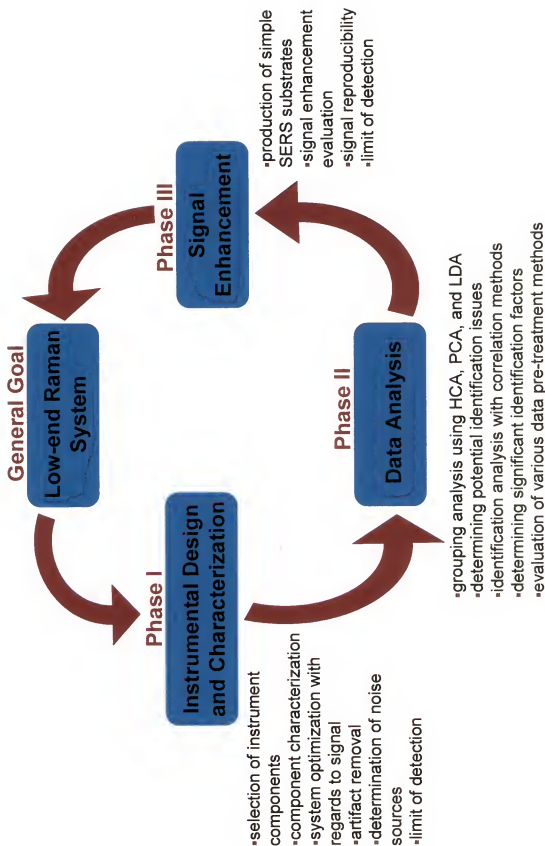


Figure 7-1. Illustrative summary of research.

Improvement in instrumentation is possible with a higher power diode laser integrated into the system as well as use of a diode laser with 830 nm excitation. The laser housing could also be fiber-coupled, which would greatly reduce the need for optical alignment. Additionally, the effects and correction of optical feedback (into the laser) is an option.

In the area of data analysis, difference spectra could be used in combination with correlation analysis and sample identification. This is a relatively new approach in the Raman field and could prove to be useful with the low-end system.⁷⁸ Research efforts could also focus on instrument calibration and standards to allow better instrument-to-instrument comparison of spectra. This would have far-reaching ramifications because universal Raman spectral libraries could be created. Lastly, a variety of other established chemometric methods could be applied to identification analysis such as partial least squares (PLS) and artificial neural networks (ANN).

Continued development of simple and inexpensive SERS substrates is another viable research path. Nontraditional means of modification could also be explored. One such method is substrate submersion in liquid nitrogen prior to analysis to increase the signal.

Since the long-range objective of the inexpensive Raman system is use in biological/biomedical applications, two small viability studies were conducted and could be used as research springboards. First, a series of human urine samples were analyzed. The purpose was to (1) determine whether Raman spectra could be obtained and (2) assess the presence of in-class variations. Collections from 4 subjects over 5 days were evaluated. The resulting averaged spectra are shown in Figure 7-2. The spectral shifts appear consistent between subjects, but the variation in continuum background is

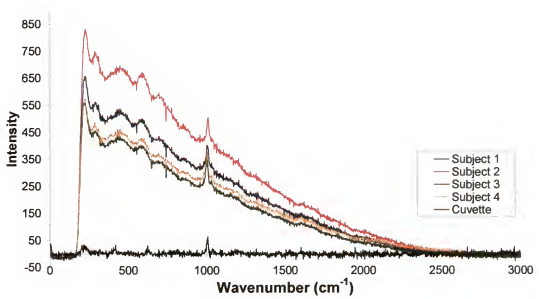


Figure 7-2. Raman spectra of human urine.

significant, indicating that in-class variations will continue to be a factor as samples increase in complexity. Second, raw and boiled egg spectra were acquired and compared. Since the proteins are denatured in the cooking process (which influences conformation and chemical structure), there was curiosity as to whether these changes could be detected with the low-end system. Egg whites did not produce an observable difference; however, the egg yolk spectra did (see Figure 7-3). The findings suggest that protein and fat based biological samples are not out of the realm of possibility. These promising results may open a wide range of application directions.

To move into the area of tissue analysis, such as skin, it is suggested that various layers of chicken skin be sequentially placed on top of a diamond chip and the spectra recorded. Chicken skin behaves similarly to human skin and diamond has one distinctive Raman band at 1331 cm^{-1} . Laser depth penetration and angle dependence could be examined, providing valuable information for other skin/tissue studies.

Not all applications need to be biological in nature. For example, application research could involve the use of the instrument as a solvent analyzer. This would require the ability to perform mixture classifications. Another potential direction is coupling the Raman system with a laser-induced breakdown spectroscopy (LIBS) system to obtain quasi-simultaneous molecular and atomic information. The spectra could then be correlated for sample identification purposes and would find use in materials science and art restoration.

While a number of disadvantages exist for Raman spectroscopy (e.g., weak signals, lack of standards, etc.), researchers continue to find the technique useful and beneficial for an array of interest areas. Superior structural detail, technological developments,

signal enhancement, and specialized chemometric methods will sustain Raman as an essential spectroscopic technique.

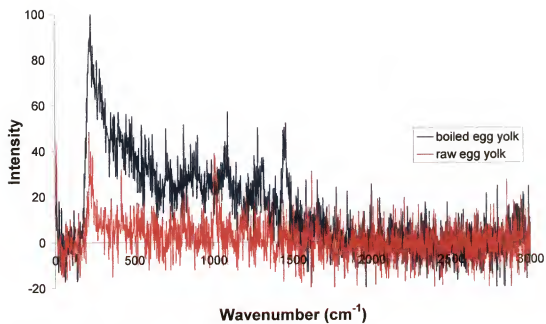


Figure 7-3. Raman spectra of raw and boiled egg yolk.

LIST OF REFERENCES

1. Settle, F., Ed.; *Handbook of Instrumental Techniques for Analytical Chemistry*; Prentice Hall PTR: New Jersey, 1997.
2. Raman, C.V.; Krishnan, K.S. *Nature*. **1929**, *121*, 501.
3. Gardiner, D. J., Graves, P. R., eds. *Practical Raman Spectroscopy*; Springer-Verlag: Berlin, 1989.
4. McCreey, R.L. *Raman Spectroscopy for Chemical Analysis* in Chemical Analysis Series ed. by J.D. Winefordner, *157*, John Wiley & Sons, Inc.: New York, 2000.
5. Pappas, D. Smith, B.W.; Winefordner, J.D. *Talanta*. **2000**, *51*, 131.
6. Chase, B. *Applied Spectroscopy*. **1994**, *48*, 14A.
7. Tessier, P.M.; Christesen, S.D.; Ong, K.K.; Clemente, E.M.; Lenhoff, A.M.; Kaler, E.W.; Velez, O.D. *Applied Spectroscopy*. **2002**, *56*, 1524.
8. Ebert, W.L. *Physical Chemistry of Glasses*, **1993**, *34*, 58.
9. Shiang, J.J.; Risbud, S.H.; Alivisatos, A.P. *Journal of Chemical Physics*. **1993**, *98*, 8432.
10. Enculescu, A.; Stegginga, J.R. *American Pharmaceutical Review*. **2002**, *5*, 81.
11. Giles, J.H.; Shackman, J.G.; Denton, M.B. *American Pharmaceutical Review*. **2002**, *5*, 45.
12. Veiga, F.; TeixeiraDias, J.J.C.; Kedzierewicz, F.; Sousa, A.; Maincent, P. *International Journal of Pharmaceutics*. **1996**, *129*, 63.
13. Goodacre, R.; Timmins, E.M.; Burton, R.; Kaderbhai, N.; Woodward, A.M.; Kell, D.B.; Rooney, P.J. *Microbiology*. **1998**, *144*, 1157.
14. Premasiri, W.R.; Clarke, R.H.; Womble, M.E. *Lasers in Surgery and Medicine*. **2001**, *28*, 330.
15. Lawson, E.E.; Barry, B.W.; Williams, A.C. *Journal of Raman Spectroscopy*. **1997**, *28*, 111.
16. Petrich, W. *Applied Spectroscopy Reviews*. **2001**, *36*, 181.
17. Enejder, A.M.K.; Koo, T.; Oh, J.; Hunter, M.; Sasic, S.; Feld, M.S., Horowitz, G.L. *Optics Letters*. **2002**, *27*, 2004.

18. Choo-Smith, L.P.; Edwaeds, H.G.M.; Endtz, H.P.; Kros, J.M.; Heule, F.; Barr, H.; Robinson, J.S.; Bruning, H.A.; Puppels, G.J. *Biopolymers*. **2002**, *67*, 1.
19. Urlab, E.; Popp, J.; Roman, V.E.; Kiefer, W.; Lankers, M.; Rossling, G. *Chemical Physics Letters*. **1998**, *298*, 177.
20. Hardcastle, F.D.; Wachs, I.E.; *Journal of Raman Spectroscopy* **1995**, *26*, 397.
21. Mulvaney, S.P.; Keating, C. D. *Analytical Chemistry*. **2000**, *72*, 145R.
22. Murata, K.; Kawakami, K.; Matsunga, Y.; Yamashita, S. *Analytica Chimica Acta*, **1997**, *344*, 153.
23. Sridhar, S.; Collette, T.; Garrison, A.W.; McCutcheon, S.C.; Wolfe, N.L. *Environmental Science and Technology*. **1999**, *33*, 3469.
24. Walker, P.A.; Shaver, J.M.; Morris, M.D. *Applied Spectroscopy*. **1997**, *51*, 1394.
25. Kiefert, L.; Hanni, H.A.; Chalaïn, J.P.; Weber, W. *Journal of Gemmology*. **1999**, *26*, 501.
26. Koivula, J.L. *Gems and Gemology*. **1998**, *34*, 281.
27. Hanni, H.A.; Schubiger, B.; Kiefert, L.; Haberli, S. *Gems Gemol*. **1998**, *34*, 102.
28. Gilmore, D.A.; Gurka, D.; Denton, M.B. *Applied Spectroscopy*. **1995**, *49*, 508.
29. Smith, G.D.; Clark, J.H. *Reviews in Conservation*. **2001**, *2*.
30. Chalmers, J.M.; Griffiths, P.R., eds. *Handbook of Vibrational Spectroscopy*; John Wiley & Sons Ltd.: Chichester, 2002.
31. Bell, S.E.J.; Burns, D.T.; Dennis, A.C.; Matchett, L.J.; Speers, J.S. *Analyst*. **2000**, *125*, 1811.
32. Kalasinsky, V.F. *Applied Spectroscopy Reviews*. **1996**, *31*, 193.
33. White, P.C.; Munro, C.H.; Smith, W.E. *Analyst*. **1996**, *121*, 835.
34. Brown, R.; Caphart, M.; Faustino, P.; Frankewich, R.; Gibbs, J.; Leutzinger, E.; Lunn, G.; Ng, L.; Rajagopalan, R.; Chiu, Y.; Sheinin, E. *LCGC*. **2001**, *19*, 74.
35. Hurst, W.S.; Choquette, S.J.; Etz, E.S.; Maslar, J.; Podobedov, V.; Blackburn, D.H.; McCreery, R. Chemical Science and Technology Laboratory. Process Measurements Division, Technical Activities Report, FY 2000.
36. Kellner, R.; Mermet, J.-M.; Otto, M.; Widmer, H. M., eds.; *Analytical Chemistry*; Wiley-VCH: Weinheim, 1998.

37. Hanlon, E. B.; Manoharan, R.; Koo, T-W; Shafer, K. E.; Motz, J. T.; Fitzmaurice, M.; Kramer, J. R.; Itzkan, I.; Dasari, R. R.; Feld, M. S. *Phys. Med. Biol.* **2000**, *45*, R1.
38. Laserna, J. J., ed.; *Modern Techniques in Raman Spectroscopy*; John Wiley and Sons: Chichester, 1996.
39. Ingle, J. D.; Crouch, S. R.; *Spectrochemical Analysis*; Prentice Hall: New Jersey, 1988.
40. Skoog, D. A.; Holler, F. J.; Nieman, T. A.; *Principals of Instrumental Analysis*, 5th Ed.; Harcourt Brace College Publishers: Philadelphia, 1998.
41. Woodbury, G.; *Physical Chemistry*. Brooks/Cole Publishing Company: Pacific Grove, CA, 1997.
42. Szymanski, H. A., ed.; *Raman Spectroscopy: Theory and Practice*; Plenum Press: New York, 1967.
43. Gardiner, D. J., Graves, P. R., eds. *Practical Raman Spectroscopy*; Springer-Verlag: Berlin, 1989.
44. Asher, S. A.; Munro, C. H.; Chi, Z. *Laser Focus World*. **1997**, July, 99.
45. Metz, C. R.; *Schaum's Outlines of Theory and Problems of Physical Chemistry*, 2nd Ed.; McGraw-Hill: New York, 1989.
46. Ramanujam, N. in *Encyclopedia of Analytical Chemistry*. Meyers, R.A., ed. John Wiley & Sons Ltd: Chichester, 2000, 20.
47. Rolfe, P. *Annual Reviews in Biomedical Engineering*. **2000**, *2*, 715.
48. Sweedler, J. V.; Ratzlaff, K. L.; Denton, M. B., Eds. *Charge-Transfer Devices in Spectroscopy*; VCH Publishers: New York, 1994.
49. Lewis, I. R.; Edwards, H. G. M., Eds. *Handbook of Raman Spectroscopy*; Marcel Dekker, Inc.: New York, 2001.
50. Milonni, P. W.; Eberly, J. H. *Lasers*; John Wiley and Sons: New York, 1988.
51. Svelto, O. *Principals of Lasers*, 2nd Ed.; Plenum Press: New York, 1982.
52. Thorlabs Technical Data Sheet on Sanyo DL7140-201 (ThorLabs, Inc., Newton, New Jersey).
53. Carrabba, M.N.; Rauh, R.D.; U.S. Pat. 5,112,127, **1992**
54. Puppels, G.J.; Colier, W.; Olminkhof, J. *Journal of Raman Spectroscopy*. **1991**, *22*, 217.

55. Shim, M. G.; Wilson, B. C.; Marple, E.; Wach, M. *Applied Spectroscopy*. **1999**, *53*, 619.
56. Lewis, I.R.; Griffiths, P.R. *Applied Spectroscopy*. **1996**, *50*, 12A.
57. Williams, K.P.I. *Journal of Raman Spectroscopy*. **1990**, *21*, 147.
58. Schwab, S.D.; McCreery, R.L. *Analytical Chemistry*. **1984**, *56*, 2199.
59. Greek, L.S.; Schulze, H.G.; Haynes, C.A.; Blades, M.W.; Turner, F.B. *Applied Optics*. **1996**, *35*, 4086.
60. McCreery, R. L.; Fleischmann, M.; Hendra, P. *Analytical Chemistry*. **1983**, *55*, 146.
61. InPhotonics Technical Note #13: <http://www.inphotonics.com/technote13.pdf>.
62. Niemczyk, T.M.; Delgado-Lopez, M.; Allen, F.S.; Clay, J.T.; Arneberg, D.L. *Applied Spectroscopy*. **1998**, *52*, 513.
63. Kaiser Optical Systems, Ann Arbor, MI; Owen, H.; Tedesco, J.M.; Slater, J.B.; U.S. Patent 5,337,004, **1994**.
64. InPhotonics User Manual, RamanProbe Fiber Optic Sampling Probe, version 2.11.
65. Wilson, R.G. *Applied Optics*. **1998**, *37*, 3201
66. Ratowsky, R. P.; Yang, L.; Deri, R. J.; Kallman, J. S.; Trott, G. *Optics Letters*. **1995**, *20*, 2048.
67. Ratowsky, R. P.; Yang, L.; Deri, R. J.; Chang, K. W.; Kallman, J. S.; Trott, G. *Applied Optics*. **1997**, *36*, 3435.
68. Weesner, F.; Longmire, M. *Spectroscopy*. **2001**, *16*, 68.
69. Allred, C.D.; McCreery, R. *Applied Spectroscopy*. **1990**, *44*, 1229.
70. OceanOptics S2000 Manual: <http://www.oceanoptics.com/technical/s2000.pdf>
71. OceanOptics grating information:
<http://www.oceanoptics.com/technical/gratingscharts.asp>
72. Sony Technical Data Sheet on ILX511 CCD Linear Image Sensor (Sony Electronics, San Jose, California).
73. Smith, B. W.; Farnsworth, P. B.; Winefordner, J. D.; Omenetto, N. *Optics Letters*. **1990**, *15*, 823.
74. Sommer, A.J.; Stewart, S.A. *Applied Spectroscopy*. **1999**, *53*, 483.

75. Workman, J.; *Handbook of Organic Compounds: NIR, IR, and UV-Vis Spectra Featuring Polymers and Surfactants*; Academic Press: San Diego, CA, 2001.
76. Driscoll, W.G., ed. *Handbook of Optics*, McGraw-Hill Book Company: New York, 1978.
77. Matou, K.; Ni, Y. *Electronics Letters*. **2002**, 38, 1078.
78. Lavine, B. K. *Analytical Chemistry*. **2000**, 72, 91R.
79. Strouf, O.; *Chemical Pattern Recognition*; Research Studies Press: New York, 1986.
80. Allen, V.; Kalivas, J. H.; Rodriguez, R. G. *Applied Spectroscopy*. **1999**, 53, 672.
81. Gornushkin, I. B.; Smith, B. W.; Nasajpour, H.; Winefordner, J. D. *Analytical Chemistry*. **1999**, 71, 5157.
82. Gornushkin, I. B.; Smith, B. W.; Potts, G. E.; Omenetto, N.; Winefordner, J. D. *Analytical Chemistry*. **1999**, 71, 5447.
83. Gornushkin, I. B.; Ruiz-Medina, A.; Anzano, J. M.; Smith, B. W.; Winefordner, J. D. *Journal of Analytical Atomic Spectroscopy*. **2000**, 15, 581.
84. Anzano, J. M.; Gornushkin, I. B.; Smith, B. W.; Winefordner, J. D. *Polymer Engineering and Science*. **2000**, 40, 2423.
85. website: <http://www.domme.ntu.ac.uk/people/alotfi/personal/recycle/plastic.html>
86. Brereton, R.G. *Chemometrics: Data Analysis for the Laboratory and Chemical Plant*; John Wiley & Sons Ltd.: England, 2003.
87. Otto, M. *Chemometrics: Statistics and Computer Application in Analytical Chemistry*; Wiley-VCH: Weinheim, 1999.
88. Meloun, M.; Militky, J.; Forina, M.; *Chemometrics for Analytical Chemistry: PC-Aided Statistical Data Analysis*; Ellis Horwood Limited: New York, 1992.
89. Brereton, R. G. *Chemometrics: Applications of Mathematics and Statistics to Laboratory Systems*; Ellis Horwood: New York, 1990.
90. Beebe, K.R.; Pell, R.J.; Seasholtz, M.B.; *Chemometrics: A Practical Guide*; Wiley & Sons, Inc.: New York, 1998.
91. Massart, D. L.; Kaufman, L. *The Interpretation of Analytical Chemical Data by the Use of Cluster Analysis*; Robert E. Krieger Publishing Co.: Malabar, Florida, 1989.


92. Meier, P. C.; Zund, R. E. In *Chemical Analysis Series: A Series of Monographs on Analytical Chemistry and Its Applications*; Winefordner, J. D., ed; John Wiley and Sons: New York, 2000; Vol. 153.
93. Ostrovskii, D.I.; Yaremko, A.M.; Vorona, I.P. *Journal of Raman Spectroscopy*. **1997**, 28, 771.
94. Vickers, T.J.; Wambles, R.E.; Mann, C.K. *Applied Spectroscopy*. **2001**, 55, 389.
95. Gornushkin, I.B.; Eagan, P.E.; Novikov, A.B.; Smith, B.W.; Winefordner, J.D. *Applied Spectroscopy*. **2003**, 57, 197.
96. Zander, C.; Enderlein, J.; Keller, R.A., eds. *Single Molecule Detection in Solution: Methods and Applications*; Wiley-VCH:Germany, 2002.
97. Filmore, D. *Today's Chemist at Work*. **2002**, 15.
98. Kniepp, K.; Kniepp, H.; Itzkan, I. *Chemical Reviews*. **1999**, 99, 2957.
99. Nie, S.; Feng, Z. *Applied Spectroscopy*. **2002**, 56, 300.

BIOGRAPHICAL SKETCH


Paige Elizabeth Eagan was born on May 26, 1977, at Carswell Air Force Base in Ft. Worth, Texas. Her parents are Colonel (Ret.) Patrick D. Eagan and Mrs. Nancy Eagan. Paige spent her childhood as a military dependent and had the opportunity to live in a number of locations: Texas, Nebraska, Guam, California, Alabama, Florida, Virginia, Georgia, and Ohio. While in Florida, Paige and her family were blessed with the addition of her sister, Kristen.

Paige attended The University of the South in Sewanee, Tennessee, for undergraduate studies. In May of 1999, she received a Bachelor of Science degree in Chemistry. Paige continued her education in chemistry as part of the Analytical Chemistry Division at the University of Florida, where she earned a Doctor of Philosophy in August of 2003.


I certify that I have read this study and that in my opinion it conforms to acceptable standards of scholarly presentation and is fully adequate, in scope and quality, as a dissertation for the degree of Doctor of Philosophy.


James D. Winefordner, Chair
Graduate Research Professor of Chemistry


I certify that I have read this study and that in my opinion it conforms to acceptable standards of scholarly presentation and is fully adequate, in scope and quality, as a dissertation for the degree of Doctor of Philosophy.


Richard A. Yost
Professor of Chemistry


I certify that I have read this study and that in my opinion it conforms to acceptable standards of scholarly presentation and is fully adequate, in scope and quality, as a dissertation for the degree of Doctor of Philosophy.


David H. Powell
Scientist of Chemistry

I certify that I have read this study and that in my opinion it conforms to acceptable standards of scholarly presentation and is fully adequate, in scope and quality, as a dissertation for the degree of Doctor of Philosophy.


Martin T. Vala
Professor of Chemistry

I certify that I have read this study and that in my opinion it conforms to acceptable standards of scholarly presentation and is fully adequate, in scope and quality, as a dissertation for the degree of Doctor of Philosophy.


Katherine N. Scott
Professor of Nuclear and Radiological
Engineering

This dissertation was submitted to the Graduate Faculty of the Department of Chemistry in the College of Liberal Arts and Sciences and to the Graduate School and was accepted as partial fulfillment of the requirements for the degree of Doctor of Philosophy.

August 2003

Dean, Graduate School